Development of Microparticles Created from Physically Modified Starch Granules for the Uptake and Release of Drugs

by

David Jonathan Wulff

A thesis

presented to the University of Waterloo

in fulfillment of the

thesis requirement for the degree of

Doctor of Philosophy

in

Chemical Engineering - Nanotechnology

Waterloo, Ontario, Canada, 2021

Examining Committee Membership

The following served on the Examining Committee for this thesis. The decision of the Examining Committee is by majority vote.

External Examiner	Dr. Todd Hoare Associate Professor Department of Chemical Engineering McMaster University
Supervisors	Dr. Marc Aucoin Professor Department of Chemical Engineering University of Waterloo
	Dr. Frank Gu Professor Department of Chemical Engineering and Applied Chemistry University of Toronto (Adjunct, University of Waterloo)
Internal Members	Dr. William Anderson Professor Department of Chemical Engineering University of Waterloo
	Dr. Raymond Legge Professor Emeritus Department of Chemical Engineering University of Waterloo
Internal-external Member	Dr. Ehsan Toyserkani Professor Department of Mechanical and Mechatronics Engineering University of Waterloo

Author's Declaration

This thesis consists of material all of which I authored or co-authored: see Statement of Contributions included in the thesis. This is a true copy of the thesis, including any required final revisions, as accepted by my examiners.

I understand that my thesis may be made electronically available to the public.

Statement of Contributions

Other than starch digestibility, amylose content, and static light scattering particle size analysis, all laboratory work was performed by me. Experimental design, planning, and result interpretation were done by me, with occasional input from Dr. Ariel Chan, Dr. Frank Gu, and Dr. Marc Aucoin

The work presented in **Chapter 2** is a manuscript entitled intended for publication. I am the primary author of this manuscript reviewing work by others in this field with input from Dr. Frank Gu for the first draft.

The work presented in **Chapter 3** is a published short communication: Wulff, David, Marc G. Aucoin, and Frank Gu. 2020. "Helium Ion Microscopy of Corn Starch." Starch - Stärke 1900267. I am the primary author of the publication with minor input from Dr. Frank Gu and Dr. Marc Aucoin. Dr. Marc Aucoin also provided assistance with editing.

The work presented in **Chapter 4** is a published journal article: Wulff, David, Ariel Chan, Qiang Liu, Frank X. Gu, Marc G. Aucoin. "Characterizing internal cavity modulation of corn starch microcapsules." Heliyon, Volume 6, Issue 10, 2020, e05294. I am the primary author of the publication with input on experimental design and analysis from Dr. Ariel Chan, Dr. Qiang Liu, Dr. Frank Gu and Dr. Marc Aucoin. Dr. Marc Aucoin also provided assistance with editing.

The work presented in **Chapters 5 and 6** contains work performed entirely by me with input on experimental design and analysis from Dr. Marc Aucoin, Dr. Ariel Chan and Dr. Frank Gu.

Abstract

Controlled release drug delivery systems are, depending on the desired effect, generally an improvement over conventional drug delivery. Through material design, drugs can be delivered with temporal and spatial control, ideally delivering a therapeutically relevant dose for a relevant duration. Hydrogels, a network of cross-linked water-soluble polymers, are a common choice of material for creating such a delivery system, due to their general similarity to biological tissue because of their high-water content. Hydrogels can be used in a variety of formats for drug delivery, with options on length scales from nanometers to centimeters, with microparticles being a common choice. When used biologically, it is important that the polymers used are biocompatible. One polymer option is starch, the polymer obtained from starch granules. The work presented in this thesis aims to use hydrogel-like microparticles created from native starch granules through a simple swelling process for a controlled release drug delivery system. In working towards this goal, the starch granule swelling process and swelled starch itself are characterized.

First, helium ion microscopy (HIM) was used to characterize the morphology of native corn starch. HIM is a relatively new method, which is similar to scanning electron microscopy, but instead of using an electron beam, a beam of He^+ is used. HIM can create images that have high contrast, high depth-of-field, and can resolve features down to a few nanometers. The method has been particularly useful for nanomaterials research and has been used on a number of materials, such as nanoporous SiO_2, cellulose nanofibrils, and mammalian cells. To the best of my knowledge, this is the first report of this method for imaging starch. The images I produced are capable of resolving features of starch not possible with scanning electron microscopy (SEM). With some areas of starch structure still not well understood, further characterization with HIM can assist with improving the understanding of starch's structure. "Blocklets," which are

theorized substructures of starch were not observed using HIM. These structures are often referred to in the literature, but evidence for their existence is contentious.

Next, the process of making starch microcapsules (a term used in this thesis for swelled particles made from native normal corn starch granules) by manipulating physical conditions was studied. When heated in water, starch swells and undergoes partial gelatinization. The swelling process for normal corn starch was controlled with heating temperature and heating time. As a result of particle size and particle solubility being correlated with swelling extent, these properties were also controlled. The internal cavity present in native corn starch granules increased in size as the particles swelled. This size of the internal cavity was modulated through control of swelling extent. It was hypothesized that a microparticle with an internal cavity could allow for an improvement of controlled release compared to a similar microparticle without an internal cavity. The internal cavity of SMCs was characterized using SEM, HIM, brightfield microscopy, polarizing light microscopy, and confocal laser scanning microscopy. The swelling process and the resulting change in internal cavity size was mathematically modeled.

To evaluate the most appropriate SMCs for use in drug delivery, the starch swelling process, differences between SMCs created from different starch types, and a number of properties of SMCs were studied. The response of pea, potato, wheat, waxy corn, and normal corn starch to various heating temperatures were evaluated. The morphological changes of the SMCs were characterized using SEM and brightfield microscopy. The effect of swelling on particle size distributions was measured and the polydispersity increased as expected. Normal corn starch type appeared to be best suited for use in a drug delivery system. With swelling power being a key measurement for characterizing SMCs, the effect of centrifugal force was evaluated; higher force led to lower measurements of swelling power.

The digestibility of microparticles is a key factor for particles intended for oral drug delivery, and so the *in vitro* digestibility of SMCs was evaluated. Greater swelling led to higher digestibility. As a method of altering the rigidity of SMCs to potentially lock-in drugs, the outer shell of the SMCs was cross-linked. The cross-linking resulted in inhibited swelling when the SMCs were subjected to greater heating. Selective water uptake in SMCs was observed when SMCs were placed in a solution of bovine serum albumin (BSA), suggesting that SMCs are limited in the size of molecule they can carry.

Finally, preliminary investigations into the ability of SMCs to be loaded with a drug and to subsequently release it were conducted. A challenge with characterizing loading of microparticles is the interstitial and intraparticle volume of water amongst tightly packed microparticles, the sum of which I term "drug-accessible water." Often the effect of this volume is ignored when determining loading capacity, but to properly characterize loading, this volume must be accounted for. Additionally, when characterizing adsorption, it is generally assumed that the hard sphere size exclusion is negligible. However, this assumption is not reasonable for large molecules. To improve loading characterization, these factors must be considered. SMCs were loaded with methylene blue (MB) and the drug-accessible-water volume was determined. The data was fit to a Langmuir adsorption isotherm, and adsorptions of 3.61, 2.14, and 2.06 mg/g for native normal corn starch, SMC65, and SMC70 were observed, respectively. Due to greater swelling and resulting greater drug-accessible-water volumes, the opposite trend was observed for loading capacities, where native normal corn starch, SMC65, and SMC70 had loading capacities of 3.81, 5.11, and 9.65 mg/g, respectively. The fraction of the drug-accessible water that is interstitial verses intraparticle was also estimated based on a comparison of experimental results with geometrically calculated theoretical swelling powers. An experimental method was used to directly calculate the interstitial volume. In addition, confocal laser scanning microscopy (CLSM) with the fluorescent dyes RITC-dextran and FITC-BSA as

model drugs, was used to visualize drug loading and to determine where drugs were loaded spatially within the SMCs. Drug can be found in the internal cavity of SMCs.

In conclusion, swelled normal corn starch granules show promise for use in a drug delivery system. Modulation of heating temperatures and times allowed for control of the swelling extent and of the size of the internal cavity. The microcapsules are candidates for use in a controlled release drug delivery system. Further work to characterize the interaction between the microparticles and more model drugs should be conducted. In addition, *in vitro* testing in simulated intestinal and gastric fluids needs to be conducted to determine the drug release capabilities.

Acknowledgements

Firstly, I would like to thank my supervisors: Dr. Frank Gu and Dr. Marc Aucoin. To Dr. Gu, thank you for accepting me into your research group and facilitating my project collaboration with Agriculture and Agri-Food Canada. Without this support, my research would not have been conducted. To Dr. Marc Aucoin, thank you for adopting me into your research group at a time when I was wondering if I would be able to finish my research at UW. I cannot thank you enough for your support and guidance and for believing in me.

To Dr. Qiang Liu, my advisor at Agriculture and Agri-Food Canada, thank you for agreeing to collaborate with me on the project and for your assistance with use of AAFC resources.

To Dr. Ariel Chan, thank you for your assistance in the 2nd and 3rd years of my research. Your guidance, encouragement, and support in the initial stages of my research into starch swelling and characterization was invaluable.

To my thesis committee members, Dr. William Anderson, Dr. Raymond Legge, and Dr. Ehsan Toyserkani, thank you for providing guidance and support towards my research. And to my external examiner, Dr. Todd Hoare, thank you for providing your time to evaluate my thesis.

Many thanks to all the research members in both lab groups for your support and friendship. While I appreciate all of you, with some of you I had particularly interesting and helpful conversations which shaped some aspects of my research and, potentially more importantly, my view of the world. In particular, I'd like to thank, in no particular order, Harish Krishnakamar, Aaminah Ahmad, Jeff Watchorn, Sandy Liu, Zac Young, Andrew Holmes, Mostafa Saquib, Stuart Linley, Paul Chen, and Mark Bruder.

To Elizabeth Donner, at AAFC, thank you for helping me with collecting samples and for running analysis on various starch samples.

I would like to thank the administrators and staff of WIN and the Chemical Engineering Department at UW for your support and assistance with taking courses, TAships, facilitating interesting lectures, and lab equipment.

I would like to thank my parents, Donald and Margaret, for your endless love, support, and encouragement. You both instilled a love of learning and encouraged my curiosity from a young age. To my siblings, Jennifer, Graham, Michael, Timothy, Jonathan, Matthew, and Hannah, you each inspire me and encourage me to be a better person, and for that I'm grateful.

To my wonderful partner Tessa, I could not have asked for more encouragement and support through the final stages of my academic journey. The last few months have had both many highs and many lows, but you made each day better.

To my friends who I've made through playing ultimate frisbee, running on the UW cross-country team, and triathlon training, thanks for giving me a way to vent excess energy and for often widening my perspective on life.

Financial support from the Agriculture and Agri-food Canada through the Research Affiliate program and from UW's Graduate Research Studentship, Graduate Scholarship and the Engineering Doctoral Domestic Student Award is gratefully acknowledged.

Dedication

To my late cousin Rebecca – we miss you and your endless positivity.

The world lost one of its best much too early.

Table of Contents

List of Figures

List of Tables

List of Abbreviations

AFM – atomic force microscopy

Asp – aspartic acid

b – Langmuir adsorption isotherm

BSA – bovine serum albumin

CLA – conjugated linoleic acid

CLSM – confocal laser scanning microscopy

CMS – carboxymethyl starch

$d_{3,2}$ – Sauter mean diameter

$d_{4,3}$ – mean volume weighted diameter

Da – Dalton

DAO – diamine oxidase

DAW – drug-accessible water

DDS – drug delivery system

DS – diclofenac sodium OR degree of substitution

DSC – differential scanning calorimetry

E – enhancement factor

EE – encapsulation efficiency

FITC - fluorescein isothiocyanate

FTIR – Fourier transform infrared

FU – furosemide

FWHM – full width at half maximum

GDGE – glycerol diglycidyl ether

Glu – glutamic acid

HBSS - Hank's balance salt solution

HES – hydroxyethyl starch

HIM – helium ion microscopy

IgG – immunoglobulin G

LC – loading capacity

MA – methacrylate

MB – methylene blue

MBA - N,N'-methylene bis-acrylamide

MW – molecular weight

MWCO – molecular weight cut off

NC – normal corn

NMR – nuclear magnetic resonance

OCT – optimal cutting temperature

OSA – octenyl succinate anhydride

O/W – oil-in-water

O/W/O – oil-in-water-in-oil

PBS – phosphate buffer solution

PCL – poly-ε-caprolactone

PEG - polyethylene glycol

P(EG)-MA - polyethylene glycol methacrylate

PF – packing factor

q_m – maximum adsorption capacity

$r_{h,n}$ – radius of hole in native granule

$r_{h,s}$ – radius of hole in swelled particle

$r_{p,n}$ – radius of native granule (particle)

$r_{p,s}$ – radius of swelled particle

RITC – Rhodamine B isothiocyanate

RDS – rapidly digestible starch

RS – resistant starch

SAXS – small angle x-ray scattering

SD – standard deviation

SDS – slowly digestible starch

SEC – size exclusion chromatography

SEM – scanning electron microscopy

SIF – simulated intestinal fluid

SGF – simulated gastric fluid

SLS – static light scattering

SMC – starch microcapsule

SP – swelling power

SPI – soy protein isolate

SSF – soluble starch fraction

STMP – sodium trimetaphosphate

STPP – sodium tripolyphosphate

TEM – transmission electron microscopy

TEMPO - 2,2,6,6-tetramethyl-1-piperidinyloxy

TGA – thermogravimetric analysis

UV – ultraviolet

W/O – water-in-oil

W/W – water-in-water

WAXS – wide angle x-ray scattering

XRD – x-ray diffraction

Chapter 1: Introduction

1.1 Overview

Conventional delivery of drugs, with all its upsides, has some downsides too. Often the dose needed to cause a therapeutic effect can have negative side effects or can even cause toxicity. Controlled release drug delivery systems offer one way to improve spatial and temporal control of drug release. Hydrogels are often the material of choice due to their high water content which is similar to biological tissue (Li & Mooney, 2016). By forming the hydrogels into microparticles or nanoparticles, the delivery system can be customized and can decrease the invasiveness of the system. To be used for drug delivery, the polymers used to form the hydrogel must be biocompatible. Being both inexpensive, widely available, and biocompatible, starch is an ideal candidate for creating a hydrogel to be used for controlled release drug delivery. Starch has also been used in conventional drug delivery as a natural excipient in tablets and capsules (Builders & Arhewoh, 2016).

In the initial stages of our research, we characterized the internal cavity that is found in normal (as opposed to high-amylose or waxy) corn starch. Another term for corn starch is maize starch. When starch granules, the 1-100 μm diameter energy storage system of most plants (Tester et al., 2004), are heated in an excess of water, they swell and undergo gelatinization, the process by which the starch polymers (amylose and amylopectin) become fully dissociated and hydrated. Through investigating the swelling process of normal corn starch, we observed that the internal cavity swells in size as the particles swell. Partially swelled granules can be created by halting the swelling process, creating hydrogel-like microcapsules through a relatively simple method. Our goal was to utilize this natural microcapsule and to determine if it could be used to encapsulate drugs which could later be released in a controlled fashion. As the particles swell, the ratio between the outer wall and the internal cavity changes, potentially allowing for tunable diffusion

profiles of drugs through the outer wall. Unlike most other work which has created starch-based microparticles with a bottom-up approach where the starting materials are fully hydrated starch polymers (i.e. not in granular form), our approach was a top-down approach which could have the benefit of creating microparticles with properties not possible with a bottom-up approach.

Despite the fact that starch is widely used in many industries and that research on starch structure has been ongoing since the 1930s (Badenhuizen, 1956), and the structure of starch granules is not entirely understood with gaps in our understanding of molecular packing and features on the nanoscale (Bertoft, 2017). Starch granule structure is quite complex and depends on the starch source (Pérez & Bertoft, 2010; Shujun Wang & Copeland, 2015). In addition, while there is a lot of research on native granules and on gelatinized starch, research on partially swelled starch has been minimal. Further, research on the changes of the internal structure of partially swelled starch is very sparse.

The work presented in this thesis aims to create a drug delivery system using microcapsules created from native starch granules. In pursuit of this aim, we contribute to the field's understanding of internal starch structure in native granules and in partially swelled granules. We also perform preliminary investigations into the ability of the swelled microcapsules for loading and releasing drugs and demonstrate proof-of-concept for this capability.

1.2 Research Objectives

The primary objectives of my research were as follows:

- To characterize the starch swelling process to allow for the creation of starch microcapsules made from partially swelled starch granules
- To probe the structure of partially swelled starch through several types of microscopy

- To characterize various properties of starch microcapsules which are relevant for their use in drug delivery
- To evaluate the ability of starch microcapsules to encapsulate and release drugs

1.3 Thesis outline

After this introductory chapter, this thesis consists of one chapter on literature review (Chapter 2), four chapters with experimental results (Chapters 3-6) and one concluding chapter (Chapter 7).

Chapter 2 consists of a comprehensive literature review of recent developments in the field of starch-based microparticles for use in drug delivery. It covers methods for producing such microparticles and the various characterization methods of the microparticles and of their drug loading and release capabilities.

Chapter 3 discusses the use of helium ion microscopy (HIM) for imaging of starch granules, a novel use for the relatively new microscopy method. We demonstrate its capacity for resolving features of starch on the order of ~10 nm and compare the images to images produced with scanning electron microscopy (SEM).

Chapter 4 focuses on the swelling process of normal corn starch granules for producing starch microcapsules (SMCs). It demonstrates the ability to control the swelling extent and the soluble starch fraction through heating temperature and heating time. The microcapsules are characterized to understand their internal structure and how the internal cavity changes as a result of microparticle swelling. A mathematical model is produced to describe the swelling behavior which closely matches our experimental results.

Chapter 5 focuses on establishing the most suitable type of swelled starch for use in a drug delivery system and on understanding relevant aspects of these swelled SMCs. Various starch types are evaluated, and we determine normal corn starch in the swelling range of 60-70 ˚C to be most suitable. With the goal of loading the particles through adsorption for the purpose of controlled release of drugs, we evaluate particle size

distributions, swelling extent characterization, digestibility, composition changes, cross-linking effects, zeta potential, and selective water uptake.

Chapter 6 contains preliminary investigations of drug loading into and release from SMCs. We use the model drug methylene blue to measure the adsorption capacity of the microcapsules. We demonstrate use of a method for quantifying drug adsorption while accounting for drug which is absorbed into the particles but not adsorbed. We evaluate the interaction between several model drugs and SMCs to attempt to characterize the interstitial volume between particles when they are tightly packed. Confocal laser scanning microscopy is used to observe loading of fluorescent model drugs.

Chapter 7 concludes the thesis by providing an overview of important findings and by suggesting recommendations and outlook for the work.

Chapter 2: Literature review

2.1 Introduction

Controlled-release drug delivery systems (DDSs) can provide both spatial and temporal control of drug release, offering the potential to improve bioavailability and to reduce toxicity to unintended areas (Li & Mooney, 2016). Controlled release can be attained by designing particles that either (a) act as a physical barrier to slow diffusion, (b) use polymers that are environmentally responsive (e.g. to temperature, enzymes, or pH), (c) degrade over time, or (d) have a combination of the previous methods. Starch-based particles can be designed with these attributes in mind and are an exciting option as starch has the benefit of being easily accessible, inexpensive, and biocompatible. While starch may be used in formats ranging from nanometers to centimeters, our review focuses on starch-based microparticles (i.e. 1-1000 μm in diameter).

There are many ways in which starch-based microparticles can be used for drug delivery. Most research on such DDSs has focused on the microparticles being used orally for the delivery of drugs to the colon or small intestine. By avoiding the release of drugs into the stomach and/or the small intestine, less drug is lost through degradation in the gastrointestinal tract. Lower loss leads to higher absorption into the bloodstream, allowing for increased bioavailability, which has multiple advantages. Another benefit is that starch-based DDSs can improve the delivery of poorly water soluble drugs (Jiang et al., 2014). In addition, while drugs are typically delivered to increase their concentration in the blood stream, in some cases the intended site of action is the colon itself; the use of starch-based particles can be helpful in these instances as well. For example, Ahmad et al. (2013) created a starch-based DDS with the intent of using it for treatment of colon cancer. Work has also been done with the intent of using starch-based DDSs for other purposes, such as for rapid hemorrhage control (Su et al., 2019), topical wound healing (Rehan et al., 2019), gastroretentive oral delivery (Lemieux et al., 2015), and intranasal administration (Mao et al., 2004). It is also worth noting that starch-based microparticles have been used medically without the delivery of drugs

for treating liver cancer through transarterial chemoembolization (TACE) (Goerg et al., 2019; Schicho et al., 2018) and in vaccines as an immunostimulant (Moreno-Mendieta et al., 2017, 2019; Wikingsson & Sjöholm, 2002).

Starch is a polymer that is derived from plant sources. Its natural state in the plant is as a starch granule, which can range from 1 – 100 μm in diameter, with size highly dependent on plant type (Tester et al., 2004). This granule consists of two types of polysaccharides: amylose and amylopectin (Fig. 2.1). Although occasionally confusing, "starch" can refer to either the starch granule or the starch molecules – amylose and amylopectin. The composition of starch varies widely depending on the plant source. However, amylose typically makes up 20-30% of the granule with the remainder being amylopectin (Singh et al., 2003a). Both amylose and amylopectin consist of repeating units of glucose monomers. Amylose is a linear polymer linked by α-(1-4) glycosidic bonds, while amylopectin is a branched polymer linked by linear α-(1-4) glycosidic bonds with branch points occurring every 20-30 units with α-(1-6) glycosidic bonds (Karim et al., 2000). Amylopectin molecules typically have molecular weights that are 10 times that of amylose (Zhong et al., 2006). Starch granules also have slight amounts of protein, fatty acids, and minerals that can affect the properties (Rosicka-Kaczmarek et al., 2016; Zhu, 2015). Corn starch tends to be the most common type of starch used, likely because: a) it is the most highly researched type of starch, and thus the most characterized, b) it is easily available in most regions, and c) there are various strains which allow for either high amylose and low amylopectin or low amylose and high amylopectin contents.

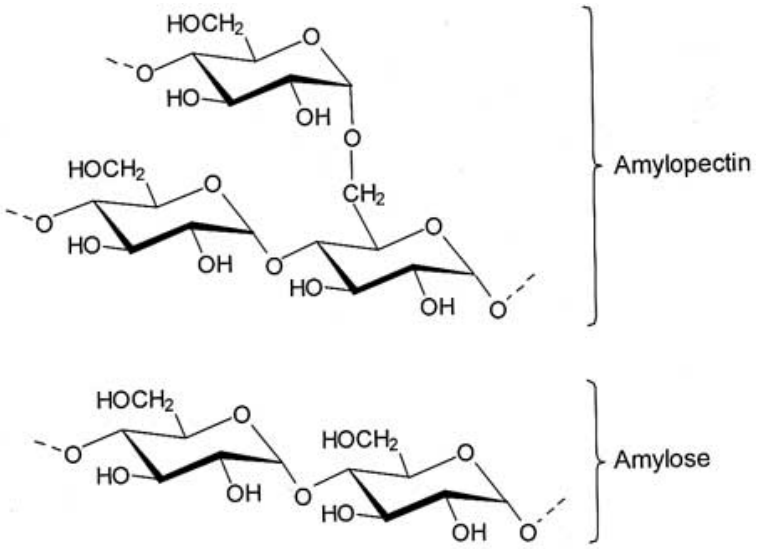

Figure 2.1: The constitutive polymers of starch: amylose and amylopectin

Although starch is often used in its unmodified form simply as amylose and amylopectin, starch can also be modified to improve its properties. Examples of modified starch are carboxymethyl starch, acetylated starch, hydroxyethyl starch, octenyl succinyl anhydrous (OSA) starch, starch acetate, vinyl-grafted, and acryloyl starch. Various block co-polymers can also be created from starch, one example being starch-PEG.

The scope of this review includes discussion of starch-based particles, which have either been evaluated for drug delivery capabilities or have been created with such an application in mind. These particles are often called many things, with ‘microparticle’ being the broadest descriptor. Some researchers have taken liberties with how they describe starch-based particles, however there are some general guidelines. ‘Microcapsule’ is typically used to describe particles that have an outer shell structure and inner core structure; the core may either be solid or non-solid. ‘Microsphere’ is typically used to describe particles which are mostly spherical and homogenous throughout. ‘Microgel’ is typically used to describe particles which are strictly a hydrogel. In this review, we generally refer to all particles using the general term of microparticles. For microparticles to be considered “starch-based” at least half of the weight of the particles should come from starch itself.

The focus of this review is on microparticles where the particles are both intended for drug delivery and demonstrate some capability for drug release. Although some work has been done with starch-based microparticles for delivery of oils (Xiao et al., 2019), food ingredients (Maia et al., 2019; Nogueira et al., 2020), nutrients (Adejoro et al., 2019), and microorganisms (Avila-Reyes et al., 2014; Muhammad et al., 2018), such work isn't covered in this review. Some research has also been conducted on use of starch-based films to deliver drugs directly (Tuovinen et al., 2004) or through the use of films that contains drug-loaded microparticles (Bie et al., 2016; Huo et al., 2016). These types of systems will also not be covered in this review. This review covers production methods, drug loading and release, and potential applications for starch-based microparticles intended for use in drug delivery.

2.2 Starch-based microparticles

The first step of starch-based drug delivery is to create the microparticles. Similar to how there are many ways to make polymer-based microparticles, the same is true with starch-based microparticles. It is challenging to categorize the microparticles into types because there is some overlap with the various types. Common formation techniques include cross-linking, emulsification, and ionotropic gelation. Often multiple techniques are combined.

Nearly all research has focused on microparticles that were created using a bottom up approach: creating something larger by starting with smaller components. In general, native starch granules are first broken down into their component molecules — amylose and amylopectin — through gelatinization. To gelatinize starch granules, they are heated (typically at a temperature between 40-140˚C) in a solution with an excess of water (typically between 0.5-20% (w/w)) for a period of time (typically 15 min to 2 hours). With an excess of water, higher heating temperatures and longer heating times lead to greater gelatinization. Gelatinization can also occur when starch granules are treated with an alkaline solution without heating (Ragheb et al., 1995). However, this method isn't commonly used. The gelatinization process can be altered when plasticizers (Ismail et al., 2016; Lara & Salcedo, 2016; Nashed et al., 2003) or neutral salt solutions

(Jay-Lin Jane, 1993) are used instead of pure water. This solubilized starch is often the starting point for creating microparticles. In addition, starch can also be modified through functionalization or co-polymerization.

2.2.1.1 Preparation of starch-based microparticles

To create particles from a solution of starch or a starch-based polymer, the polymer must be formed into a particle-like shape in some way. Methods for achieving such a shape are spray drying, emulsification, or dripping of the polymer into another solution to extract the solvent while leaving the polymer. In some cases, physical attractive forces are enough to maintain a rigid microparticle structure. In other cases, ionic or chemical cross-linking is used to hold the particles together or to improve their rigidity. Various methods are frequently combined to allow for better control in order to produce the most suitable particles for the intended application. A summary of recent work is provided in Table 2.1.

2.2.2 Spray drying

Spray drying is a process in which dry particles are produced by dispersing a liquid mixture or solution into a hot gas. To make starch-based microparticles for drug delivery through spray drying, typically gelatinized or homogenized starch and drug are added to form an aqueous slurry. When the slurry is atomized into the hot gas (typically air), the water evaporates, and the starch physically entraps the drug through intermolecular forces as the microparticle forms. Often non-starch components such as gelatin (H. Chen et al., 2017; Trindade & Grosso, 2000) or xanthan gum (He et al., 2016) are added to the slurry to improve loading capabilities or to provide stability to the loaded drugs in the microparticles.

It is worth noting that while freeze drying has some similarities to spray drying, freeze drying by itself generally cannot be used to create particles as there is no mechanism in the process that can cause a homogenous hydrogel to separate into particles. Freeze drying is a useful process for drying already-formed particles, as freeze drying can minimize some of the negative effects of conventional drying. Both spray drying and freeze drying can be used for loading particles with drugs.

Palma-Rodriguez et al. (2013) used spray drying to encapsulate ascorbic acid, also known as vitamin C, using native rice starch, and modified (acid-treated and subsequently gelatinized) rice, maize, and potato starch. To form the particles, a 15% w/w mixture of starch in water with ascorbic acid (10% by weight, relative to starch) was spray dried at 7 mL/min with inlet and outlet temperatures of 160˚C and 110˚C, respectively. The particles were stored at 4˚C at low humidity. The morphology of their particles varied considerably. The native rice starch particles (mean diameter of 7.2 μm) resembled "popcorn" balls, which the authors report being held together by protein structures. As for the acid modified rice starch, the particles (mean diameter of 7.0 μm) had a smooth appearance, the result of fully gelatinized starch molecules coalescing uniformly during spray drying. The modified maize and potato starch were similarly smooth with mean diameters of 5.8 μm and 5.7 μm, respectively. The authors reported on the stability of the ascorbic acid, based on how much was retained over a period of a few weeks. They found that the native rice starch microcapsules had the least amount of ascorbic acid degradation, while the modified starch microparticles all had considerably higher degradation. However, the native rice starch microparticles had a lower encapsulation efficiency of 58% compared to encapsulation efficiencies ranging from 64-98% for the modified starch microparticles. The authors suggested a positive correlation between how much ascorbic acid was on the surface and the rate of degradation with storage. Similar work was subsequently done by Hoyos-Leyva et al. (2018) using native taro starch where they created similar "popcorn" balls loaded with L-ascorbic acid with a total encapsulation efficiency of 99%. The authors suggested that forming such microparticles from native granules is only possible with small granules of less than 10 μm in diameter and a sufficiently high protein content as the binding agent. They also reported an inverse correlation between the relative humidity and the rate of degradation of ascorbic acid.

Liu et al. (2007) used sweet potato starch to encapsulate diclofenac sodium (DS, MW: 318 g/mol) with spray drying. Native starch (2, 3, or 4% w/v) and DS (1 or 2% w/v) were added together in water and heated at 80˚C for 2 hours to cause gelatinization of the starch. The liquid was spray dried with a feed rate of 2 mL/min and an inlet temperature of 130˚C. Particle diameters showed dependence on the amount of starch,

with particles made with 2% starch having a mean diameter of 10.3 μm and particles made with 4% starch having a mean diameter of 13.1 μm. In all ratios used, the encapsulation efficiency was above 95%. Release was tested into PBS at 37˚C through a cellulose dialysis membrane with greater than 70% release of DS in 6 hours for all particle types. The authors fit the release data to the Higuchi equation with a good fit, indicating that release is governed by Fickian diffusion. They did not, however, mention the molecular weight cut-off of the dialysis membrane or provide a control for diffusion of pure DS through the dialysis membrane.

A different approach for encapsulating drugs involves spray coating a drug-containing core. The core contains the drug and an accessory polymer and can be made through extrusion spheronization and then dried. A bottom-spray fluidized-bed coater is then used to coat the microparticle cores with a starch-based polymer, which acts to slow the release of the encapsulated drugs. This method has been used to encapsulate both 5-aminoslicylic acid (J. Chen et al., 2018; Situ et al., 2014) and insulin (Situ et al., 2014, 2015).

Another approach that involves spray drying is spray freeze-dying, whereby the liquid feed is sprayed right into liquid nitrogen. Rochelle and Lee (2007) created microparticles from hydroxyethyl starch using this method. While, the particles encapsulated and stabilized bovine liver catalase (MW: 250 kDa), the stabilization was poor without also using trehalose and mannitol as stabilizers. The particles were intended to be used as a ballistic injection method whereby the particles are accelerated to a high speed to allow for penetration of the epidermis. However, it appears that such a project has yet to become available on the market.

2.2.3 Cross-linking

Cross-linking is a common technique for linking together multiple polymers. When used to create microparticles, cross-linking imparts mechanical stability and stiffness. It can also prevent motion of the polymer, potentially slowing or preventing the release of any entrapped drugs within the polymer matrix. Typically cross-linking is used in conjunction with another method, such as emulsification, but there has

been considerable work creating starch-based microparticle only through cross-linking. The basic principle involves reacting modified starch with a cross-linker in a homogenous solution without stirring. Once the cross-linking takes place, the result is a large single cross-linked structure that is theoretically a single molecule. To arrive at the final microparticle, this single mass is broken up mechanically into microparticle-sized pieces and then washed and dried to obtain the final particles.

Yuan Li et al. (2009) were the first to use such a method to create starch-based microparticles. Oxidized starch (DS: 30-100%) was first produced using the oxidation catalyst 2,2,6,6-tetramethyl-1-piperidinyloxy (TEMPO). This process oxidizes alcohol groups at the C-6 to carboxyl groups. Sodium trimetaphosphate (STMP) is then used to cross-link the starch at pH 10 with heating at 40˚C by reacting with alcohol groups on adjacent polymer chains. STMP was used in varying weight ratios between 10-40%. After the cross-linking takes place, the gel is pushed through a nylon cloth with a 75 μm mesh size to form the microparticles through mechanical fragmentation. After washing with ethanol and then acetone to remove the water with minimal deformation to the mesh, the particles are dried. Most particles are about 10-20 μm in size. The authors report that properties such as charge density and cross-linking density can be controlled. Due to the negative charge of the particles, they make an ideal candidate for encapsulating positively charged functional molecules. The authors also report environment-dependent release, with high pH, high salt concentrations, and enzymes all being capable of triggering release. This method has been used by many others to create the same particles and has been researched for delivering lysozyme (MW: 14.3 kDa; pI: 11.35) (Yuan Li, Kadam, et al., 2012; Bao Zhang et al., 2014, 2017; Bao Zhang, Wei, et al., 2015), ascorbic acid (MW: 176 g/mol) (Bao Zhang, Li, et al., 2015), anthocyanins (MW: ~300 g/mol) (Z. Wang et al., 2013), and beta-carotene (537 g/mol) (Shanshan Wang, Chen, Shi, et al., 2015). A variation of the method that used glycerol diglycidyl ether (GDGE) as the cross-linker has also been researched (L. Zhao et al., 2015).

2.2.4 Emulsification

The most well-researched form of creating starch-based particles for use in drug delivery is through emulsification. Often this method is combined with either cross-linking, which improves the structural rigidity of microparticles and prevents or slows diffusion of encapsulated drugs, or with spray drying, which causes coalescence of the particles through physical interactions. When starch is used in its unmodified form, it encapsulates hydrophilic molecules well, and either water-in-oil (W/O) or water-in-water (W/W) emulsions are used to create the particles. With modifications to make the starch polymer more hydrophobic, oil-in-water (O/W) or oil-in-water-oil (O/W/O) emulsions can be used to encapsulate hydrophobic molecules. Sometimes modifications to the starch polymer result in a structure that has both hydrophilic and hydrophobic properties which can improve loading of some molecules.

There are often several variables that are used to tune the properties of the microparticles. Common parameters that are varied in the production process include temperature, solvents, reaction time (with or without cross-linking), degree of substation when modified starch is used, and drug and reagent concentrations. Particle size is typically highly dependent on the viscosities of the two phases, on the stirring speed (or droplet size if dripping method is used), and on the ratio of the two phases.

2.2.4.1 W/O emulsion

W/O emulsions provide a useful method for organizing water-soluble polymers into spherical structures. If used for encapsulation of hydrophilic drugs, generally the drugs can be loaded either during or after particle formation. If intended for delivery of hydrophobic drugs, the particles should be formed prior to drug loading. Surfactants can be used to help with stabilizing the emulsion during particle formation.

García-González et al. (2012) used a W/O emulsion method to produce microparticles. They first mixed native corn starch, water, canola oil, and in some formulations, glycerol monostearate, as a surfactant to form a W/O emulsion. Water:oil phase ratios of 1:1, 1:2, and 1:3 were used. After heating the emulsion in a pressure vessel at various temperature between 95˚C and 140˚C to cause gelation of the starch, the mixture

was slowly cooled to 45˚C with stirring. The particles were then isolated using centrifugation and soaked in ethanol at 4˚C for 48 hours to allow for starch retrogradation – the process of thermodynamic reorganization of starch polymers over time. The authors found that higher gelatinization temperatures, higher stirring speeds, and the use of a surfactant all led to smaller particle sizes. Specific surface areas of up to 112 m^2/g were achieved. The particles were subsequently loaded with ketoprofen (MW: 254 g/mol) using a supercritical CO_2 method to adsorb the drug.

Jiang et al. (2014) used a W/O emulsion to create microparticles 20-100 μm in size. Soluble starch (type not specified) was added to water and homogenized with methylbenzene, chloroform, and Span® 80 as the organic phase in a W/O ratio of 8:100. After storing the emulsion at -20˚C (time not provided), solvent exchange was used to convert the hydrogel to an alcogel. The authors claim that the freezing process causes ice-crystal formation that leaves pores when the ice is displaced by ethanol and the particles are subsequently dried. The drug lovastatin (MW: 405 g/mol) was loaded into the particles by soaking the particles in a solution of lovastatin dissolved in chloroform. The chloroform was then evaporated, allowing lovastatin to precipitate into and onto the particles. Release of lovastatin into PBS was tested and demonstrated first-order release over about 60 min.

Baimark and Srisuwan (2013) created microparticles from a simple process, whereby solubilized starch was added dropwise to ethyl acetate with stirring. Since water is miscible in ethyl acetate, the water is extracted from the droplet and the remaining starch polymer aggregates together to form the particles (mean size of 34 μm). Blue dextran (MW not specified by authors, but 2,000 kDa is most common) as a model drug was loaded into the particles by adding it with the starch solution before the dropwise solvent extraction step. Drug-free particles displayed a porous internal morphology.

The previous three methods created particles through physical interactions. A key limitation of physical interaction is their low mechanical strength. By combining emulsification with cross-linking, high strength particles with controllable size can be created. Lemioux et al. (2015) formed mucoadhesive microparticles by cross-linking carboxymethyl starch (CMS) in a W/O emulsion. Carboxylation is used to convert starch

to an ionic hydrophilic polymer that allows for pH-controlled release of encapsulated drugs (Lemieux et al., 2009). The particles were created by adding CMS (DS: 0.1 – 1.5), STMP as the cross-linker, and furosemide (FU; MW: 331 g/mol) as the model drug together in a basic solution as the aqueous phase to the organic phase that consisted of cyclohexane, chloroform, and Span® 80. The W/O emulsion was allowed to react for 4 hours to cause cross-linking of the particles within the aqueous phase. The particles were then washed with isopropyl alcohol. The authors tested release from the particles into Hank's balance salt solution (HBSS), both at pH 1.0 and 7.4. They reported low swelling of the particles at pH 1.0, the result of low electrostatic repulsion between the negatively charged polymers. This led to slow release of FU, with first order-like release over about 2 hours. Under pH 7.4 conditions, however, FU was fully released within about 5 min. The authors' intent with the particles was to use them as a gastroretentive oral drug delivery system. The authors also found that the particles had higher mucoadhesion to gastric mucosa than to intestinal mucosa.

A similar process was used by Zhao et al. (2008) to create microparticles by use of a W/O emulsion with gelatinized starch as the aqueous phase, and with cyclohexane, chloroform, Span® 60, and Tween® 60 as the organic phase. N,N'-methylene bis-acrylamide (MBA) was used to cross-link the starch at 50˚C for 2h. Particles had a mean diameter of 18.2 μm. After washing, adsorption isotherms were created with methylene blue (MW: 320 g/mol) at various temperatures. It was observed that cooler temperatures corresponded to higher adsorption, with adsorption at 25˚C resulting in a saturation adsorption capacity of 0.1064 mmol/g of particles (equivalent to 34 mg/g). Pereira et al. (2013) also used MBA to cross-link vinyl-grafted starch by creating W/O emulsion and allowed cross-linking to take place for 30 min. The particles had an average particle size between 400-500 μm and were loaded with curcumin (MW: 368 g/mol) through soaking to a total loading capacity of 82 mg/g.

After first developing a simple method to create starch microparticles with only cross-linking, as described in Section 2.3.2, Li et al. (Yuan Li, Kleijn, et al., 2011; Yuan Li, Norde, et al., 2012; Yuan Li, Zhang, et al., 2011) created a similar method where spherical particles were made using a W/O emulsion, but then were

cross-linked with STMP to increase stiffness of the particles. Oxidized starch and STMP, as cross-linker, were added together in a basic solution and then emulsified with an excess of hexane and Span® 80. By immediately filtering the emulsion through a 10 μm membrane 10 times, a homogenous size distribution was obtained. The emulsion was heated at 40˚C for 40 min to allow for completion of cross-linking. Lastly, particles were washed with methanol and then stored in water. The particles demonstrated high loading of lysozyme (MW: 14.3 kDa) through adsorption of up to ~3 g/g. More recently, D. Li et al. (2020) used the same process to form microparticles, but then subsequently loaded the microparticles with nanoparticles through electrostatic interactions, where the nanoparticles had a positive charge attracting them to the negatively charged oxidized starch in the microparticle. The nanoparticles were made from amphiphilic lysozyme (made through partial enzymolysis at Glu and Asp sites) and loaded with quercetin (MW: 302 g/mol).

A variation of the W/O emulsion was used by Fang et al. (2008), where rather than emulsifying both the oil and aqueous phases together as is common, they dripped the aqueous phase into the oil phase. The aqueous phase consisted of a basic solution with solubilized starch and STMP. When dripped into the oleic phase of liquid paraffin, Span® 80, and Tween 80® at 50˚C, microparticles formed and were hardened through cross-linking by STMP for 5h. After washing the particles with organic solvents and a saline solution, the particles were vacuum dried. The dried particles had a mean $d_{4,3}$ diameter of ~19 μm. A soaking method was used to load the particles with methylene blue to a maximum loading capacity of 330 mg/g; loading was dependent on temperature, drug concentration, media type, and time.

2.2.4.2 W/W emulsion

This method takes advantage of two aqueous solutions with vastly different viscosities to create an emulsion.

Wöhl-Bruhn et al. (2012) used UV cross-linking in a W/W emulsion to create microparticles from hydroxyethyl starch (HES) grafted with polyethylene glycol methacrylate (P(EG)-MA). The polymer,

HES-P(EG)$_n$MA, with n = 6 or 10, had degrees of substitution between 0.3 – 1.2. HES-P(EG)$_n$MA (2% w/w), the cross-linking initiator (Irgacure®2959, 0.1% w/w), and a model drug (70 kDa FITC-dextran or FITC-IgG) were added together to form the first aqueous phase (W_1). A 30 wt.% solution of 12,860 g/mol PEG was used as the second aqueous phase (W_2). Both phases were mixed with a vortex mixer for 1 min to form the W/W emulsion; various W_1:W_2 ratios were used for different formulations. Cross-linking was done with 366 nm light for 30 min and then particles were washed with DI water and freeze-dried. Mean diameter ranged from about 5 to 40 μm and was dependent on polymer solution concentration and the PEG:polymer ratio in the W/W emulsion. Cryo-SEM revealed a highly porous interior (Fig. 2.5). Controlled release (which appears first-order) into PBS of FITC-dextran with the HES-P(EG)$_{10}$MA particles showed faster release (65% release at 30 days) than the HES-P(EG)$_6$MA particles (45% release at 30 days). However, release by 400 days was about 90% for both. When α-amylase was added to the release media, release occurred faster.

Elfstrand et al. (2009) had previously used a similar method. The W_1 phase contained ~22 wt.% starch and 0.95 wt.% protein (either insulin or bovine serum albumin [BSA]) and the W_2 phase was a 38 wt.% solution of 20,000 g/mol PEG. Both phases were mixed together and then incubated at 6˚C for times between 5-48 hours, followed by incubation at 37˚C for times between 5-24 hours. Unlike the other work by Wöhl-Bruhn et al. (2012), no cross-linker was used, and the particles were held together with physical interactions only.

2.2.4.3 O/W emulsion

Panyoyai et al. (2017) encapsulated tocopheryl acetate (MW: 473 g/mol), also known as vitamin E acetate, into microcapsules made from modified waxy maize starch using spray drying. The starch was modified by grafting octenyl succinate, a molecule with a polar 8-carbon tail, at just below 3% content, to induce some hydrophobicity to the starch. Since tocopheryl acetate is a relatively viscous oil and insoluble in water, it was dissolved in ethanol and then homogenized with the modified starch in water to form an O/W emulsion with a starch:tocopheryl acetate weight ratio of 19:1. This emulsion was spray dried with a feed

rate of 7.5 mL/min with inlet and outlet temperatures of 120˚C and 75˚C, respectively. The particles were then stored at -30˚C. The authors reported an encapsulation efficiency of 90% and studied the release into ethanol at temperatures ranging from -30 to 70˚C. They found the release profile reached equilibrium in about 1 min with a total release of only about 10% of the encapsulated tocopheryl acetate. They also found a strong positive correlation between release temperature and release extent.

Deng et al. (2014) used octenyl succinate anhydride (OSA) starch to create spray dried microparticles with encapsulated β-carotene (MW: 537 g/mol), a hydrophobic molecule that is a precursor to vitamin A. The OSA starch used had a DS of 1.9% (C. Li et al., 2013). The authors compared OSA starch to soy protein isolate (SPI) as encapsulating materials, and they used various ratios of OSA starch, SPI, and β-carotene (with soy oil as carrier). After homogenization of the feed components to create an O/W emulsion (with total solid contents between 10-20%), the emulsion was spray dried with a feed rate of 10mL/min with inlet and outlet temperatures of 160˚C and 85˚C, respectively. The particles were stored in a desiccator at 4˚C until further use. The authors found that using a 1:1 blend of OSA starch:SPI resulted in the highest encapsulation efficiency, while using only OSA starch resulted in the lowest. Stability was also studied with various temperatures, humidities, with/without sunlight, and with different storages times. While much of the results show no clear trends, OSA starch-only microparticles seemed to have the best β-carotene retention with storage at 60˚C. They also found little difference in β-carotene retention regardless of whether particles were exposed to sunlight.

He et al. (2016) similarly used OSA starch (DS: 0.16) to encapsulate conjugated linoleic acid (CLA), a type of fatty acid. The authors used both OSA starch only and mixtures of OSA starch and xanthan gum in 60:1, 80:1, and 100:1 w/w ratios. Each suspension was homogenized with 25% w/w CLA to form an O/W emulsion that was used as the feed for spray drying. Spray drying was done with inlet and outlet air temperatures of 160 and 75˚C, respectively. The authors reported particle sizes of 5-6 μm and found that the addition of xanthan gum provided a protective effect from oxidation for the CLA. They also reported the addition of xanthan gum conferred resistance to acid hydrolysis and enzymatic degradation, resulting

in the 60:1 ratio microparticles having ~3% release of CLA in simulated stomach conditions compared to ~6% release with particles made with OSA starch only. Similarly, when comparing release into simulated intestinal conditions, they observed ~10% release for the 60:1 ratio particles compared to ~50% release from the particles made with OSA starch only.

Okunlola et al. (2017) acetylated yam starch to introduce hydrophobicity that was then used to encapsulate a hydrophobic drug using a O/W emulsion. Repaglinide (MW: 453 g/mol) as the model drug and the acetylated starch (DS: ~2.6) in 1:5, 1:8, and 1:10 w/w ratios were added to chloroform and mixed. A thin stream of this solution was added to a 0.5% w/v aqueous solution of sodium carboxylmethylcellulose with stirring, causing particles to form. The particle sizes were highly dependent on the drug:polymer ratio, with higher amounts of drug resulting in smaller particles. The authors reported encapsulation efficiencies between 75-93% and extended release over 12 hours.

Balmayor and colleagues (Balmayor, Feichtinger, et al., 2009; Balmayor, Tuzlakoglu, et al., 2009) used a method to encapsulate hydrophobic molecules using a blend of starch and poly-ε-caprolactone (PCL) to increase the hydrophobicity. The blend of polymers composed the oleic phase for formation using an O/W emulsion with solvent evaporation. However, the particles were not strictly "starch-based," as they used a 30:70 weight ratio of starch:PCL to create the particles.

2.2.4.4 O/W/O emulsion

One final emulsion method is to create a double emulsion where starch is used as the shell material to encapsulate a hydrophobic drug in an inner oleic phase. The double emulsion allows for the hydrophilic starch-based phase to form into particles, while still encapsulating a hydrophobic molecule.

Similar to the O/W emulsion and cross-linking methods previously described where TEMPO-oxidized starch is used to create microparticles, S. Wang et al. (2015) created microspheres using an O/W/O method. Oxidized starch (DS: 0.9) was created through TEMPO-mediated oxidation. A double emulsion process was used to obtain an $O_i/W/O_o$ emulsion with the inner oil phase (O_i) consisting of β-carotene in corn oil,

the aqueous phase (W) consisting of oxidized starch (primarily), whey protein isolate, and Fe^{2+} ions, and the outer oil phase (O_o) consisting of paraffin oil with Span® 80. After the double emulsion was created, oxygen gas was pumped into the solution with stirring, to oxidize the Fe^{2+} into Fe^{3+} in order to induce cross-linking between the carboxyl groups. Particles were washed with hexane and methanol, and then resuspended in pH 3 HCl solution where they had a mean diameter of 39 μm. The authors reported that the particles were stable at acidic stomach conditions (pH<2), but that the particles were disrupted in intestinal conditions (pH 7) to release the β-carotene.

Ahmad et al. encapsulated the hydrophobic model drugs metronidazole (2012), 5-fluorouracil (2012), and irinotecan hydrochloride (2013) with an O/W/O emulsion. The O_i phase consisted of the drug and magnesium stearate in methylene chloride, and the W phase consisted of starch and Tween® 80 in water. After homogenizing these two phases into an O/W emulsion, this emulsion was added dropwise into liquid paraffin containing 1.5% v/v Span® 80 as the O_o phase. The particles were heated at 40˚C to promote extraction of water. After separating the particles with centrifugation, the particles were washed with hexane. Other than testing the effect of varying starch:drug ratios, where generally a higher starch content led to larger particles, the authors did not test the effect of other variables. As a result, it is hard to draw any conclusions about the effect of stirring speeds, reaction times, or other ratios. The authors conducted *in vivo* studies on rats for each drug, and in each they observed selective release into the colon, which the authors attribute to mucoadhesion and microbial degradation in the colon.

2.2.5 Ionotropic gelation and polyelectrolyte complexation

Ionotropic gelation, also called ionic cross-linking, is a process which uses polyelectrolytes (polymers with repeating units which carry a charge) to form ionic cross-links in the presence of counter ions to create a hydrogel. Nanoparticles, microparticles, and millimetre-sized particles can all be created using this process. Polyelectrolyte complexation is a slightly different process with a similar result: instead of counter ions, a polyelectrolyte polymer with opposite charge is used. Typically, a small gauge needle is used to drip one

solution into another, with each drop from the needle forming one particle. Historically, alginate has been the main polyelectrolyte used to create such hydrogels (Daly et al., 2020; J. Li & Mooney, 2016), but recently work has be done with incorporating modified starch to improve the properties of the hydrogels.

Blemur et al. (2016) created microspheres using ionotropic gelation with carboxymethyl starch (CMS) made from high amylose corn starch and alginate (the salt of alginic acid) for encapsulation of diamine oxidase (DAO, MW: ~184 kDa for dimer). A ~2% solution containing CMS (DS: 0.2), sodium alginate, and DAO in roughly a 19:4:3 wt. ratio was added from a height of 4 cm with a 26-gauge needle (inner diameter 0.26 mm) into a 10% $CaCl_2$ solution under stirring. Both CMS and alginate have a negative charge, so when added to a solution with the bivalent ion Ca^{2+}, ionotropic gelation occurs, and a microsphere is formed. The authors report encapsulation efficiency of about 90%, with enzyme activity of about 50% after vacuum drying. They also evaluated the stability of the enzyme in simulated intestinal fluid; they reported that although enzyme activity in the microspheres was lower compared to the free enzyme control for the first 12 hours, for the following 12 hours, the activity was maintained at about 60% while the free enzyme activity decreased to close to zero.

Rehan et al. (2019) also used ionotropic gelation to create microcapsules from starch and alginate. Their intent was to create an antioxidant, antimicrobial, and wound-healing cotton gauze by incorporating bioactive microcapsules. They created a solution with 2% sodium alginate and 4% starch, along with guava leaf powder extract. After soaking gauze in the solution for 15 min, the gauze was soaked in a solution with 0.05M $CaCl_2$ to induce cross-linking, which created microcapsules. The leaf extract is a combination of bioactive compounds – primarily phenols, flavonoids, and essential oils. The authors report antimicrobial, antioxidant, UV protection, and wound healing properties. The wound healing studies were done on rats with induced wounds.

Quadrado and Fajardo (2020) created BSA-loaded microparticles through polyelectrolyte complexation using carboxymethyl starch (CMS) made from rice starch and chitosan. Chitosan is a cationic polymer and is thus able to complex with the anionic CMS. A 3% (w/v) solution of chitosan and BSA at pH 5 was added

dropwise from a height of 1 cm into a 4% (w/v) solution of CMS (DS: 0.5) at pH 8.5 to form the microparticles. The CMS solution also contained 0.1% w/v sodium tripolyphosphate (STPP), which is a cross-linker, and the authors did not include a control, so it is not possible to isolate the difference between the effect of polyelectrolyte complexation and the effect of the STPP. Particles were about 1 mm in diameter and had a BSA encapsulation efficiency of 67%. Release into SGF (pH 1.2) and SIF (pH 6.8) was tested, and the authors reported pH dependent release, with slightly faster release into SGF. However, they completed the release study with dialysis membrane with a molecular weight cut-off (MWCO) of 12,000 Da, and BSA has a molecular weight of ~66,000 Da, calling their results into question.

2.2.6 Other methods

Su et al. (2019) created microspheres from corn starch through cross-linking with epichlorohydrin followed by enzymolysis. Their intent was to use the microspheres as a hemostatic agent for control of blood loss. It appears the particles might have been partially gelatinized in conjunction with the cross-linking process, as a result of heating at 50˚C in a pH 13 solution, based on their appearance. This process is unique in that it is a top-down approach for making the particles. As such, the particles retain some of the original form of the native granules, as confirmed by the authors using FTIR spectroscopy and XRD. Large pores (~1 μm in diameter) were created by treating the particles with glucoamylase and α-amylase for 6 h at 50˚C. After loading the particles with tranexamic acid (MW: 157 g/mol), a fibrinolytic agent, through freeze drying, the particles were able to effectively induce blood clotting to prevent blood loss *in vivo* on rabbits with ear artery and liver injuries. In addition, the particles induced clotting faster, and with less blood loss, than a product currently on the market (Arista®).

In another unique method, Luo et al. (2019) created microparticles through self-assembly of short chain glucans, which were derived from waxy maize starch. The short chain glucans were created by debranching gelatinized starch with pullulanase at 37˚C for times between 1 – 7 days. After centrifuging the treated starch, the supernatant was added to a solution with chitosan and incubated at 4˚C, inducing self-assembly

through recrystallization of the short chain glucans. Chitosan was also used as a steric stabilizer to minimize self-aggregation of the short chain glucan clusters. The use of chitosan resulted in a much more highly monodisperse distribution and imparted a positive zeta potential to the particles. The particles had mean sizes between 0.23 - 5.2 μm that were controllable based on the length of debranching time and pullulanase concentration. The authors loaded the particles through soaking in drug solutions. Due to their positive charge, the microparticles adsorbed Evans blue (MW: 961 g/mol) and Brilliant blue (MW: 749 g/mol), which are both negatively charged, to high loading capacities of 223 mg/g and 206 mg/g, respectively. An *in vitro* release test into SGF followed by SIF demonstrated selective release into SIF only.

2.3 Characterization of starch-based microparticles

2.3.1 Size and size distribution

An important variable for any particle-based controlled DDS is particle size. The size differences between nanoparticles, microparticles, and macroscopic particles determine how the particles can be used. For example, particles which are intended for intravenous injection need to be between 10-100 nm in diameter (J. Li & Mooney, 2016), excluding use of microparticles. Where microparticles lie on the 1-1000 μm range generally has little effect on how they can be used, but their size can affect rate of drug release (W. Chen et al., 2017; Dash et al., 2010). In addition, size distribution can play an important role in how uniformly release is controlled. A wide size distribution could mean a significant difference in how drug is released the largest particles to the smallest, depending on the release mechanism. Typically, diameter is reported for particle sizes. However, often only the ambiguous term “size” is used; we suggest authors clearly state what they are reporting to minimize any possible confusion.

Laser light scattering is a common method of determining sizes and size distributions of microparticles. While there are different specific techniques and configurations with how light scattering is used to determine particles sizes, the general method can determine sizes between tens of nanometers and up to a few millimeters. While typically particles are imaged while wet in water (Maaran et al., 2014), ethanol

(García-González et al., 2012), or isopropanol (Bordenave et al., 2014; Sasaki & Matsuki, 1998), dry imaging is also possible, depending on the method used. One limitation is that the method assumes homogeneity and sphericity of the particles (Dhital et al., 2010). Another limitation of light scattering is that it provides no information on the morphology of the particle. With some assumptions, it is possible to use light scattering results to calculate the specific surface area of the particles (Maaran et al., 2014).

Coulter counters, capable of determining diameters a little beyond the micron range, may also be used to determine sizes of starch-based particles. The device takes advantage of the Coulter principle: when a particle in an electrolytic solution passes through orifice, concurrent with an electric current across the orifice, the impedance changes proportionally to the volume of the particle. The orifice must be correctly sized depending on the size range of the particles. The method is limited to particles in solution that have low conductivity. Indeed, Tester and Morrison (1990) discovered that with moderate swelling of starch granules, a Coulter counter was not able to correctly determine swelling extent, due to the granules becoming conductive. This method also has the advantage of being able to count the number of particles in solution.

Scanning electron microscopy, while typically used to observe morphology, can also be used to determine particle dimensions. This method is somewhat laborious, as the images must first be taken and then analyzed manually, or with software to determine dimensions (Farrag, Sabando, et al., 2018; Lecorre et al., 2012; Rehan et al., 2019). Similarly, confocal laser scanning microscopy (M Schirmer et al., 2013), optical microscopy (Lemieux et al., 2015), and helium ion microscopy (Wulff, Aucoin, et al., 2020) can be used in the same way.

2.3.2 Swelling

When drug release is controlled by swelling extent, characterizing this extent is important. Swelling ratio (Kowalski & Ptaszek, 2016), hydration capacity (Kim & Huber, 2013), and swelling power (Bordenave et al., 2014) are all simple methods that use the weight ratio of the wet swelled particles to the dry particles.

Unfortunately, there is not a standard method, and some researchers have come up with their own definitions. We would suggest the use of swelling power as it both intuitive and the simplest. Similarly, swelling factor uses a volume ratio of particles, but if used as initially described by Tester and Morrison (1990), the particles must not be permeable to or adsorb blue dextran (2,000 kDa). One advantage of this method is that the interstitial volume between particles is not a factor in the result, unlike with the weight-based methods. Swelling kinetics can also be determined by measuring swelling extent as a function of time (Wulff, Chan, et al., 2020 [Chapter 4 in this thesis]). Often swelling analysis is done at various temperatures (Fundueanu et al., 2010) or in various media with different ion concentrations (Yuan Li et al., 2009) or pHs (de Oliveira Cardoso et al., 2020; Yuan Li et al., 2009).

While less quantitative, starch microparticles have also been observed with optical microscopy during swelling to visually observe how they change (Wojtasz et al., 2016).

2.3.3 Shape, morphology, and internal structure

Scanning electron microscopy (SEM) is typically the method used for determining particle shape and morphology for starch-based particles. It is quick and creates high-resolution images. Since starch is a poor conductor, typically starch is sputter coated with gold between 10-50 nm in thickness (He et al., 2016; Nayak et al., 2018; Phromsopha & Baimark, 2014), however platinum (Desam et al., 2018) or iridium (Farrag, Sabando, et al., 2018) have also been used. SEM can resolve features of starch down to high tens of nanometers. Helium ion microscopy (HIM), a relatively new method that instead uses a scanning helium ion bean, has also been used to observe starch granule features down to low tens of nanometers (Wulff, Aucoin, et al., 2020) and could be useful for characterization of starch-based microparticles. With either method, particles are often sectioned or cracked open to observe their interior. A limitation of these methods is that the particles need to be dry. Transmission electron microscopy (TEM), while less commonly used compared to SEM, has also been used to image starch microparticles (Östh et al., 2003; Xu et al., 2018).

Confocal laser scanning microscopy (CLSM) is a particularly useful technique for observing the interior of microparticles intended for use in drug delivery. Particles can be loaded with fluorescent probes in the same way that drugs would be loaded and then imaged with CLSM. Due to the nature of CLSM, it is possible to see exactly where the probes are within the microparticle at a specific Z-plane. By combining a Z-stack of XY-plane images, a 3D image of the probes within the particle can be created. Any fluorescence molecule may be used, and fluorescein-based probes (e.g. FITC, FITC-dextran or FITC-BSA) are most commonly used (Bie et al., 2016; J. Chen et al., 2018; Östh et al., 2003), but starch microparticles have also been imaged using β-carotene (Shanshan Wang, Chen, Liang, et al., 2015), Nile Red and Blue (Yusoff & Murray, 2011), RITC-dextran (Wulff, Chan, et al., 2020) and Coumarin 6 (Sun et al., 2018; Xu et al., 2018). CLSM is capable of resolving features in the low hundreds of nanometers.

2.3.4 Thermal analysis

Thermal analysis techniques can provide insight into the molecular arrangement within the starch-based microparticles. Differential scanning calorimetry measures the amount of heat required to increase the temperature of samples and gives an indication of the degree of crystallinity, and the nature of that crystallinity. While native starch shows very distinct endothermic peaks from the melting of crystallites (Jenkins & Donald, 1998; Shujun Wang et al., 2016), generally starch-based microparticles are quite amorphous and show a less clear peak or no peak at all (Kittipongpatana, 2013; Lemieux et al., 2015). The method can also provide insight into the interaction between the microparticle and loaded drug (de Oliveira Cardoso et al., 2020) or into the stability of the loaded drug (Okunlola et al., 2017). Thermal gravimetric analysis (TGA) has also been used to characterize starch-based microparticles intended for drug delivery, providing insight into their thermal stability (Farrag, Ide, et al., 2018; Peng et al., 2011). The relevance of TGA data for particles intended for drug delivery is minimal, however.

2.3.5 Spectroscopy

Spectroscopy, while not frequently used in this particular area of research, can be a useful tool for evaluating the presence or absence of chemical groups in starch-based microparticles. X-ray diffraction (XRD) has been used to confirm drug loading (Nayak et al., 2018), absence of cross-linking agent (B. Li et al., 2009), and structural properties of microparticles (Farrag, Sabando, et al., 2018). Similarly, Fourier transform infrared spectroscopy (FTIR) can be used to study the interaction between loaded drug and microparticle (Desai, 2007; Hoyos-Leyva et al., 2018; Nayak et al., 2018; Panyoyai et al., 2017) or to evaluate modifications to the particles (B. Li et al., 2009; Momeni & Mohammadi, 2009; Okunlola et al., 2017; Bao Zhang, Wei, et al., 2015). Nuclear magnetic resonance (NMR), while rarely used to evaluate starch-based microparticles themselves, can be used to assess modifications to polymers used to create the microparticles.

Table 2.1: Summary of work in literature on starch-based microparticles for drug delivery

Particle type/name	Particle fabrication method	Starch polymer used	Other polymer used	Particle size	Drug loaded	Drug solubility	Drug encapsulation method	Drug loading during or after particle formation	Drug loading capacity	Drug encapsulation efficiency	Drug release test method	50% drug release time	90% drug release time	Specific intended application	in vivo studies done?	Key findings	References
CMS microspheres	W/O emulsion with cross-linking	Carboxymethyl starch	None	~90	Furosemide	Water soluble at neutral and high pHs	Emulsification and cross-linking	During	50 mg/g	50%	Into HBSS at pH 1 and 7.4	pH 1: 5-25 min. pH 7.4: <2 min	pH 1: 15-60 min. pH 7.4: ~2 min	Gastroretentive delivery	Not done	High swelling at pH 7.4 leads to rapid release of drug.	(Lemieux et al., 2015)
Starch microspheres	Cross-linking of native starch with subsequent enzyme treatment	Native corn starch	None	~10	Tranexamic acid	Water soluble	Freeze drying	After	5-100 mg/g	100%	Not done	Not done	Not done	Rapid hemorrhage control	Blood clotting tested on ears and livers of rabbits	The drug-loaded particles where able to better induce blood clotting on wounds compared to particles without drug and on par with a comparable product available on the market (Arista®).	(Su et al., 2019)
Starch microparticles	Recrystallization of debranched short chain glucans and chitosan	Short chain glucans from waxy maize starch	Chitosan	0.2-5	Rhodamine, Brilliant Blue, Evans Blue	Water soluble	Soaking of particles in drug solutions	After - adsorption	Up to 223 mg/g	Up to 78%	Into SGF and SIF	SGF: not reached. SIF: ~5 hours	SGF: not reached. SIF: ~12 hours	Intestine-targeted release	Not done	Although the authors attempted to load both negatively and positively charged molecules, only the negatively charged molecules were successfully loaded, which they attributed to the loading mechanism primarily being electrostatic interaction with the positively charged chitosan.	(Luo et al., 2019)
Microgel particles	Large scale cross-linking and subsequent grinding/sieving	Carboxymethyl starch	beta-cyclodextrin	10-25	Ascorbic acid	Water soluble	Soaking of particles in ascorbic acid solution	After - adsorption	Up to 1.9 g/g	Up to 69.5%	Into SGF and SIF	SGF: not reached. SIF: ~20min	SGF: not reached. SIF: ~60 min	Intestine-targeted release	Not done	Higher amounts of beta-cyclodextrin allowed for higher loading and higher encapsulation efficiency of ascorbic acid.	(Bao Zhang, Li, et al., 2015)
Oxidized starch microgel	Large scale cross-linking and subsequent grinding/sieving	TEMPO oxidized potato starch	None	10-50	Anthocyanins	Water soluble	Soaking of particles in anthocyanin solution	After - adsorption	Up to 62 mg/g	Not provided	Into SGF and SIF	SGF: not reached. SIF: <15min	SGF: not reached. SIF: <15min	Intestine-targeted release	Not done	Loading capacity was dependent on the degree of oxidation of starch, particle cross-linking extent, and ionic strength and pH of anthocyanin solution.	(Z. Wang et al., 2013)
Cross-linked anionic microspheres	W/O emulsion with cross-linking	"water soluble starch"	None	~19	Methylene blue	Water soluble	Soaking of particles in methylene blue solution	After - adsorption	18-330 mg/g	7-84%	Into saline solution	~2 hours	~15 hours	Not stated	Not done	Drug loading was higher with longer soaking times and higher drug concentrations and was maximal at room temperature and with a NaCl solution.	(Fang et al., 2008)
Starch-based microgel-lysozyme complexes	Large scale cross-linking, grinding/sieving, and adsorption of additional polymer	Carboxymethyl starch	Chitosan	~20	Lysozyme	Water soluble	Soaking of particles in lysozyme solution	After - adsorption	Up to 6.6 g/g	Not provided	Into SGF and SIF	SGF: not reached. SIF: ~45min	SGF: not reached. SIF: ~2.5 hours	Intestine-targeted release	Not done	Loading capacity was dependent on the degree of substitution of starch and ionic strength and pH of lysozyme solution. Coating the microgel particles with through electrostatic interactions with CMS and chitosan slowed the release of lysozyme.	(Bao Zhang et al., 2014, 2017; Bao Zhang, Wei, et al., 2015)
Oxidized starch microgel	Large scale cross-linking and subsequent grinding/sieving	TEMPO oxidized potato starch	None	10-20	Lysozyme	Water soluble	Soaking of particles in lysozyme solution	After - adsorption	Up to 5 g/g	Not provided	Into citric acid-PBS	~30 min	~2 hours	Not stated	Not done	Loading capacity was dependent on the degree of oxidation of starch, particle cross-linking extent, and ionic strength and pH of lysozyme solution, and release was highly dependent on ionic strength and pH of release solution.	(Yuan Li et al., 2009; Yuan Li, Kadam, et al., 2012; L. Zhao et al., 2015)
Oxidized starch microgel	W/O emulsion with cross-linking	TEMPO oxidized potato starch	None	10-20	Lysozyme	Water soluble	Soaking of particles in lysozyme solution	After - adsorption	3 g/g	Not provided	Not done	-	-	Not stated	Not done	Higher loading with lysozyme occurred at low pH and low ionic strength	(Yuan Li, Kleijn, et al., 2011; Yuan Li, Norde, et al., 2012; Yuan Li, Zhang, et al., 2011)
Carboxymethyl starch/chitosan microspheres	Polyelectrolyte complexation	Carboxymethyl starch	Chitosan	1230	Bovine serum albumin	Water soluble	Physical entrapment through polyelectrolyte complexation	During	~100 mg/g	~67%	Into SGF and SIF	SGF: ~6 hours. SIF: ~20 hours	SGF: ~48 hours. SIF: ~60 hours	Intestine-targeted release	Not done	Release into SIF was slightly slower than release into SGF, but the total amount released was nearly the same.	(Quadrado & Fajardo, 2020)

Starch spherical aggregates	Spray drying	Taro starch granules	None	20.8	Ascorbic acid	Water soluble	Spray drying	During	99 mg/g	99%	Not done	-	-	Improved drug stability	Not done	Particles were able to protect against ascorbic degradation at high temperature and humidity.	(Hoyos-Leyva et al., 2018)
Carboxymethyl starch/alginate microspheres	Ionotropic gelation	Carboxymethyl starch	Alginate	~600-800	Diamine oxidase	Water soluble	Physical entrapment through ionotropic gelation	During	Not provided	82-95%	Not done	-	-	Intestine-targeted release	Not done	Encapsulation of the enzyme maintained high activity compared to non-encapsulated enzyme in SIF after 24 hours.	(L. Zhao et al., 2015)
Film-coated microparticles	Spray coating of drug-containing cores	Concanavalin A-conjugated resistant starch acetate	None	~500	Insulin	Water soluble	Spray coating of drug	During	~1%	Not provided	Not done	-	-	Colon-targeted release	With type II diabetic rats	The insulin-loaded particles were able to reduce plasma glucose concentrations in diabetic rats at an oral dose of 50 IU/kg, similar to the response when insulin was injected subcutaneously at a dose of 35 IU/kg.	(Situ et al., 2015)
Hydroxyethyl starch-based hydrogel microspheres	W/W emulsion with cross-linking	Hydroxyethyl starch (grafted with MA or PEG-MA)	None	~8-40	FITC-dextran and FITC-IgG	Water soluble	Emulsification	During	Up to 14.5 mg/g	Up to 99%	Into phosphate buffer and into PBS with alpha-amylase	~20 days	~100 days	Not stated	Not done	The release rate was tunable based on which polymers were grafted onto hydroxyethyl starch.	(Wöhl-Bruhn et al., 2012)
Starch microspheres	W/W emulsion and subsequent freeze drying	Mechanically treated and acid hydrolyzed waxy maize starch	None	~100	Insulin and BSA	Water soluble	Emulsification and freeze drying	During	Insulin: Up to 21.2 mg/g. BSA: Up to 51.3 mg/g	Insulin: Up to 49%. BSA: Up to 126%	Into PBS with amylase	~10 min	~30 min	Sustained release - oral	Not done	BSA was more easily loaded into the particles. Recrystallization was a factor in particle formation. Protein release in the presence of amylase was faster.	(Elfstrand et al., 2009)
Polysaccharide-based microparticles	W/O emulsion with solvent diffusion	Potato starch	None	32	Blue dextran	Water soluble	Emulsification	During	89.5 mg/g	89.5%	Not done	-	-	Not stated	Not done	When the same production was used to create particles from starch, chitosan, and alginate, the main effect was different particle sizes which the authors attribute to differences in viscosities.	(Baimark & Srisuwan, 2013)
Porous starch microsphere foam	W/O emulsion with solvent exchange	"Soluble starch"	None	20-100	Lovastatin	Poorly water soluble	Vacuum drying	After	140-390 mg/g	39-68%	Into water at 37˚C with pH 7	~5 min	~30 min	Oral dissolution enhancement	With beagle dogs	Unlike most other research where particles are utilized to slow release of drug, this work demonstrated the ability of microparticles to accelerate release of poorly soluble Lovastatin.	(Jiang et al., 2014)
Starch-based microspheres	W/O emulsion with cross-linking	Vinyl-grafted cassava starch	None	400-500	Curcumin	Poorly water soluble	Soaking of particles in curcumin solution	After	82 mg/g	82%	Into SGF and SIF	SGF: ~36 hours. SIF: not reached	SGF: ~96 hours. SIF: not reached	Sustained release - oral	Not done	High toxicity against tumor cell lines compared to control was observed.	(Pereira et al., 2013)
Microspheres	O/W emulsion with solvent evaporation	Acetylated starch	None	30-350	Repaglinide	Poorly water soluble	Emulsification	During	Not provided	75-93%	Into PBS	~5 hours	~10 hours	Sustained release - oral	Not done	Higher porosity lead to faster drug release. They report that the release mechanism was a combination of erosion and diffusion.	(Okunlola et al., 2017)
Mucoadhesive microparticles	O/W/O emulsion with solvent evaporation	Rice starch	None	210-367	5-fluorouracil	Poorly water soluble	Emulsification	During	Not provided	90-93%	Into goat caecal content	~7 hours	~18 hours	Colon-targeted release	With rats	In vivo studies indicated selective release into the colon with minor release occurring in the stomach and small intestine.	(Ahmad, Akhter, Anwar, et al., 2012)
Starch-poly-epsilon-caprolactone microparticles	O/W emulsion with solvent diffusion	Corn starch	Poly-epsilon-caprolactone	100-150	Bone morphogenic protein 2 (BMP2) and dexamethasone	Poorly water soluble	Emulsification	During	Not provided	25% for BMP2	Into PBS	~12 hours	~5 days	Sustained release - injectable	Not done	The use of SPCL allow for encapsulation and release of osteogenic hydrophobic drugs with a minor effect on cell viability of unloaded microparticles.	(Balmayor, Feichtinger, et al., 2009)
Starch-poly-epsilon-caprolactone microparticles	O/W emulsion with solvent evaporation	Corn starch	Poly-epsilon-caprolactone	6-914	Dexamethasone	Poorly water soluble	Emulsification	During	Not provided	75-94%	Into PBS	~30 hours	~23 days	Sustained release - tissue engineering	Not done	Polymer concentration and stirring rates had significant effects on particle sizes and morphologies.	(Balmayor, Tuzlakoglu, et al., 2009)
Starch-based aerogel microspheres	W/O emulsion and starch retrogradation	Corn starch	None	212-1226	Ketoprofen	Not water soluble	Supercritical CO2 absorption	After	1.1 mg/m^2	0.16	Not done	-	-	Not stated	Not done	Faster stirring speeds and the use of a surfactant led to smaller particles sizes.	(García-González et al., 2012)
Oxidized starch microparticles	W/O emulsion with cross-linking	TEMPO oxidized potato starch	Lysozyme	1-2	Quercetin	Not water soluble	Absorption into porous microparticles	After - electrostatic absorption	~1400 mg/g	Not provided	Into SGF and SIF	SGF: not reached. SIF: ~30 min	SGF: not reached. SIF: ~3.5 hours	Intestine-targeted release	With rats	Loading takes advantage of the charge difference between lysozyme and oxidized starch. Release is highly medium dependent allowing for majority of release into SIF. Higher cross-linking leads to lower drug loading. Drug loaded into	(D. Li et al., 2020)

																particles showed higher retention in GI tract vs. control.	
Oxidized starch microgels	Large scale cross-linking and subsequent grinding/sieving	TEMPO oxidized potato starch	None	~20	beta-carotene	Not water soluble	Absorption into porous microparticles	After - electrostatic absorption	4 - 18 mg/g	Not provided	Into SGF and SIF	SGF: not reached. SIF: ~20min	SGF: not reached. SIF: ~60min	Intestine-targeted release	Not done	The degree of oxidation, the ratio of cross-linker to starch, the ionic strength, and the pH all affected loading capacity of the particles. Low release in SGF and high release in SIF was achieved.	(Shanshan Wang, Chen, Shi, et al., 2015)
Microcapsules	O/W emulsion with spray drying	OSA starch	None	15	Tocopheryl acetate	Not water soluble	Spray drying	During	Not provided	90%	Into ethanol	~10 seconds	~60 seconds	Not stated	Not done	Total drug release was higher at higher temperatures	(Panyoyai et al., 2017)
Spray dried microcapsules	O/W emulsion with spray drying	OSA starch	Xanthan gum	5-6	Conjugated linoleic acid	Not water soluble	Spray drying	During	17-19 mg/g	85-96%	Into SGF and SIF	SGF: not reached. SIF: ~10 min	SGF: not reached. SIF: ~60 min	Intestine-targeted release	Not done	Adding xanthan gum to the particles improved protection against oxidation but also reduced the total amount of CLA released.	(He et al., 2016)
Oxidized starch microspheres	O/W/O emulsion with cross-linking	TEMPO oxidized potato starch	None	5-100	beta-carotene	Not water soluble	Emulsification and cross-linking	During	2.3 mg/g	Not provided	Into SGF and SIF	SGF: not reached. SIF: ~15min	SGF: not reached. SIF: ~45min	Intestine-targeted release	Not done	Particles demonstrated rapid release in SIF with only minimal release in SGF. Stability of beta-carotene was improved through encapsulation in particles.	(Shanshan Wang, Chen, Liang, et al., 2015)
OSA-starch microparticles	O/W emulsion with spray drying	OSA starch	Soy protein isolate	0.8-16.4	beta-carotene	Not water soluble	Emulsification	During	Not provided	21-39%	Not done	-	-	Improved drug stability	Not done	Blended particles with both soy protein isolate and starch provided higher encapsulation efficiency but lower redispersion compared to particles with only starch.	(Deng et al., 2014)
Irinotecan hydrochloride loaded microspheres	O/W/O emulsion with solvent evaporation	Rice starch	None	25-33	Irinotecan hydrochloride	Moderately water soluble	Emulsification	During	Up to 932.3 mg/g	92-97%	Into diluted rat caecal content	~6 hours	~16 hours	Colon-targeted release	With rats	In vivo studies indicated selective release into the colon with minor release occurring in the stomach and small intestine.	(Ahmad et al., 2013)
Starch-based bioactive microspheres	O/W/O emulsion with solvent evaporation	Rice starch	None	111-485	Metronidazole	Moderately water soluble	Emulsification	During	Up to ~778 mg/g	76-91%	Into goat caecal content	~4 hours	~20 hours	Colon-targeted release	With rats	In vivo studies indicated selective release into the colon with minor release occurring in the stomach and small intestine.	(Ahmad, Akhter, Ahmad, et al., 2012)
Starch film-coated microparticles	Spray coating of drug-containing cores	Debranched high amylose corn starch	Microcrystalline cellulose	Not provided	5-ASA	Low water solubility	Spray coating	During	~16%	Not provided	Into SGF and SIF	~1 hour	~4 hours	Colon-targeted release	With mice	A thicker outer coating layer lead to less drug release. In vivo results showed colon targeting capability.	(J. Chen et al., 2018)
Starch film-coated microparticles	Spray coating of drug-containing cores	Debranched high amylose starch	Microcrystalline cellulose	~600	5-ASA and insulin	Low water solubility	Spray coating	During	800 mg/g	N/A	Into SGF for 2h, SIF for 6h, and SCF for 8h	~16 hours	Not reached	Colon-targeted release	With type II diabetic rats	Higher resistant starch content, higher coating thickness, and longer heat treatment time all slowed the release of 5-ASA from the particles (data only provided for 5-ASA)	(Situ et al., 2014)

2.4 Drug loading

Drug loading is clearly a key step in creating a drug delivery system. Two important classifiers in drug loading are (a) whether the loaded drugs are hydrophobic or hydrophilic and (b) whether drugs are loaded during or after the particles are formed. Typically, when drugs are loaded during particle formation, the drugs are held within the particles by physical entrapment, the result of the physical barrier created by outer layers of particle. When drugs are loaded after the particles have been created, typically the drugs must diffuse into the particles, with the primary mechanism being adsorption. It is also conceivable to use a hybrid method, whereby particles are loaded through adsorption but then an outer layer is added to the particles to "lock in" the adsorbed drugs. The method used to load the drugs depends on the method for producing the microparticles and on the type of drug being loaded. Due to its hydrophilic nature, starch is best suited for encapsulating hydrophilic drugs. Loading of hydrophobic drugs is possible as well, but often requires modifications to the starch.

Drug loading capability depends on the nature of the microparticles, how the microparticles are formed, at what point the drugs are loaded into the particles, and the nature of the drugs (e.g. size, charge, hydrophilicity, and functional groups). Both small molecule drugs and large molecule drugs (typically proteins) can be encapsulated with starch-based microparticles. Loading is typically characterised through evaluating the drug encapsulation efficiency (EE) and the drug loading capacity (LC), also known as drug retention. While some authors take liberties with how these terms are defined, EE is typically defined as EE = (drug loaded into and/or onto the particles)/(total drug used for the loading process), and LC is typically defined as LC = (drug loaded into and/or onto the particles)/(total weight of the unloaded microparticles).

2.4.1 Loading of hydrophilic drugs

When drugs are loaded through soaking microparticles in a solution with the drug, the method is a somewhat agnostic formation method. The loading capacity primarily depends on how much of the particle's polymer mesh is accessible to the drugs, and on the net strength of the intermolecular forces between the drug and the polymer mesh are. The surface area accessible to the drugs depends on the porosity and pore size of the mesh, in addition to the diffusibility of the drug. Typically adsorption equilibrium is reached within a few hours (El Mouzdahir et al., 2007; Yuan Li, Kadam, et al., 2012; Yuhua Li et al., 2019), as long as adsorption is not significantly hindered by diffusion.

Adsorption can be used to load microparticles with hydrophilic drugs to a high loading capacity. While there are numerous theories that describe adsorption behaviour, the primary factors that affect capacity loading of a specific drug are the equilibrium concentration of the drug and the accessible mesh surface. Typically, adsorption capacity is measured in units of mass of drug loaded to mass of microparticle.

Yuan Li et al. (2009) and Zhao et al. (2015) have completed some foundational work in evaluating the adsorption capability of starch-based microparticles, particularly with hydrophilic molecules. Both sets of work used two different methods to create the microparticles; however, the result of both are cross-linked (either with STMP or GDGE) microparticles made from oxidized starch, which the authors claim to have the same physicochemical properties. Lysozyme (MW: 14.3 kDa) was loaded into the particles through adsorption, which was able to be loaded to a capacity of 5 g/g (L. Zhao et al., 2015). Loading, as measured through adsorption capacity, was dependent on the degree of oxidation of the starch, the pH of the loading solution, salt concentration, and cross-linking extent (Yuan Li et al., 2009; L. Zhao et al., 2015). The use of oxidized starch to create the particles conferred a highly negative charge to the particles that allowed for high loading of the positively charged lysozyme. In other research, Li et al. (2012) created their particles

loaded with lysozyme, but then they used polyelectrolyte complexation to create a shell on the outside of the particles with poly-lysine and poly-glutamic acid. This shell added an additional barrier between the encapsulated lysozyme and the external environment that slowed release of the lysozyme. Z. Wang et al. (2013) created particles with the same method and loaded them with anthocyanins (MW: 271- 331 g/mol), which are positively charged, to a maximum capacity of 62 mg/g. This comparison indicates that proteins are capable of higher loading than small molecule drugs.

Zhang et al. (2014; 2015) created starch-based microparticles made from carboxymethyl starch (CMS) that were intended for delivery of hydrophilic drugs. Particles were created with only CMS, and also with both CMS and cyclodextrin. Both lysozyme and ascorbic acid were loaded with lysozyme to a maximum loading capacity of about 6 g/g (2014). This loading was about 3x higher than that of ascorbic acid which had a maximum loading capacity of 1.9 g/g (2015). The group found that higher amounts of β-cyclodextrin led to higher loading capacity of ascorbic acid (2015).

Small molecule dyes are commonly used to assess the adsorption properties of starch-based microparticles. Methylene blue has been loaded into microparticles made from a W/O emulsion and STMP cross-linking process; loading capacity was affected by loading temperature, loading time, loading concentration, and dissolution medium, with a maximum loading of 327.3 mg/g (Fang et al., 2008). Microparticles made from debranched starch and chitosan were successfully loaded with Evans blue and Brilliant blue (Luo et al., 2019). Although both these dyes have negative charges, the particles had a positive zeta potential due to the addition of chitosan, which allowed for loading of up to about 200 mg/g. The same microparticles failed to encapsulate two positively charged molecules with low molecular weight (Luo et al., 2019).

It is also possible to load microparticles with hydrophilic drugs in a method similar to adsorption through freeze drying or spray drying. While the drugs are not adsorbed in the strict sense, such loading more closely

resembles adsorption than physical entrapment by the particles. This method also allows for higher loading than would be possible with only adsorption, but most of the drug will be released nearly instantly. Tranexamic acid was loaded into starch microparticles through a combination of adsorption and freeze drying up to a loading capacity of 100 mg/g. However, the authors did not characterize how much was actually adsorbed prior to the lyophilization step. Spray drying was used to load ascorbic acid into microparticles made from aggregated taro starch granules with a loading capacity of 20.9 mg/g (Hoyos-Leyva et al., 2018). Similar work was also previously conducted using fully gelatinized starch to encapsulate ascorbic acid with spray drying which had a maximum loading capacity of up to 98 mg/g (Palma-Rodriguez et al., 2013).

Other non-adsorption-based methods that rely on physical entrapment are often used for encapsulation of hydrophilic drugs. Ionic gelation has been used to form particles by dripping carboxymethyl starch and alginate, which are both negatively charged, along with diamine oxidase into a solution with Ca^{2+}, which acted as the counter ion (Blemur et al., 2016). Polyelectrolyte complexation was used by Quadrado and Fajardo (2020) to encapsulate BSA as a model protein to about 100 mg/g with carboxymethyl starch (CMS) and chitosan as counter polyelectrolytes.

Comparison of loading capability between microparticle DDSs can be hard as there is little consistency between studies. We suggest that if a study is trying to provide proof of concept for a DDS, then at least one commonly-used model drug should be used, depending on the final application intent. BSA and lysozyme are already commonly used as model proteins, which is helpful, but establishing commonly-used model cationic, anionic, and neutral small molecule drugs and large non-protein drugs could be helpful for the field. Such overlap with model drugs can also assist reviewers, and authors themselves, with evaluating validity of the study results.

2.4.2 Loading of hydrophobic drugs

Starch-based microparticles can be loaded with hydrophobic drugs in a variety of ways. A common method is to modify the hydrophilic starch to introduce hydrophobic domains, allowing for encapsulation of hydrophobic molecules. Tocopheryl acetate (MW: 473 g/mol) was loaded into microparticles made from octenylsuccinyl-ated starch through spray drying (Panyoyai et al., 2017). The drug was loaded prior to spray drying through dissolution, along with starch and ethanol. Solvent diffusion or extraction using an O/W emulsion is also a convenient way to load hydrophobic drugs and has been used to load repaglinide (MW: 453 g/mol) and dexamethasone (MW: 392 g/mol). Repaglinide was loaded into acetylated starch microparticles by dispersing a solution containing the drug, starch, and chloroform into water (Okunlola et al., 2017). Similarly, dexamethasone was loaded into microparticles made from a blend of starch and polycaprolactone by adding the drug with the starch mixture in methylene chloride into a water-soluble polymer solution (Balmayor, Tuzlakoglu, et al., 2009). The methylene chloride is extracted out of the particles in the O/W emulsion with vacuum drying, leaving the drug-loaded microparticles. Microparticles made with a W/O emulsion can also be used to encapsulate hydrophobic drugs and has been used to encapsulate furosemide (MW: 331 g/mol) with carboxymethyl starch-based microparticles (Lemieux et al., 2015) and to encapsulate curcumin (MW: 368 g/mol) with vinyl-functionalized starch microparticles (Pereira et al., 2013). These methods are made possible by modifying the solubility of the drug during loading. Extrusion spheronization has been used to encapsulate mesalazine (aka 5-aminoslicylic acid) (MW: 153 g/mol) by creating a core made from the drug and then coating the outside with modified (debranched and retrograded) starch (J. Chen et al., 2018; Situ et al., 2014).

Microporous materials can be particularly advantageous for delivery of crystalline drugs that have low water solubility. By restricting the drug's ability to form large crystals within the microparticle, surface

area can be maximized, and dissolution can occur faster, thus increasing the bioavailability. Lovastatin (MW: 405 g/mol) (Jiang et al., 2014) and nitrendipine (MW: 360 g/mol) (Y. Zhao et al., 2015), both sparingly soluble in water, were loaded into starch microparticles by soaking the particles in organic solvents containing the solubilized drugs. Vacuum dying caused the drugs to precipitate onto and into the particles, but the starch prevented large crystals from forming. Both systems demonstrated higher subsequent dissolution rates of the drugs into aqueous solutions. Another way in which starch microparticles can encapsulate hydrophobic drugs is through use of a O/W/O emulsion. This was demonstrated by Wang et al. to encapsulate β-carotene with a LC of 2.3 mg/ mixed with corn oil within an outer shell made from cross-linked starch (Shanshan Wang, Chen, Liang, et al., 2015). Wang et al. (Shanshan Wang, Chen, Shi, et al., 2015) also encapsulated β-carotene with a slightly different variation using a whey protein isolate to stabilize the oil into a nanoemulsion that was then absorbed into cross-linked oxidized starch microparticles; the authors reported low release in simulated gastric fluid and high release in simulated intestinal fluid.

2.5 Drug release

Drug release from starch-based microparticles is the most important aspect of a DDS. For a starch-based system, release is dependent on the nature of the particles themselves, their environment, and the encapsulated drug. When release is tested *in vitro*, the testing method used is important for characterising release. Due to the size of microparticles, they are primarily used for either controlled release or sustained release. Since the field of research on starch microparticles for drug delivery is still relatively young – compared to conventional drug delivery – and small, most work has focused on *in vitro* testing. However, some *in vivo* studies with animal models have also been conducted.

Through testing the release *in vitro*, much can be learned about the nature of the particles. Typically, this is done by placing the particles into either (a) a solution of PBS (sometimes with enzymes), (b) into simulated gastric fluid (SGF, pH 1.2) and simulated intestinal fluid (SIF, pH 6.8), or (c) SGF, SIF, and simulated colonic fluid (SCF, pH ~7). Generally testing is done at 37˚C to mimic human body temperature. Since release testing into PBS is fairly simple, it makes it easier to isolate the release mechanism. However, its usefulness is limited since it is not similar to how the system would respond if taken orally. When release is tested, the data is often fit to a drug release model (e.g. zero order, first order, Higuchi, etc.) to evaluate the nature of the release. For example, Pereira et al. (2013) fit their release data to four different models and found that it was best fit with the Hixson-Crowell model, which indicated that the particles are eroding as drug is released.

In cases where the drug is loaded through adsorption after particle formation, release is typically governed by desorption. Release can also be done in various conditions to evaluate the effect of each. Bao Zhang et al. (2014) loaded their carboxymethyl starch microparticles with lysozyme through adsorption and found that release was highly dependent on release media pH and ionic strength. Greater release at higher pHs and higher ionic strength was observed, due to decreases in the binding affinity between lysozyme and the particles.

Sometimes the particles are separated from the release media with a dialysis membrane. One limitation to dialysis is the diffusion of drug through the dialysis membrane. When release is relatively quick, it is possible that this diffusion can affect the results, depending on the size of drug and the dialysis membrane molecular weight cut off (MWCO). If proper controls are done with the non-encapsulated drug, this effect can be controlled for. However, a number of published manuscripts lack such a control.

Often, when selective release into the small intestine is desired, drug release into SGF is first done, followed by release into SIF. The ideal result is no release into SGF, but quick release into SIF. Such a system was created by Luo et al. (2018), where their starch microparticles loaded with dyes demonstrated minimal release into SGF, but released ~50% of the encapsulated dyes when in SIF within ~5 hours.

The addition of amylase, which degrades starch, also increased the rate of drug release, as expected. The addition of α-amylase increased the rate of release of FD70 and FITC-IgG from HES-based microparticles (Wöhl-Bruhn et al., 2012) and of insulin and BSA from starch microparticles (Elfstrand et al., 2009).

One aspect that could be improved in the field of testing drug release is standardization of release testing methods to allow for comparison between studies. Consistency with release media, release times, and reporting of the results would help to advance the field. In addition, proper controls must be used to evaluate the effect of each variable; too often these are not done. When release studies are done into SGF followed by release into SIF, the effect of each by itself cannot be known over the total release time; we suggest that controls for release into each SGF and SIF be done.

When evaluating *in vitro* drug release over time, there are generally three ways to report the same data. The first is to report the cumulative amount of drug released in weight or moles. The second is to report the cumulative percentage release of encapsulated drug – often the final release percentage is less than 100%. The third is to report the cumulative percentage of the total releasable drug – this value should be 100% at the final time point. The second method is most commonly used. We suggest that the drug release be reported in all three ways for proper comparisons to be made. In some systems (e.g. a degradable system), it is expected that the encapsulated drug and total releasable drug is equivalent as time approaches infinity. It is also important that experiments are conducted for long enough to reach equilibrium. Another reporting method that would enable comparison between studies is to report the time it takes for 50% ($t_{50\%}$) (J. Li &

Mooney, 2016; Yuan Li, Zhang, et al., 2011; Okunlola et al., 2017) and/or 90% ($t_{90\%}$) (Lemieux et al., 2015; Lenaerts et al., 1991) of the total releasable drug to be released; releasable drug should be used (as opposed to unencapsulated drug) as it is more representative of how the microparticles would release the drug for in a medical application and allows for useful comparisons. It is also worth mentioning that if sustained release is desired, even if a particular drug/microparticle combination demonstrates burst release followed by sustained release, a possible solution could be to cause the burst release to occur in vitro before using the DDS for *in vivo* treatment.

2.6 Pharmaceutical applications

Since the field of starch-based microparticles for drug delivery is still a relatively new and small field, there appear to be no pharmaceutical products on the market currently. However, we briefly discuss some intended applications.

Colon-targeted and intestine-targeted delivery is the primary goal of most research, and most *in vivo* studies have had this application in mind. Particles must encapsulate drugs and then selectively release the drugs into either the small intestine or the colon. By creating particles which are pH and enzyme responsive, such selective release can be achieved, as previously described. Oral delivery of quercetin loaded microparticles allowed for selective delivery to the small intestine with in vivo testing on rats (D. Li et al., 2020). In a number of other studies, specific delivery of various drugs to the colon has been demonstrated (Ahmad et al., 2013; Ahmad, Akhter, Ahmad, et al., 2012; Ahmad, Akhter, Anwar, et al., 2012; J. Chen et al., 2018). Oral delivery of insulin-loaded starch-coated microparticles also reduced glucose plasma concentrations to a similar extent, compared with subcutaneous injection in rats (Situ et al., 2014, 2015), potentially paving the way for oral delivery methods for insulin.

2.7 Conclusion

Starch-based particle systems are a promising method for drug delivery. In addition to being widely available, starch has many properties that make it a great contender for use in drug delivery including biocompatibility, low toxicity, and high tunability. The methods for producing starch-based particles have been well researched and there are a wide variety of methods that may be used to create drug delivery systems. A combination of the synthesis methods is often used to create the best system possible for the delivery mechanism desired. Research on loading and release of drugs has been conducted with a number of starch-based microparticle systems and has demonstrated significant potential. This research has mostly focused on *in vitro* studies and leaves much work to be done on testing *in vivo* efficacy.

Chapter 3: Helium Ion Microscopy of Corn Starch

This chapter is modified from a published short communication as follows:

Wulff, David, Marc G. Aucoin, and Frank Gu. 2020. "Helium Ion Microscopy of Corn Starch." Starch - Stärke 1900267.

Other types of starch (potato, wheat, and Hylon VII starch) were imaged but not included in the manuscript and are provided in Appendix A.

3.1 Summary

Normal corn starch granules were imaged using a helium ion microscope (HIM). This relatively new imaging technique produced high-resolution images of both the interior and exterior of the granules that allowed features to be observed which had previously not been seen with SEM. Of particular interest is the mesh-like structure which was observed in the interior when starch granules were sectioned with a metal blade, a structure not currently part of existing models of starch architecture. HIM imaging provides a new way to characterize starch in the ongoing quest to elucidate its internal structure.

3.2 Introduction

Helium ion microscopy (HIM) is a relatively new characterization method that utilizes a gas field ionization source to create He^+ ions. The impact from the beam of He^+ ions that are scanned across the sample generates secondary electrons, which are then detected. HIM offers high source brightness, low energy spread, and small diffraction effects to produce high contrast, high depth-of-field images (Ward et al., 2006). These properties make the technique a useful tool for nanoscale research. Helium ion microscopy has been used for imaging nanoporous SiO_2 (Burch et al., 2018), cellulose nanofibrils (Ketola et al., 2019), mammalian cells (Sato et al., 2018), and other biological samples (Joens et al., 2013). To the best of our

knowledge, we report on the first time that HIM has been used to image starch. Despite much research into the structure of starch, unknowns still remain. In particular, the proposed blocklet structure (Gallant et al., 1997) still has not been clearly defined or characterized. Further, the molecular arrangement of amylopectin within starch granules is still an active area of research (Bertoft, 2017). Use of HIM for studying both internal and external starch structure can assist with answering these questions.

The present study achieved high-resolution HIM images of the interior and exterior of normal corn (maize) starch granules, allowing new features smaller than 10 nm to be resolved, previously unseen through the use of SEM imaging. We contrast our HIM images with similar SEM images. Interestingly, we did not observe any blocklet-like structures in either the interior or exterior of granules. It is also worth noting that in addition to our HIM images being very high-resolution, the SEM images which we produced for comparison are the highest-resolution SEM images of starch of which we are aware.

3.3 Materials and methods

3.3.1 Materials

Unmodified normal corn (maize) (S4126, Lot #: MKBT0621V) starch was purchased from Sigma-Aldrich (Oakville, Canada). The apparent amylose content of the starch was 27.8% as determined the method of Williams et al. (Williams et al., 1970). A moisture content of 14.3% was determined by calculating the difference in weight as a fraction of the initial weight after drying for 16 hours at 100˚C. The granules used for microscopy were not the same granules used in the amylose content or moisture test and were not modified other than for imaging preparation.

3.3.2 Imaging of starch

A thick mixture of starch in water was created by combining 250 mg of corn starch with 250 µL of water in a 1.5 mL centrifuge tube. The mixture was frozen by directly immersing the tube in liquid nitrogen. The frozen starch-and-water pellet was removed from the tube and mounted to a cold (-18˚C) metal disc using optimal cutting temperature (OCT) compound (VWR, Mississauga, Canada), which rapidly freezes to keep the sample in place. The pellet was then sectioned, while still frozen, in 10 µm increments using a cryomicrotome (Shandon Cryomicrotome SME, Thermo, Mississauga, Canada) with a metal triple-facet cryomicrotome blade (VWR, Mississauga, Canada). The part of the pellet that was sectioned was not in contact with the OCT fluid. The sectioned starch granules were placed in a new 1.5 mL microcentrifuge tube and washed with an excess of acetone (1 mL) to remove any water. After centrifuging the samples (1000 g for 1 min) and decanting the excess acetone, the samples were placed in a vacuum desiccator for 4 hours to remove the acetone. The dry samples were lightly sprinkled onto double-sided carbon tape attached to the specimen stubs. Gold sputtering was performed for 60 seconds for an approximate coating thickness of 5 nm. A (scanning) helium ion microscope (Orion Plus HIM, Carl Zeiss, North York, Canada) at a working distance of 6-7 mm, a dwell time of 0.2-1 µs, and a beam current of about 1 pA was used to collect the HIM images. A scanning electron microscope (SEM, Quanta FEG 250, FEI, USA) at 20-30 keV with a working distance of 9-10 mm was used to produce the SEM images.

3.4 Results and Discussion

To compare the imaging capability of HIM to that of SEM, we imaged granules using both microscopes. The native corn starch granules had been subject to the exact same preparation method for both types of imaging. However, due to the sectioning process, not all particles are sectioned, and, if a particle is

sectioned, there is variation in where across the particle it is sectioned. In addition, orientation of the particles varies, and the particles can only be imaged from the top. The images presented here are characteristic of the numerous images taken and showcase the three different perspectives: 1) the interior of particles which do not display an internal cavity, 2) the interior of particles which do display an internal cavity, and 3) the exterior of particles.

Figure 1 features sectioned granules that do not reveal an internal cavity. The granules might indeed have internal cavities; however, the observation of the cavity is dependent on both the sectioning and the location of the cavity. A comparison between Figs. 1A and 1C demonstrates the general difference between SEM and HIM images at relatively low magnification. The HIM imaging capability at high magnification is most clearly seen by comparing Figs. 1B and 1D, which are images of regions in Figs. 1A and 1C, respectively. In Fig. 1B, a mesh-like structure can be clearly seen. The mesh-like structure has "bundles" which are roughly 10-40 nm in thickness with pore sizes roughly 5-50 nm in size. Some of the pores seem to lead further into the granule which could play a role in starch porosity. Neither of the prominent models of starch structure, namely the "cluster model" and the "building block backbone model", which are based on characterization using AFM, NMR, SEM, WAXS, SAXS, SEC, and DSC, explicitly describe such a mesh-like structure. Small angle X-ray scattering (SAXS) shows a 9-10 nm repeat distance which has been suggested to be the result of repeating crystalline and amorphous lamellae, however there does not seem to be much similarity between the bundles seen in these HIM images and the repeating lamellae structures. Fig. 1D demonstrates that resolving features smaller than about 50 nm is difficult with SEM.

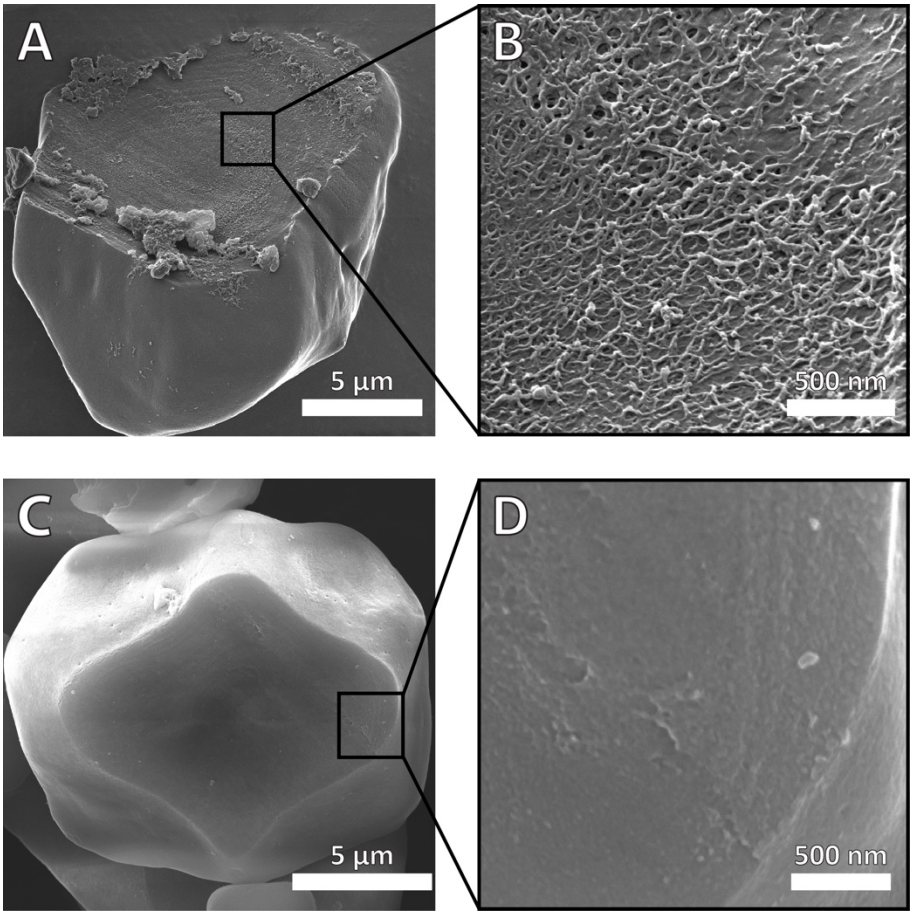

Figure 3.1: Comparison of HIM and SEM images of the interior of sectioned normal corn starch without an observable internal cavity. (A) An HIM image of the sectioned granule and (B) a high-magnification image of the area demarcated by the black square in (A). (C) An SEM image of a comparable sectioned granule and (D) a high-magnification image of the area demarcated by the black square in (C).

Figure 3.2 shows granules in which an internal cavity was observed. Most native granules have an internal cavity (see Chapter 4). The comparison between the HIM images (Figs. 3.2A and 3.2B) and SEM images (Figs. 3.2C and 3.2D) demonstrates the difference in imaging quality between the two microscopy methods. In both Fig. 2A and 2C, growth rings are observed. The better resolution that HIM provides is most clearly seen in Fig. 2B where a mesh-like structure may be observed. When compared to the SEM image at

equivalent magnification (Fig. 3.2D), a heterogenous surface is observed, but it is hard to determine what that heterogeneity represents.

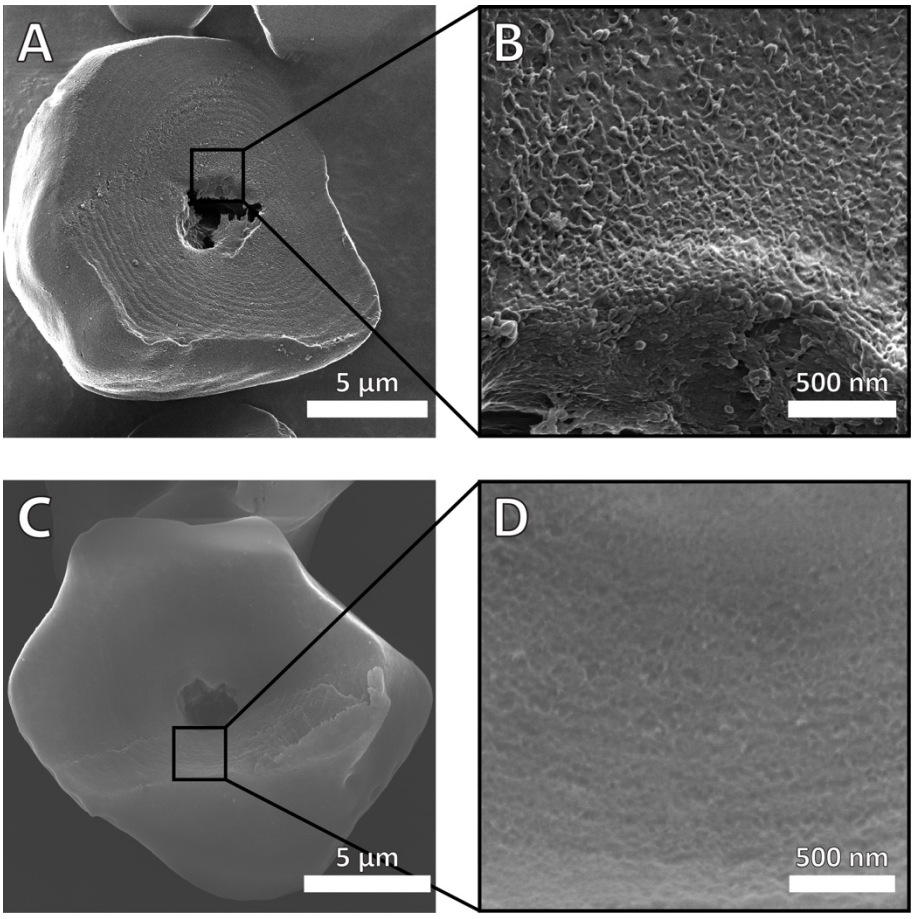

Figure 3.2: Comparison of HIM and SEM images of the interior of sectioned normal corn starch with an observable internal cavity. (A) An HIM image of the sectioned granule and (B) a high-magnification image of the area demarcated by the black square in (A). (C) An SEM image of a comparable sectioned granule and (D) a high-magnification image of the area demarcated by the black square in (C).

In addition to imaging the interior of granules, the exterior of native corn granules was also imaged (Fig. 3.3) which displays the surface morphology. The HIM images (Figs. 3.3A and 3.3B) provide a clearer

illustration of the morphology compared with the SEM images (Figs. 3.3C and 3.3D). The high-magnification images (Figs. 3.3B and 3.3D) both show surfaces with heterogenous roughness. The high-magnification HIM image (Fig. 3.3B) provides higher differentiation of the various ridge-and-valley features compared with the high-magnification SEM image (Fig. 3.3D). Unlike the images showing the interior of the granule (Figs. 3.1 and 3.2), the surface doesn't appear mesh-like. The ridges and valleys observed are roughly 20-80 nm across and seem to have depths on that same scale, with both having large variation in the shape. The height variation is comparable to that seen with AFM, with the authors attributing the unevenness to "blocklet" structures (L. Chen et al., 2019; Ohtani et al., 2000). It is also possible that the valley-like structures lead to pores that go further into the interior of the granule.

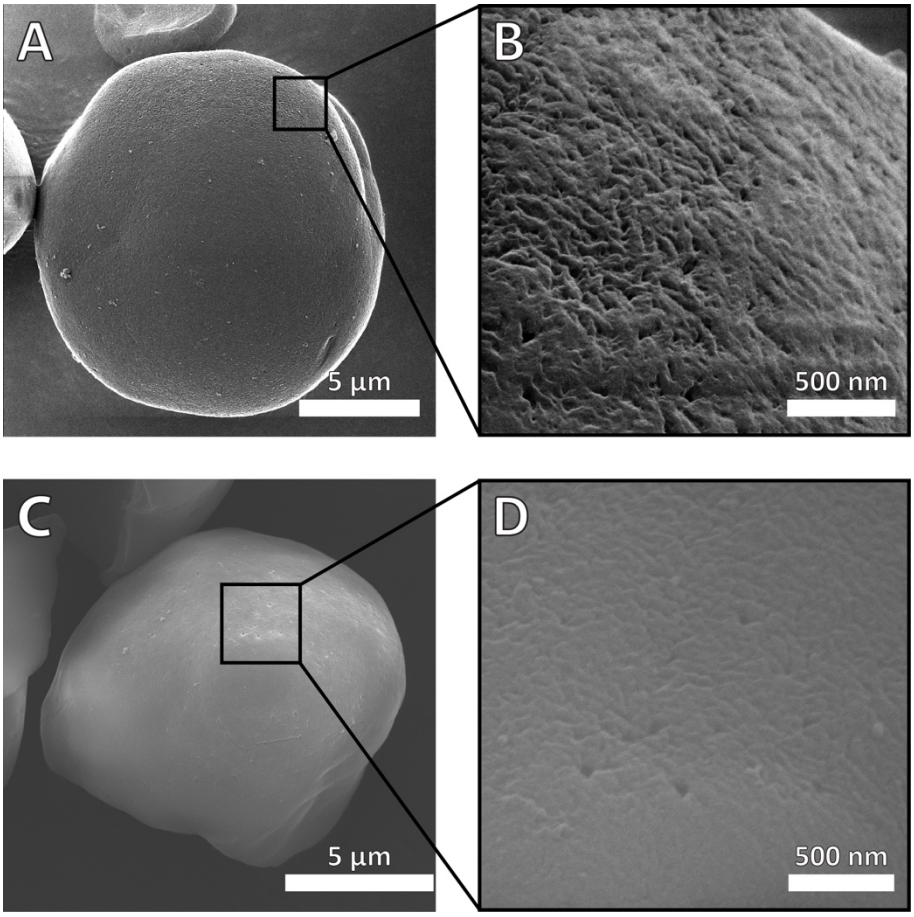

Figure 3.3: Comparison of HIM and SEM images of the exterior of normal corn starch. (A) An HIM image of the granule and (B) a high-magnification image of the area demarcated by the black square in (A). (C) An SEM image of a comparable granule and (D) a high-magnification image of the area demarcated by the black square in (C).

Interestingly, structures that should also be visible at these when resolving down to about 5 nm are so-called blocklets, which are supposed to have diameters in the range of 10-500 nm, depending on the starch type (Bertoft, 2017). After Gallant et al. (1997) reported evidence for these structures in 1997, they have been widely mentioned in literature, primarily with AFM evidence, in various starch types. There are, however, conflicting results in the literature on the properties of blocklets. In particular, there is no consensus on

blocklet sizes. Although different sizes of blocklets would be expected with different starch types due to considerable variation in granule size and other properties, we would at least expect similarity between the same starch types. Ridout et al. (2002) reported blocklets on the surface of corn starch granules on the order of 45-85 nm in size while Park et al. (2011) described small 20-30 nm blocklets within larger blocklet structures of 100-200 nm. Baker et al. (2001) have reported blocklets in the interior after sectioning corn starch in an embedding resin; they reported observing large 400-500 nm blocklets in native starch granules and smaller 10-30 nm blocklets in acid-treated starch granules. Tsukomoto et al. (2012) reported blocklets being approximately 30 nm in size (without any treatment). Although presumably all publications were referring to blocklet diameter, only Baker et al. specified that this was the case. Regardless, our HIM (and even SEM) results challenge the notion that blocklets are a part of starch structure. If these elusive blocklets are indeed a real sub-structure of starch, they have not been well defined, and evidence for their existence in the literature is relatively weak. Although the purpose of this research was not to investigate blocklets, further investigation into blocklets using HIM will be useful.

3.5 Conclusion

Helium ion microscopy is a new and exciting technique that has found uses in many applications, and now has been shown to be a valuable method for imaging starch. It is capable of resolving features smaller than 10 nm in size and has been able to reveal new levels of organization within normal corn starch that have not been observed before with SEM or AFM. In the interior of native corn starch, there appears to be a mesh-like structure which appears porous. On the exterior of native corn starch, clear ridge-and-valley morphology can be clearly seen. With further HIM imaging of starch, it should become possible to better understand its complicated structure.

Chapter 4: Characterizing internal cavity modulation of corn starch microcapsules

This chapter is a published research article as follows:

Wulff, David, Ariel Chan, Qiang Liu, Frank X. Gu, Marc G. Aucoin. "Characterizing internal cavity modulation of corn starch microcapsules." Heliyon, Volume 6, Issue 10, 2020, e05294.

4.1 Summary

Swelling of normal corn starch granules through heating in water leads to enlargement of the starch particles and a corresponding increase in internal cavity size. Through control of the swelling extent, it is possible to tune the size of the internal cavity for the starch microcapsules (SMCs). The swelling extent can be controlled through regulation of the swelling time and the swelling temperature. Since the swelling extent is correlated with particle size and solubility, these aspects may also be controlled. Imaging the SMCs at increasing levels of swelling extent using scanning electron microscopy (SEM) allowed for the internal cavity swelling process to be clearly observed. Brightfield and polarizing light microscopy validated the SEM observations. Confocal laser scanning microscopy provided further validation and indicated that it is possible to load the SMCs with large molecules through diffusion. The highly tunable SMCs are novel microparticles which could have applications in various industries.

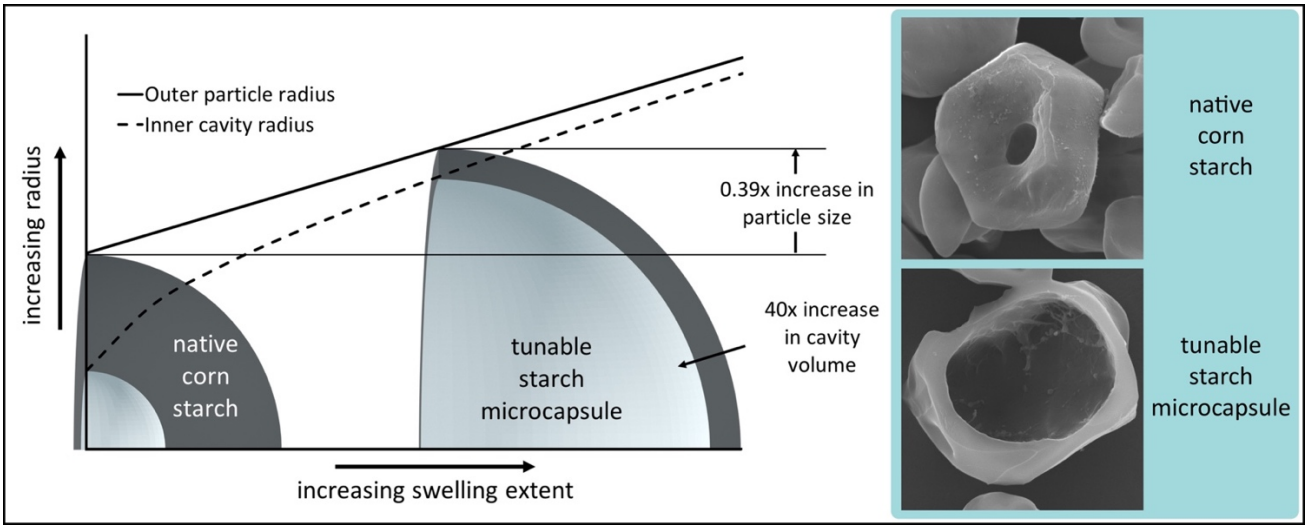

Figure 4.1: Graphical abstract for publication

4.2 Introduction

Starch is one of the most widely used biopolymers. In addition to its primary use as an energy source in food, starch has been used, typically with modifications, in the pharmaceutical, packaging, paper, plastic, cosmetic, and medical industries (Q. Liu, 2005). Despite extensive research over the past many decades, starch structure is still not fully understood (Bertoft, 2017; Zhu, 2018). Starch granules are particles with a size range of 2-100 μm and are the form in which starch molecules – amylose and amylopectin – are organized within plants in a semi-crystalline fashion (Vandeputte & Delcour, 2004). When starch granules are heated in the presence of excess water, they swell and, eventually, gelatinize, with enough time and heat. Gelatinization is the irreversible process by which starch granules transform from their ordered semi-crystalline state to a disorganized amorphous state (Ai & Jane, 2015) and is characterized by loss of granule birefringence and increased suspension viscosity (Markus Schirmer et al., 2015). Although gelatinization is typically done by heating starch granules, the same result can be achieved using high hydrostatic pressure

(Schneider Teixeira et al., 2018) and can be affected by pH and osmolarity (Simonin et al., 2011). Gelatinization occurs gradually, both within each granule, and with all of the granules collectively in the sample. Gelatinization is an important process for improving the usability of starch and is used in various industries (Builders & Arhewoh, 2016; Ratnayake & Jackson, 2007). Although most aspects of the gelatinization process are well characterized and understood (Ai & Jane, 2015; Markus Schirmer et al., 2015; Waigh et al., 2000), the changes to the internal macrostructure of starch through gelatinization have not been clearly elucidated.

It is well known that many types of starch have granules which can have an internal cavity or hole in their native state. These cavities have been reported in starch granules originating from rice (Baldwin et al., 1994; Sujka & Jamroz, 2013), wheat (Baldwin et al., 1994; Sujka & Jamroz, 2013), potato (Baldwin et al., 1994; Hall & Sayre, 1970; Sujka & Jamroz, 2013), sorghum (K C Huber & BeMiller, 2000), waxy corn (P. Chen et al., 2009, 2011), and normal corn (P. Chen et al., 2009, 2011; K C Huber & BeMiller, 2000; Sujka & Jamroz, 2013). Although it seems likely that these cavities observed in the native state are at least partly the result of drying (Baldwin et al., 1994), the exact origin remains a topic of discussion (K C Huber & BeMiller, 2000), and further work is needed. It is understood that the hilum region is an area of low organization (Błaszczak et al., 2005) and that gelatinization starts in the hilum region and proceeds radially to the periphery of the granule (Jay-lin Jane & Shen, 1993; M Schirmer et al., 2013; Singh et al., 2003b). It is likely that these two observations are related, and that gelatinization preferentially occurs in areas with less organized structure. As previously mentioned, the internal architecture changes that occur through the gelatinization process have been poorly characterized. Some research has observed an internal cavity in partially-gelatinized starch (Hall & Sayre, 1971; M Schirmer et al., 2013), but no research has studied the progression of that internal cavity at different stages of gelatinization. Little is known about what is

happening structurally inside a starch granule as it transitions from a highly organized semi-crystalline granule to a highly disorganized amorphous state through the gelatinization process. It is also worth noting that some research has characterized the remaining nonsoluble parts of fully-gelatinized starch granules, often referred to as "ghosts". These ghosts form when starch is gelatinized with little or no shear, producing structures which are hollow, highly swollen, fragile, and amylopectin-rich (Debet & Gidley, 2007; Gómez-Luría et al., 2017; Bin Zhang et al., 2014).

In this paper, we have studied the swelling process as a result of partial gelatinization and the resulting structural changes that occur. We use the term "partial gelatinization" to refer to starch granules which have been swelled but would not be considered fully gelatinized, and we refer to these particles as starch microcapsules (SMCs). The swelling extent (i.e. how swelled the particles are) is characterized through measurement of the swelling power. The internal structure of the corn starch was observed at various stages of swelling through characterization with scanning electron microscopy, brightfield microscopy, polarizing light microscopy, and confocal laser scanning microscopy. In addition to achieving our objective of characterizing the swelling process, we also determined that the SMCs which we created can be modulated in terms of both the swelling extent and the internal cavity size through a simple heating process. Both the swelling process and how the internal cavity changes as a result of the swelling were also mathematically modeled and fit to our experimental data.

4.3 Materials and methods

Normal corn (maize) starch was purchased from Sigma-Aldrich (S4126, Lot #: MKBT0621V) (Oakville, Canada). The apparent amylose content of the native starch was 27.8% as determined by the method of Williams et al. (1970). The moisture content was 14.3%, determined by the difference in weight as a fraction

of the initial weight after drying for 16 hours at 100˚C. FITC-dextran (MW 10,000) was purchased from Sigma-Aldrich.

4.3.1 Preparation of starch microcapsules (SMCs) through heating in water

The starch microcapsules (SMCs) were prepared through a simple heat-treatment process. Native normal corn starch (0.7 g, dry basis), as received from the supplier, was added with Milli-Q water (14 mL) in a centrifuge tube at a concentration of 5% w/w (native, dried starch basis). The term *native* indicates the granules are virgin or unmodified and the term *normal* distinguishes between other corn starch variants (e.g. waxy corn starch). To swell the starch, the centrifuge tube was placed in a water bath at the required heating temperature (55-85˚C) for the required time (5-240 min) with stirring of the water bath with a magnetic stirrer. The height of the water in water bath was carefully controlled to also cause gentle agitation of the centrifuge tube. After the starch was swelled, the starch mixture was cooled immediately to 20˚C by placing the centrifuge tube in a cold-water bath. Unless the particles were to be sectioned, the particles remained in solution for further use.

4.3.2 Starch swelling power

To measure the swelling power, the centrifuge tube containing the mixture of starch (native granules or SMC particles) and water were centrifuged at 1000 g for 15 minutes based on the method reported by Kim and Huber (2013). The weight of the sediment after decanting the supernatant was then measured. The swelling power was calculated using Eq. 1:

$$\text{swelling power} = \frac{\text{weight of sediment (g)}}{\text{dry basis weight of starch (g)}} \qquad (1)$$

4.3.3 Soluble starch fraction

We calculated the fraction of soluble starch using the standard approach for starch solubility analysis (Shujun Wang & Copeland, 2012) with an alternate method of calculation as noted below. The decanted supernatant (from the swelling power measurement step) was added to a pre-weighed glass vial and placed in an air oven at 105˚C until at a constant weight (~24 hours). The weight of the dried soluble starch was then measured, and the weight loss was used to calculate the amount of soluble starch in the supernatant. Since the volume of the supernatant is less than the volume of the water added initially – the result of interparticle and intraparticle water – the solubility was corrected by the ratio of these two volumes to account for this difference. This correction assumes that all water in the mixture has the same concentration of soluble starch, regardless of whether it is the supernatant or interparticle or intraparticle water. The solubility was calculated using Eq. 2:

$$\text{soluble starch fraction} = \frac{\text{weight of dried supernatent (g)} * \frac{\text{initial water volume (mL)}}{\text{supernatant volume (mL)}}}{\text{dry basis weight of starch (g)}} \qquad (2)$$

4.3.4 Starch granule size distribution

Starch particle sizes were measured using a laser particle sizer (Fritsch NanoTec Analysette 22, Fritsch GmbH, Idar-Oberstein, Germany) using static light scattering. The starch samples were suspended in water at a concentration of about 7% (w/w). The surface weighted mean diameter [D(3,2)] (i.e. Sauter diameter) was used as the representative diameter. The surface weighted mean is the equivalent diameter of a sphere which has the same volume/surface area ratio.

4.3.5 Sectioning of starch for internal particle imaging with SEM and HIM

After the SMC preparation process, the sediment was frozen through immersion in liquid nitrogen. The sample was then mounted to a cold (-18˚C) metal disc using optimal cutting temperature (OCT) compound (VWR, Mississauga, Canada), which rapidly freezes to keep the sample in place. The sample was then sectioned, while still frozen, in 10 µm increments using a cryomicrotome (Shandon Cryomicrotome SME, Thermo, Mississauga, Canada) with a metal triple-facet cryomicrotome blade (VWR, Mississauga, Canada). The samples were then placed back in a -20˚C freezer until further use. The part of the pellet that was sectioned was not in contact with the OCT fluid.

4.3.6 Scanning electron microscopy and helium ion microscopy imaging of starch

The starch samples (native and SMC) were prepared through either a) acetone washing and vacuum drying or b) freeze drying to remove residual water. The dried starch samples were sprinkled onto double-sided carbon tape attached to the specimen stubs. Gold sputtering was performed for 120 seconds for an approximate coating thickness of 10 nm for SEM imaging; 60 seconds was used for HIM imaging. A scanning electron microscope (SEM, Quanta FEG 250, FEI, USA) at 20-30 keV with a working distance of 9-10 mm was used to produce the SEM images. A (scanning) helium ion microscope (Orion Plus HIM, Carl Zeiss, North York, Canada) at a working distance of 6-7 mm, a dwell time of 0.2-1 µs, and a beam current of about 1 pA was used to collect the HIM images. Refer to Section 3.3.2 for more details on sample preparation for imaging.

4.3.7 Optical imaging of starch

The starch samples (native and SMC) were placed on a glass slide, a small drop of water was added, and a coverslip was placed on top. The slide was then imaged using an optical microscope (Axioskop, Carl Zeiss,

North York, Canada) at 50x magnification. Polarizing light images were taken using the same microscope with a set of cross polarizing light filters (Carl Zeiss, North York, Canada).

4.3.8 Fluorescent microscopy of starch

Starch samples (native and SMC) were added to a solution of fluorescein isothiocyanate conjugated with dextran (FITC-dextran) with a molecular weight of 10,000 g/mol at a concentration of 10 mg/mL and were left overnight at room temperature for loading of the particles. Right before imaging (~15-30 min before), each sample was placed on filter paper using a pipette to wick away excess liquid and then rinsed using a few drops of water. The starch was removed from the filter paper and placed on a microscope slide; a drop of water was added, and a coverslip was placed on top. Nail polish was used to seal between the edges of the coverslip and the slide to prevent evaporation and movement. Once the nail polish was dry (~5 min), the slide was placed on the microscope and images were taken using a confocal microscope (LSM 700, Carl Zeiss, North York, Canada) with illumination by the 488 nm laser using a 100x oil immersion objective.

4.3.9 Particle size and internal cavity analysis on SEM images

SEM images of sectioned particles were analyzed for particle dimensions in Photoshop (Adobe, San Jose, CA, USA) using the ruler tool. To calculate the particle diameter, the widest and narrowest diameters were measured and the two were averaged to calculate the average diameter for each particle. To calculate the internal cavity diameter, the shell thickness was first measured by averaging the thickest and the thinnest points of the particle shell and then calculated using Eq. 3:

$$\text{internal cavity diameter} = \text{particle diameter} - (2 * \text{shell thickness}) \quad (3)$$

A total of eight particles for each particle type were analyzed. The theoretical equation for modeling the internal cavity size as a function of the particle size was fitted using the initial hole size (β_i).

4.3.10 Statistical Analysis

Swelling power experiments were conducted in triplicate or quadruplicate, and values are reported as the mean±SD. The data were fitted empirically to model the observed behaviour. Lines of best fit were created in Origin graphing and data analysis software (OriginLab, Northampton, MA, USA). For the exponential equation fits, the ExpGro2 and ExpGro1 functions were used, representing two-phase exponential growth and single-phase exponential growth, respectively. For the sigmoidal equation fit, the Hill1 function was used. For the linear equation fit, the Line function was used. For the second order polynomial equation fit, a polynomial function with an order of two was used. The equations and fitted parameters are given within each plot figure.

4.4 Results and Discussion

4.4.1 Preparation of tunable starch microcapsules (SMCs)

4.4.1.1 Control of swelling power using swelling time

The tunability of the swelling extent was first studied through measuring the swelling power as a function of time (Fig. 4.2). The swelling power was measured at various swelling times with heating at 65˚C and 70˚C and with no heating (at 20˚C) as a control. All subsequent preparations of SMCs were swelled for 30 min for two reasons: 1) 30 min allowed for the swelling processes to mostly plateau as seen in Fig. 4.2, and 2) 30 min is also what other work has used to prepare swelled starch particles (Kumar et al., 2018; Ratnayake & Jackson, 2007; Shi et al., 2013; W. Wang et al., 2017). The swelling process can be modeled

using a second order exponential curve as seen with the solid lines in Figure 4.2. A similar swelling profile was observed by Desam et al. with waxy maize starch (2018). Control of swelling time is one way to control the swelling extent of the SMCs.

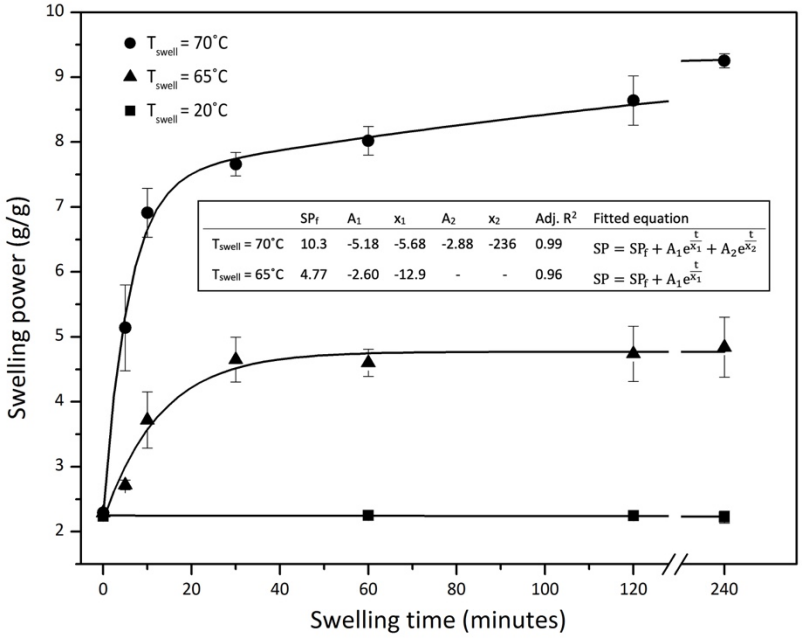

	SP_f	A_1	x_1	A_2	x_2	Adj. R^2	Fitted equation
T_{swell} = 70˚C	10.3	-5.18	-5.68	-2.88	-236	0.99	$SP = SP_f + A_1 e^{\frac{t}{x_1}} + A_2 e^{\frac{t}{x_2}}$
T_{swell} = 65˚C	4.77	-2.60	-12.9	-	-	0.96	$SP = SP_f + A_1 e^{\frac{t}{x_1}}$

Figure 4.2: The swelling power of corn starch at increasing swelling times with heating at 70˚C and 65˚C, and with a swelling control at 20˚C (n=3, mean ± SD). Exponential functions were fitted to the data, with a two-phase function used for heating at 70˚C and a single-phase function used for heating at 65˚C. The fitted parameters (SP_f, final swelling power; A_1; x_1; A_2; and x_2) and equations are provided in the inset table.

4.4.1.2 Control of swelling power using swelling temperature

The effect of temperature on the swelling power was studied by creating SMCs through heating (for 30 minutes) at 55˚C (SMC55), 60˚C (SMC60), 65˚C (SMC65), 70˚C (SMC70), 75˚C (SMC75), 80˚C (SMC80), and 85˚C (SMC85) (Fig. 4.3). As the heating temperature increases, the swelling power increases too. These results indicate that the most significant structural changes occur for the SMC65 and SMC70

samples because relative change from the native starch swelling power is the greatest for these two samples. The swelling process as a function of temperature can be modeled using a sigmoidal equation. It should be noted that the modified Hill equation as we have used it is only valid as a model up to 85˚C. A similar sigmoidal swelling profile was observed by Tester and Morrison (1990) when they measured swelling factor vs temperature for normal maize starch. Control of swelling temperature is a second way to control the swelling extent of the SMCs.

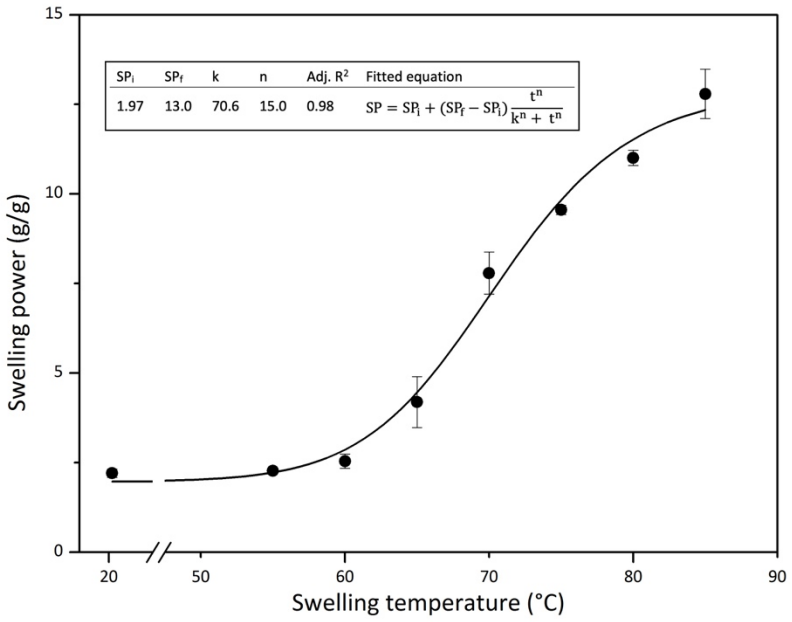

Figure 4.3: The swelling power (SP) of corn starch at increasing swelling temperatures (t) with heating for 30 min (n = 4, mean ± SD). A modified Hill equation was fitted to the data. The fitted parameters (SP_i, initial swelling power; SP_f, final swelling power; k; and n) and equation are provided in the inset table.

4.4.1.3 Control of particle size using swelling power

As the swelling power increases, it is natural to conclude that the particle sizes must increase. Static light scattering (SLS) was used to determine particle diameters and to demonstrate the effect of swelling on the

particle sizes (Fig. 4.4). Increased swelling temperatures linearly correlates to increased particle sizes. Although laser light scattering data can be used to calculate various mean diameters, the mean Sauter diameter ($d_{3,2}$) provided the best fit and thus was used. The Sauter diameter also showed the most similarity to diameters observed with other microscopy methods. The correlation between the swelling power and diameter can be used to modulate the mean particle diameter. Native starch granules have a polydisperse particle size distribution, and so, as expected, the swelled SMCs likewise have a fairly polydisperse distribution (Appendix B). It is worth noting that there are many active and passive methods for sorting microparticles while in solution (Sajeesh & Sen, 2014; Xi et al., 2017; Zhou et al., 2019), and it is expected that these SMCs would similarly be easily sortable based on their size to allow for a more monodisperse distribution if needed.

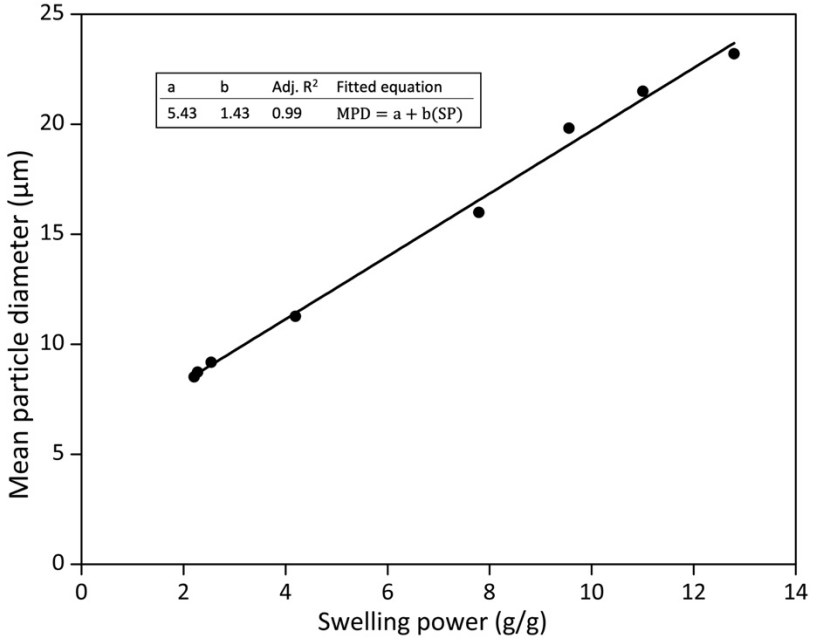

Figure 4.4: The effect of swelling power (SP) on the mean particle diameter (MPD). A linear equation was fitted to the data. The fitted parameters (a and b) and equation are provided in the inset table.

4.4.1.4 Control of soluble starch fraction using swelling power

As the particles swell and start to gelatinize, some of the polymer becomes solubilized. The soluble starch fraction (sometimes referred to by others as solubility or percent of leaching) can be plotted as a function of swelling power (Fig. 4.5). This soluble starch is quite minimal at low swelling powers but does become increasingly significant as the swelling power increases. Our data can be fitted through a second order polynomial as indicated in Fig. 4.5 by the solid line. The correlation between the swelling power and solubility can be used to control the extent of solubilization.

With normal corn starch, amylose preferentially leaches out (Doblado-Maldonado et al., 2017; Roger & Colonna, 1996). Further, the preferential leaching out of amylose in corn starch is more significant at lower heating temperatures: Doblado-Maldonado et al. (2017) observed leached material with 91.4% amylose content (determined through size exclusion chromatography) with heating at 90˚C, compared with 96.7% amylose content with heating at 70˚C (the native starch they used had an amylose content of 28.0%). It has also been suggested that that the leaching out of amylose is dependent on starch type (Vamadevan & Bertoft, 2020).

A single analysis of the amylose content on our results indicated that the soluble starch from preparing SMC70 had 68.6% amylose content, as determined through a colorimetric method (Williams et al., 1970), compared with 27.8% amylose content of the native corn starch, further supporting that amylose preferentially leeches out.

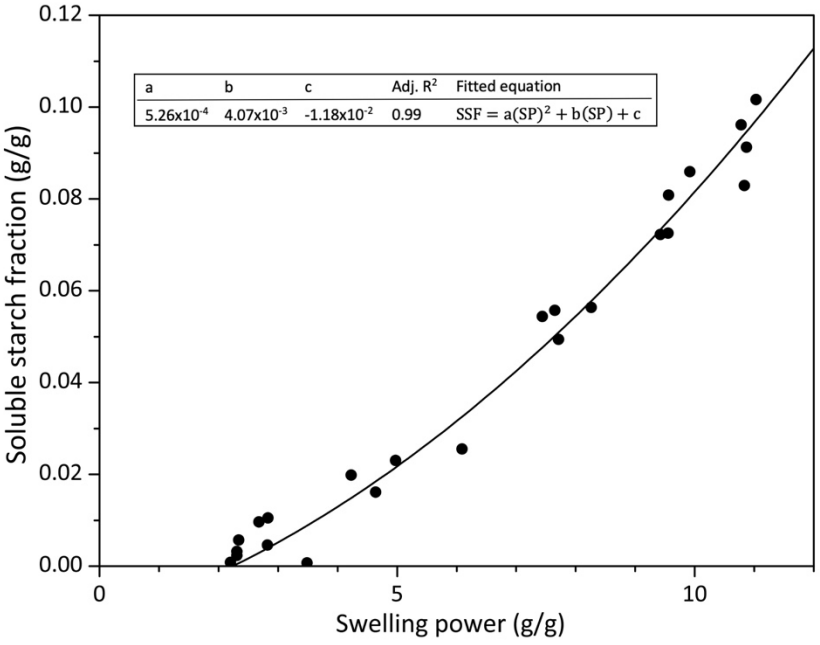

Figure 4.5: The effect of swelling power (SP) on soluble starch fraction (SSF). A second order polynomial function was fitted to the data. The fitted parameters (a, b, and c) and equation are provided in the inset table.

4.4.2 Characterization of starch microcapsules

4.4.2.1 Scanning electron microscopy

Scanning electron microscopy (SEM) provided clear images of the internal structure of the SMCs in a dry state. We observed that most native granules had an empty internal cavity (Fig. 4.6a, 4.6d, and 4.6g). The internal cavities were primarily observed as being centred around the hilum region. It has been reported that internal cavity formation is the result of drying (through creation of internal stresses) of the granules both in potato starch (Baldwin et al., 1994) and maize starch (Kerry C. Huber & BeMiller, 1997). The results in Fig. 4.6a, 4.6d, and 4.6g also indicate that the internal cavity is empty, in agreement with work

by Huber and BeMiller (2000). In contrast to our results, Gallant et al. suggested the space was filled with amorphous material (1997).

In the particles swelled at 65˚C (SMC65) (Fig. 4.6b, 4.6e, and 4.6h), larger internal cavities were observed compared to the native corn starch granules. Particles showed some variation in the appearance of internal cavity surface roughness. Of particles which were sectioned and were oriented so that the interior could be seen, all showed an internal cavity. In the particles swelled at 70˚C (SMC70) (Fig. 4.6c, 4.6f, and 4.6i), even larger internal cavities are seen compared with the SMC65 particles. With heating at 70˚C, the walls of the particles become quite thin as a result of particle expansion.

The primary mechanism for wall thinning and cavity growth is simply particle swelling. With the assumption that the starch wall volume and density is conserved, the starch cavity volume can be modeled mathematically as the particle swells (see Section 4.3.3). As we have observed that solubilization also occurs with particle swelling, this solubilization must contribute either to wall thinning and cavity growth, to a decrease in density of the starch wall, or to both. However, if we assume that starch density is constant, when the effect of solubilization (using data and correlations in Figs. 4.4 and 4.5) on internal cavity volume is calculated mathematically , it is seen that the effect is negligible (proof given in Fig. 4.11).

Our results support the idea that the starch closest to the hilum region is more loosely packed and hence most easily solubilized (Yang et al., 2016). Although there are still conflicting results regarding whether there is more amylose or amylopectin in the interior of starch granules (Bertoft, 2017), there is consensus that this interior region is more amorphous than the peripheral regions of the starch granule (Buléon et al., 1998; Vamadevan & Bertoft, 2015) and that this region gelatinizes most easily (Bogracheva et al., 1998).

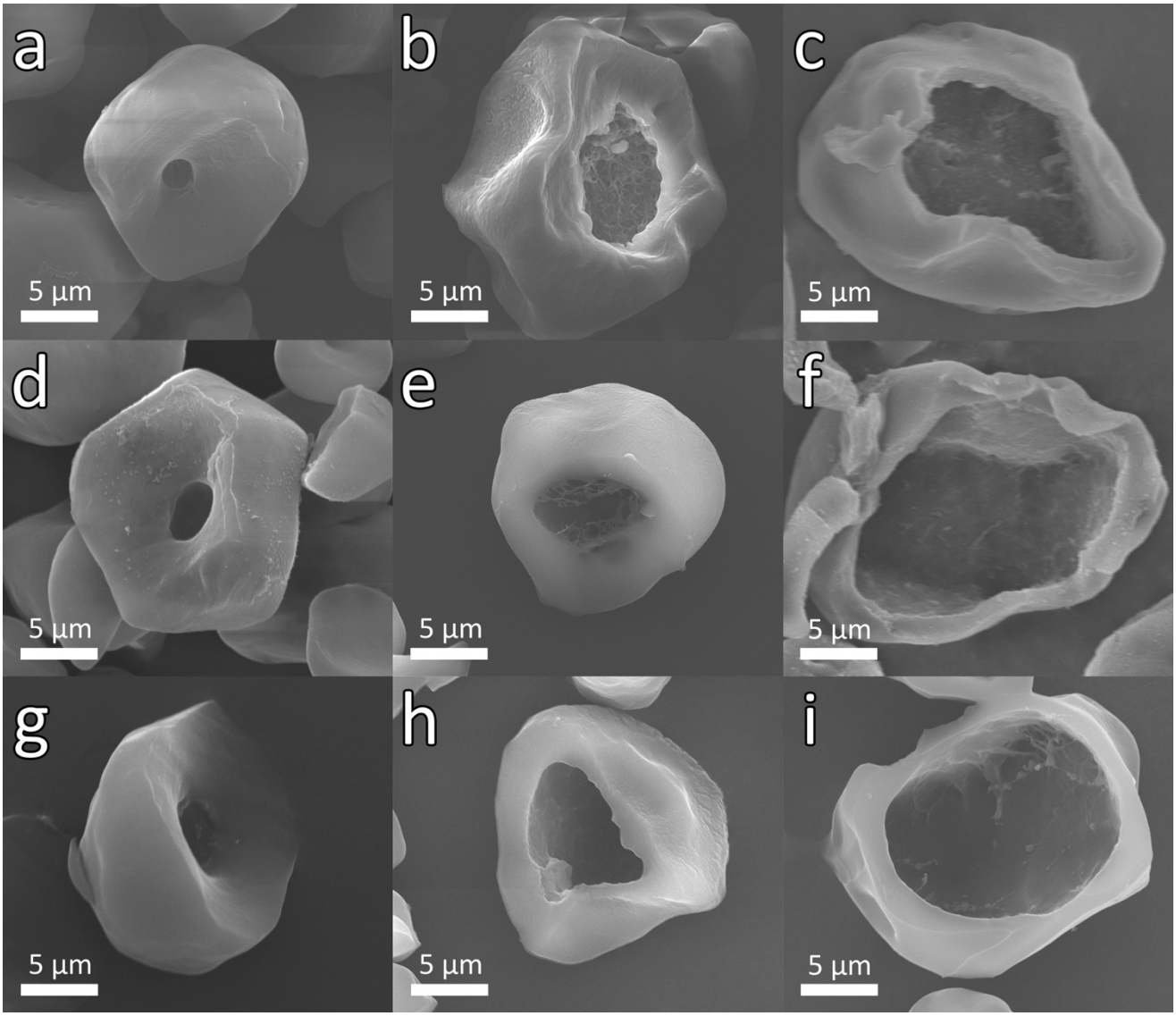

Figure 4.6: SEM images of sectioned native starch granules (a, d, and g), SMC65 particles (b, e, and h), and SMC70 particles (c, f, and i). Particles in images a, b, c, d, and f were acetone washed; e, g, h, and i were freeze dried. Scale bars indicate 5 µm.

4.4.2.2 Helium ion microscopy

Helium ion microscopy (HIM) is a relatively new characterization method which is capable of producing high-resolution images of starch, as we have previously reported (Wulff, Aucoin, et al., 2020). The results in Fig. 4.7 support what is seen in the SEM images (Fig. 4.6). In native corn starch granules, growth rings (Fig. 4.7a) and the surface morphology with a mesh-like structure (Fig. 4.7d) are clearly seen. HIM images of SMC65 (Fig. 4.7b and 4.7e) clearly show a distinct internal cavity similar what was seen with SEM. In addition, pore-like structures are seen in the wall of the particle. The images of SMC70 particles (Fig. 4.7c and 4.7f) similarly supported what we saw observed with SEM. In Fig. 4.7c, the wall of the SMC70 particle shows mesh-like features (as seen in Fig. 4.7a) and pores (as seen in Fig. 4.7b).

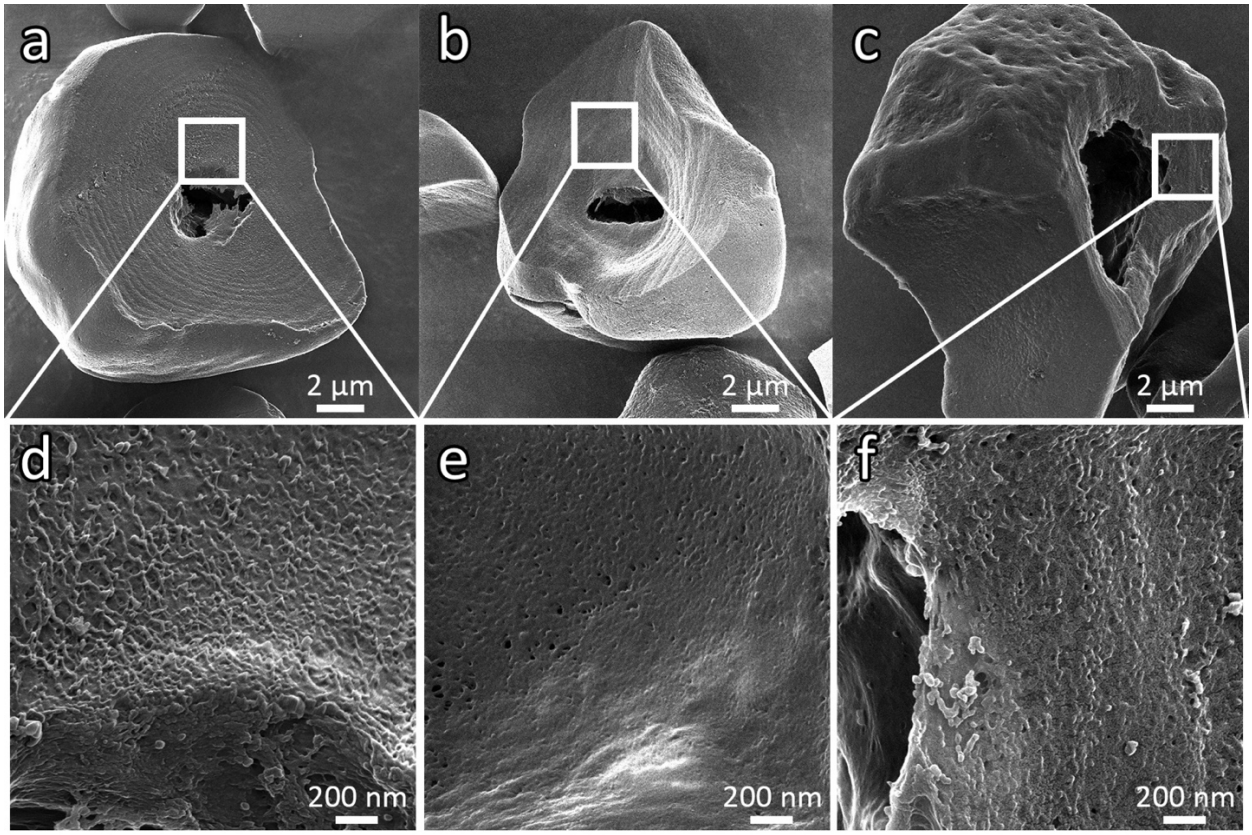

Figure 4.7: HIM images of sectioned native starch granules (a and d), SMC65 particles (b and e), and SMC70 particles (c and f). All particles were acetone washed. White boxes in the top images indicate the location of the zoomed-in bottom images. Images were taken using a Zeiss Orion Plus helium ion microscope. Scale bars indicate 2 µm (top row) and 200 nm (bottom row). Fig. 7a and 7d are adapted and reproduced with permission from (Wulff, Aucoin, et al., 2020).

4.4.2.3 Optical microscopy

Brightfield images of the swelling process (Fig. 4.8a – 4.8d) clearly show the increase in size as the particles are heated at higher temperatures and support the SEM and HIM results, but with particles which are fully wet and in solution. The particles also appear to become more translucent at they get larger. The SMC70

particles (Fig. 4.8d) have a diameter which is about double compared to the native starch granules (Fig. 4.8a), roughly in agreement with the quantitative results obtained using the laser particle sizer.

Polarizing light microscopy allows for insight into the crystallinity of the starch granules. These images show the transition from native corn (Fig. 4.8e), which is birefringent (as indicated by the characteristic 'Maltese cross'), to nearly complete loss of birefringence when heated to 70˚C (Fig. 4.8h). The 'Maltese cross' demonstrates radial organization within the starch granule and indicates a high degree of order inside the granules (Bertoft, 2017). Loss of birefringence is known to be associated with melting of crystallites (Q. Li et al., 2013) and is one way to define gelatinization (Parker & Ring, 2001).

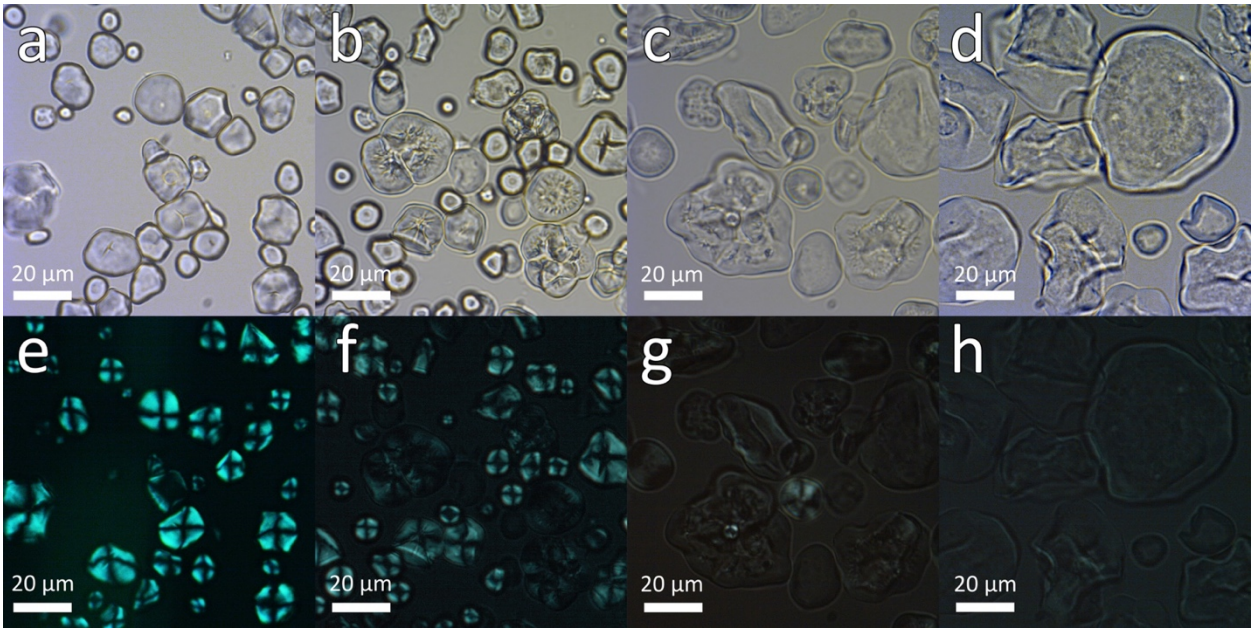

Figure 4.8: Microscopy images (brightfield, top; polarized light, bottom) of native corn starch granules (a and e), SMC60 particles (b and f), SMC65 particles (c and g), and SMC70 particles (d and h). For each sample type, the exact same particles were imaged for both brightfield and polarized images. Scale bars indicate 20 µm.

4.4.2.4 Confocal laser scanning microscopy

CLSM images (Fig. 4.9) allowed for internal structures to be seen both in a wet state and without using a microtome to physically section the starch. FITC-dextran (MW 10,000) was chosen because it shows clear identification of features in starch granules and is not selective with respect to amylose or amylopectin. As noted by Schirmer et al., there is little information on the way in which various dyes interact with starch granules (2013). Based on our method of preparation, it was possible to qualitatively analyze the diffusion of the FITC-dextran after the particles had been washed with water.

Native corn starch (Fig. 4.9a) showed some variation between particles with respect to dye localization. Some particles showed high fluorescence in the hilum region of the particles while others showed very low fluorescence there, in agreement with work by Dhital et al. (2013). This result seems to indicate that, of native granules that had an internal cavity in the hilum region, only some were permeable to FITC-dextran, which could mean that only some granules have pores or channels which are large enough for FITC-dextran to diffuse all the way to the centre of the granule. A similar result was found by Achayuthakan et al. (2012) who observed higher permeation in rice starch with MW 4,000 FITC-dextran compared to MW 10,000 FITC-dextran. In addition, of the particles which were fully permeable to FITC-dextran, the fluorescent intensity in the hilum region was very high. Based on the assumption that higher fluorescent intensity means higher concentration of FITC-dextran, this higher intensity indicated that the hilum region was empty which allowed for higher concentration of the dye. The reason for the lower fluorescence outside of the particles in Fig. 4.9a – 4.9c was likely due to the water washing step which dilutes the FITC-dextran.

In the SMCs (Fig. 4.9b – 4.9d), internal cavities and their expansion were clearly observed. Of particular interest is that the particles, particularly SMC60 and SMC65 particles, have varying internal fluorescence. When the particles were washed and placed on the microscope slide, the FITC-dextran likely started to diffuse out slowly. Of the particles which were both permeable and had a high concentration of FITC-dextran in the cavity, presumably the particles which displayed higher internal cavity fluorescence when imaged had a slower rate of diffusion out of the particles. Relative background fluorescence was brighter with the SMC images compared with the native granule image, likely as a result of the FITC-dextran which had diffused out of the particles. One final observation is the loss in circularity as the particles swell, which could be an indication of lower structural integrity of the wall.

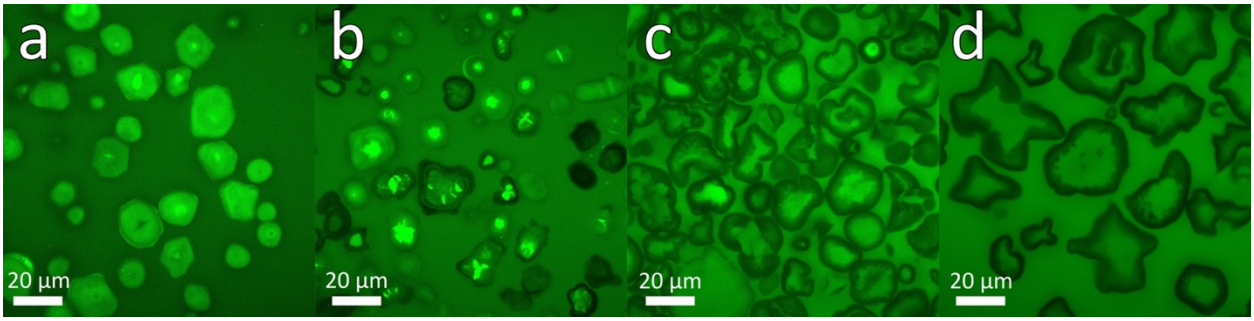

Figure 4.9: Confocal laser scanning microscopy images of native corn starch granules (a), SMC60 particles (b), SMC65 particles (c), and SMC70 particles (d). Scale bars indicate 20 µm.

4.4.3 Mathematical modeling of starch swelling

It is possible to mathematically relate swelled particles sizes to the size of the internal hole. Two assumptions must be made: 1) particles are spheres and 2) particle wall volume and density are conserved through the swelling process. The swelled microcapsule will have an internal hole radius ($r_{h,s}$) that is a function of the native granule outer particle radius ($r_{p,n}$), the native granule internal hole radius ($r_{h,n}$), and the swelled microcapsule outer particle radius ($r_{p,s}$); it can be calculated, through derivation from the equation relating the volume of a sphere to its radius using Eq. 4:

$$r_{h,s} = \sqrt[3]{(r_{p,s})^3 + (r_{h,n})^3 - (r_{p,n})^3} \qquad (4)$$

Equation 4 can also be written in an alternative dimensionless form which uses variables to describe the relative swelling extent (α) and the relative size of the internal cavity (β). α represents the ratio of swelled particle radius to native particle radius, and β represents the ratio of the swelled hole radius to the native particle radius (Fig 10). β_i represents the ratio of the initial (unswelled) hole radius to the native particle radius. These variables are calculated using Eqs. 5-7:

$$\alpha = \frac{r_{p,s}}{r_{p,n}} \qquad (5)$$

$$\beta = \frac{r_{h,s}}{r_{p,n}} \qquad (6)$$

$$\beta_i = \frac{r_{h,n}}{r_{p,n}} \qquad (7)$$

Thus, the dimensionless equation now takes the form in Eq. 8:

$$\beta = \sqrt[3]{\alpha^3 + \beta_i{}^3 - 1} \qquad (8)$$

When plotted (Fig. 4.10), the relationship between α, β, and β_i can be clearly seen. The two superimposed model particles in Figure 8 demonstrate the swelling process for a granule with $\beta_i = 0.4$, with the left particle being a native granule and the right particle being a swelled microcapsule. A small change in the outer particle radius results in a large change in the internal hole radius. It is also clear that the effect of the initial hole radius is negligible as the particle swells.

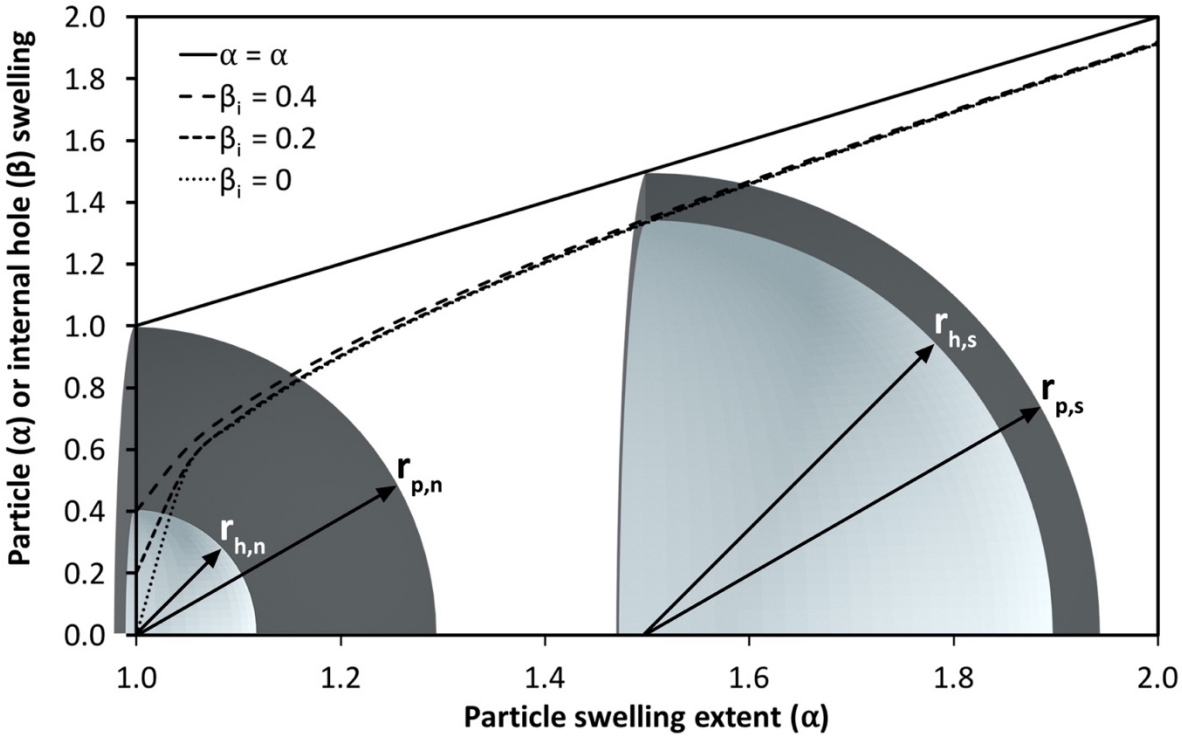

Figure 4.10: The effect of particle swelling on internal hole size can be seen by comparing the effect of increasing particle swelling extent (α) with various initial hole sizes (β_i) on swelled hole sizes (β). The superimposed particle section on the left indicates a native (n) starch granule demonstrating the radius of the hole (h) and of the outer particle surface (p), and the superimposed particle on the right indicates a swelled (s) starch microcapsule (SMC) demonstrating the same radii.

As indicated previously, the calculation of Eq. 8 assumes conservation of particle wall (i.e. the shell) volume and density. However, even when the loss of soluble starch is accounted for by use of the correlations for swelling power and solubility in Fig. 4.5, there is a less than 0.35% change in the hole radius at any given swelling power or initial hole size (Fig. 4.11). As such, Eq. 4.8 provides a very close approximation without unnecessary complication.

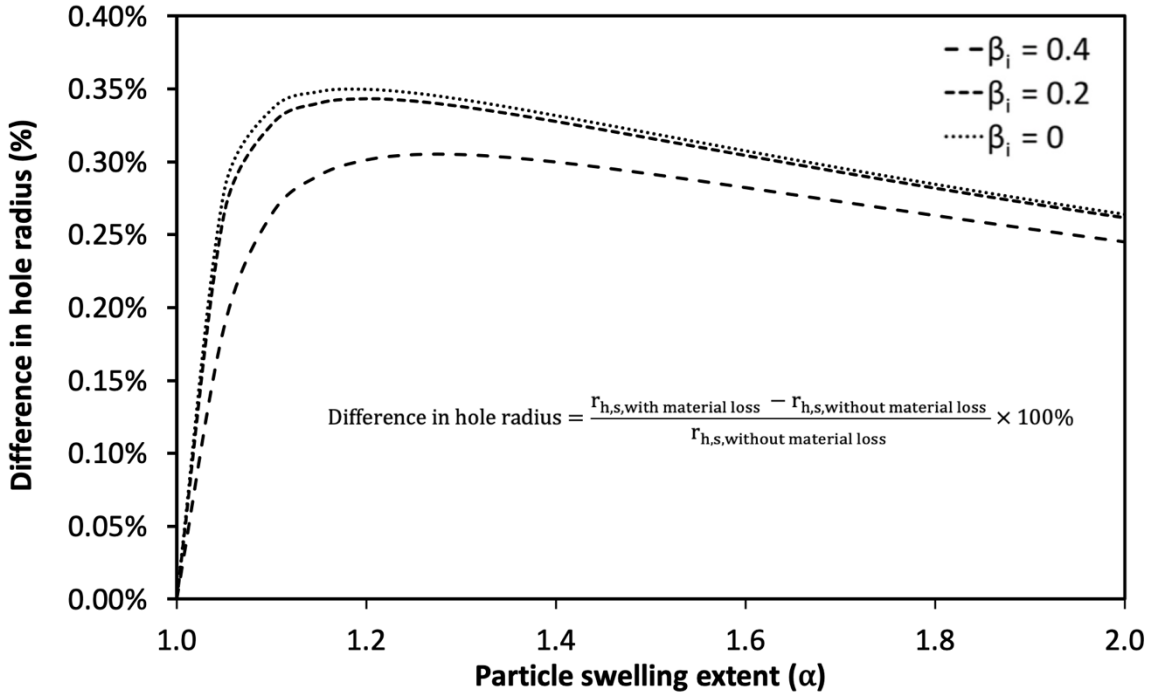

Figure 4.11: The effect of accounting for material loss when calculating the theoretical hole radius based on conservation of mass and density. The calculations are based on an initial particle radius of 4.25 μm, representative of native normal corn starch. The swelling power is calculated from the linear line of best fit (in Eq. 4), and the fraction of soluble starch is calculated based on the second order polynomial line of best fit from the swelling power (in Eq. 5). These calculations assume that a) both the solubilized and unsolubilized starch had the same density prior to any solubilization and b) the solubilized starch is only removed from the inner surface (i.e. the internal cavity side) of the particle.

4.4.4 Fitting of mathematical modeling with experimental data

The theoretical mathematical model in the previous section (Section 4.4.3) can be fit to particle size and hole size data based on SEM images of sectioned particles. Image analysis on native particles, SMC65 particles, and SMC70 particles yielded values for the relative swelling extent (α) and the relative internal

hole size (β), which can be plotted and compared to the model equation. The measured β value for native particles gives $\beta_i = 0.35 \pm 0.08$; and this value is the only value needed to fit the model, as seen in Figure 4.12, which results in a close fit. The standard deviation is primarily a result of variation in particle and hole sizes and not measurement error.

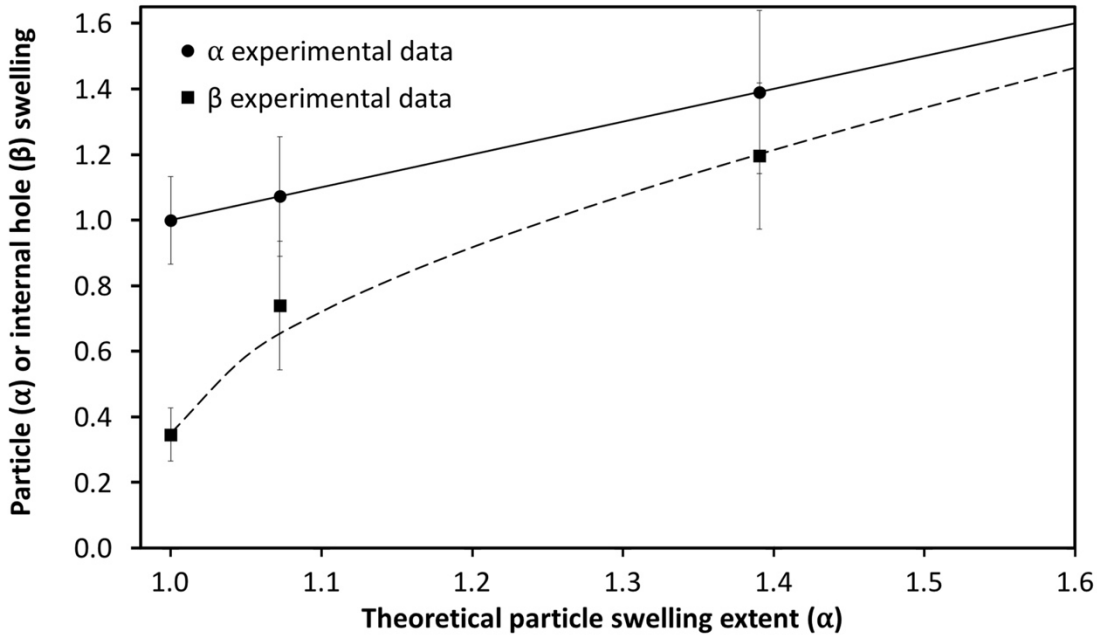

Figure 4.12: The experimental particle size and hole data fitted to the mathematical model. The fit for α represents the outer particle radius and the fit for β represents the internal hole radius. (n=8, mean ± SD)

Based on the experimental results, for SMC70 particles the average increase in particle radius is about 39% (i.e. $\alpha = 1.39 \pm 0.22$). Based on the fitted mathematical model, a 39% increase in the particle radius results in a relative internal hole size increase from 0.35 to 1.20, which means that internal cavity volume increases by a factor of 40x.

4.5 Conclusion

The starch granule swelling process in normal corn starch was studied through heating starch in an excess of water. Both the swelling temperature and the swelling time can be used to control the swelling extent of the particles, as measured by the swelling power. When the starch is swelled, there is a corresponding increase in the average particle diameter and in the amount of soluble starch, allowing for control of these properties too. The swelling process causes growth of the internal cavity, as clearly observed with SEM, HIM, and CLSM imaging. The growth of the internal cavity is primarily the result of particle expansion, and only a small increase in particle diameter corresponds to a large increase in the internal cavity volume. The particle shell becomes thinner while the structural integrity of the particle appears to be largely maintained. The swelling process was modeled mathematically in close agreement with our experimental results.

Chapter 5: Characterization of swelled normal corn starch and comparison with other starch types

5.1 Summary

Starch swelling is compared with pea, potato, wheat, waxy corn and normal corn starch through heating in water. Morphological changes are observed through brightfield and scanning electron microscopy (SEM) with internal cavities and increased particle sizes being observed. Particle size distributions are measured and assessed as a result of particle swelling. The effect of centrifugation force on the swelling power is evaluated with higher centrifugal force leading to lower swelling power measurements. In pursuit of using the particles as an oral drug delivery system, we determined that greatly swelled starch has higher digestibility compared to native starch. Cross-linking is demonstrated as a method for inhibiting swelling, with corn starch being better inhibited than pea starch. Zeta potentials for corn starch are measured to be negative. And it is demonstrated that the normal corn microparticles selectively absorb water in a solution of bovine serum albumin (BSA).

5.2 Introduction

To use partially swelled starch in a drug delivery system, it is crucial to understand partially swelled starch to a reasonable extent. Attempting to characterize drug loading and release without a good understanding of the microparticles could make that characterization process more difficult. Comparing different options for starch types is also helpful for obtaining the most suitable type.

In this work, we gain a better understanding of the starch swelling process, the differences between different types of starch, and some of the properties of partially swelled starch.

5.3 Materials and Methods

5.3.1 Materials

The following samples were purchased from Sigma-Aldrich (Oakville, Canada): normal corn (maize) starch (S4126, Lot #: MKBT0621V), wheat starch (S5127, Lot #: 28H1016), waxy corn (maize) starch (S9679, Lot #: SLBP9703V), and potato starch (S4126, Lot #: BCBJ1187V). Pea starch was purchased from Nutri-Pea Limited (Portage la Prairie, Canada). The moisture contents for normal corn, wheat, waxy corn, potato, and pea starch were 14.3%, 15.0%, 15.0%, 22.1%, and 14.2%, respectively, determined by the difference in weight as a fraction of the initial weight after drying for 16 hours at 100˚C. STMP, NaOH, and NaCl were purchased from Sigma-Aldrich (Oakville, Canada)..

5.3.2 Preparation of starch microcapsules (SMCs) through heating in water

The starch microcapsules (SMCs) were prepared through a simple heat-treatment process. Native corn starch (0.7 g, dry basis), as received from the supplier, was added with Milli-Q water (14 mL) in a centrifuge tube at a concentration of 5% w/w (native, dried starch basis). To swell the starch, the centrifuge tube was placed in a water bath at the required heating temperature (50-90˚C) for 30 min with stirring of the water bath with a magnetic stirrer. The height of the water in water bath was carefully controlled to also cause gentle agitation of the centrifuge tube. After the starch was swelled, the starch mixture was cooled immediately to 20˚C by placing the centrifuge tube in a cold-water bath. Unless the particles were to be sectioned, the particles remained in solution for further use.

5.3.3 Starch swelling power

To measure the swelling power, the centrifuge tube containing the mixture of starch (native granules or SMC particles) and water were centrifuged at 1000 g for 15 minutes based on the method reported by Kim and Huber (2013). The weight of the sediment after decanting the supernatant was then measured. The swelling power was calculated using Eq. 1:

$$\text{swelling power} = \frac{\text{weight of sediment (g)}}{\text{dry basis weight of starch (g)}} \qquad (1)$$

5.3.4 Optical imaging of starch

The starch samples (native and SMC) were placed on a glass slide, a small drop of water was added, and a coverslip was placed on top. The slide was then imaged using an optical microscope (Axioskop, Carl Zeiss, North York, Canada) at 20x magnification.

5.3.5 Sectioning of starch for internal particle imaging with SEM

After the SMC preparation process, the sediment was frozen through immersion in liquid nitrogen. The sample was then mounted to a cold (-18˚C) metal disc using optimal cutting temperature (OCT) compound (VWR, Mississauga, Canada), which rapidly freezes to keep the sample in place. The sample was then sectioned, while still frozen, in 10 µm increments using a cryomicrotome (Shandon Cryomicrotome SME, Thermo, Mississauga, Canada) with a metal triple-facet cryomicrotome blade (VWR, Mississauga, Canada). The samples were then placed back in a -20˚C freezer until further use. The part of the pellet that was sectioned was not in contact with the OCT fluid.

5.3.6 Scanning electron microscopy (SEM) imaging of starch

The starch samples (native and SMC) were first frozen in liquid nitrogen and the sectioned using a cryomicrotome in 10 μm increments. The still-frozen sectioned granules were then washed with acetone to remove water while minimizing the impact of drying on the internal structure. Acetone washing involved placing the frozen sectioned granules in an excess of acetone (at room temperature), centrifuging to separate the particles, decanting the supernatant acetone, and then placing the granules in a vacuum dryer until dry. The dried starch samples were sprinkled onto double-sided carbon tape attached to the specimen stubs. Gold sputtering was performed for 120 seconds for an approximate coating thickness of 10 nm. The starch was then viewed using a scanning electron microscope (SEM, Quanta FEG 250, FEI, USA, 10-30 keV).

5.3.7 Starch particle sizing

Starch granule sizes were measured using a laser particle sizer in wet mode (Fritsch NanoTec Analysette 22, Fritsch GmbH, Idar-Oberstein, Germany). The starch samples were suspended in water at about 7% (w/w). The surface weighted mean ($d_{3,2}$) was used for further calculations and correlations. Each data point represents analysis of over 1,700 particles.

5.3.8 In vitro starch digestibility and amylose content

In vitro starch digestibility was determined by using the Englyst method (Englyst et al., 1992) with minor modifications. Glucose content of the supernatant was measured by a glucose oxidase-peroxidase assay kit (Megazyme International Ireland Ltd., Bray, Ireland). Percentages of rapidly digestible starch (RDS, % digestible starch at 20 min), slowly digestible starch (SDS, % digestible starch at 120 − min % digestible starch at 20 min), and resistant starch (RS, 100% − % digestible starch at 120 min) were calculated.

Apparent amylose content was measured by the method Williams et al. (1970) using UV-vis spectrophotometer to measure the absorbance of the amylose-iodine complex at a wavelength of 625 nm.

5.3.9 Cross-linking of partially swelled starch

STMP-crosslinked starch samples were prepared using a modified method of Gao et al. (2014). Starch granules were prepared using our standard swelling method with about 1.3 g of normal corn starch in a 50 mL centrifuge tube. After centrifugation at 1000g for 15 min, the supernatant was decanted leaving the starch sediment. For the high STMP treatment, 1 mL of STMP solution (200 mg/mL), 2.5 mL of NaOH solution (2 mg/mL), 600 µL of NaCl solution (100 µg/mL), and 10 mL of Milli-Q water were added to the swelled starch. The mixture was heated at 50˚C in a water bath with stirring for 80 min. The solution was neutralized from a pH of ~11 to a pH of ~7 using a few drops of 37.5% HCl.

5.3.10 Zeta potential

Zeta potential was determined by electrophoretic light scattering in a Zetasizer Nano (Malvern Instruments, UK) at room temperature. For the measurements, the previously freeze-dried starch microparticle samples were diluted to 0.1 wt.% in a solution of 0.01 mM NaCl at approximately neutral pH.

5.3.11 Selective water uptake

Wet starch (native and swelled) was first frozen using liquid nitrogen and then freeze dried to leave only the dry starch particles and to preserve the granules and SMCs in their swelled form. 10 mL of BSA solution (20 mg/mL) was then added to 0.4g of freeze-dried starch. The starch and BSA solution were then placed on a bench rotator overnight. After the elapsed time, the tube was centrifuged for 5 min at 1000 g to settle out the starch granules. The supernatant was then filtered using a 0.2 µm filter, diluted 40x with water, and the UV-vis absorbance analyzed at 280 nm to determine the concentration of BSA using a standard curve.

The amount of water selectively absorbed was based on a mass balance of BSA based on the observed increase in concentration.

5.4 Results and Discussion

5.4.1 Comparing the swelling profiles of various starch types using swelling power

To evaluate the various starch types for suitability for use in a drug delivery system, we compared the swelling profiles of several starch types. Swelling power provides a simple and easy way to quantify swelling extent. Figure 5.1 demonstrates the differences in swelling power for pea, potato, wheat, waxy corn, and normal corn (NC) starch. Experiments were conducted with heating only up to 90˚C as further heating leads to disintegration and a loss of rigidity of the particles, making them unsuitable for our purposes. For each type, the swelling power increases with increasing swelling temperatures, as expected (J. Y. Li & Yeh, 2001). Our goal for evaluating a number of types of starch was to evaluate if certain types of starch should immediately be ruled out as potential candidates for a starch-based drug delivery system. While other work had studied how the swelling power changes with swelling temperatures (Cai, Cai, et al., 2014; J. Y. Li & Yeh, 2001; Tester & Morrison, 1990), none had done so across enough types with results that were fully comparable.

For potato starch, the swelling power increased significantly when heated at 60˚C and was unquantifiable beyond that point due to an unclear distinction between the supernatant and the swelled starch. A quickly rising swelling power for potato starch between 55 and 60˚C could make it difficult to target a specific swelling extent if needed for particle design. When evaluating the swelling powers of wheat, pea, waxy corn, and normal corn at T_{swell} = 65˚C, the types swell from most to least in the following order: wheat >

pea > waxy corn ≈ normal corn. Based on these results, it seemed that potato starch was likely a poor candidate for use in a drug delivery system we were trying to create.

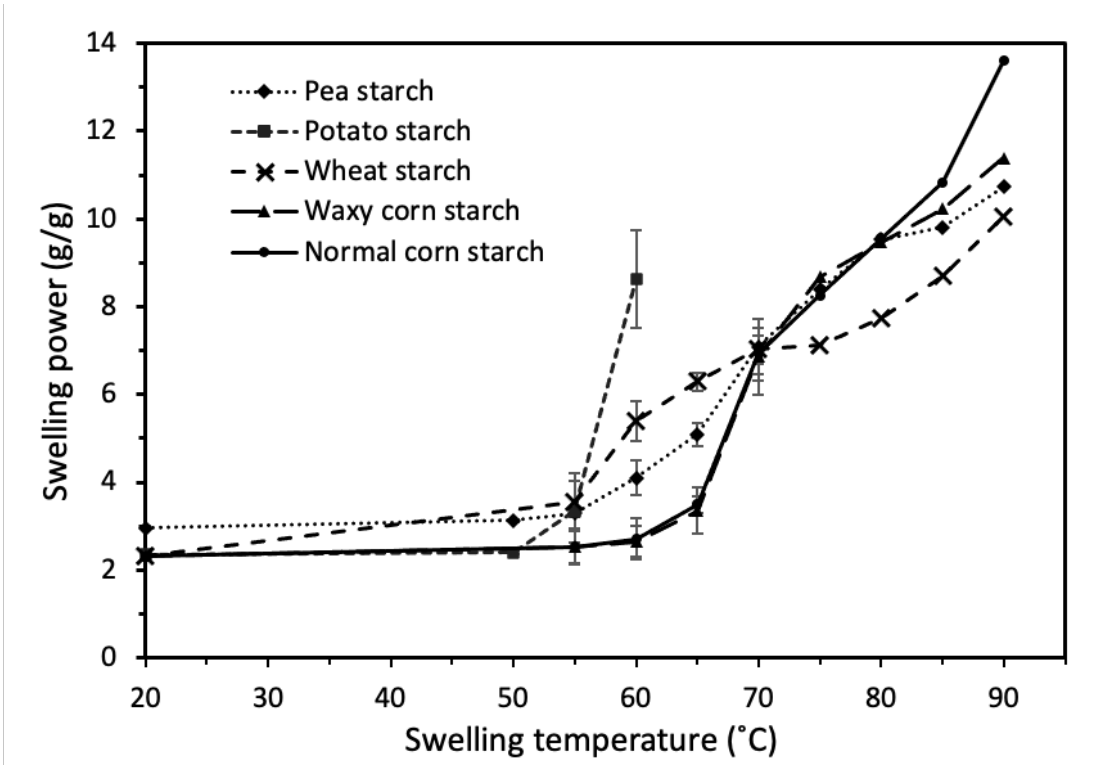

Figure 5.1: The effect of swelling temperature on swelling power of pea, potato, wheat, waxy, and normal corn starch. For T ≥ 75˚C, n = 1; all others, n=3, mean ± SD.

A progression of swelled pea starch and their swelling extent with respect to swelling temperature is seen in Figure 5.2. Visually, the samples appear to have the most drastic change in appearance for the 65˚C and 70˚C samples. When swelled in water with 5% w/w starch content, for the 80˚C and 90˚C samples the swelled starch expands to fill the entire volume and were limited by the available water. This observation is in agreement with Shujun Wang et al. (2014) where they demonstrated that for heating of wheat starch

at 92.5˚C at starch content above 6.66% w/w, the swelling was water constrained. To more accurately measure the swelling extent at high temperatures, a lower starch content should be used.

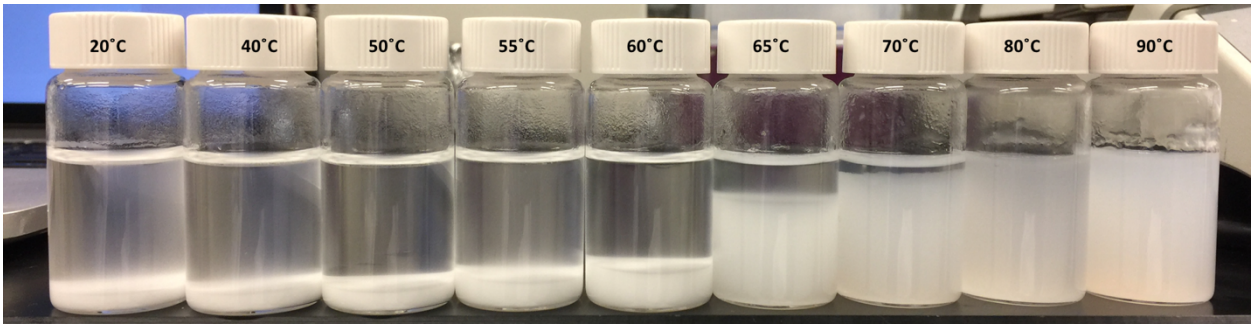

Figure 5.2: Swelling progression of swelled pea starch at increasing swelling temperatures. Temperatures at which samples were heated are indicated on the vial lids. Swelling was done for 30 min at a 5% w/w starch content.

5.4.2 Microscopy images of native and swelled starch granules of various starch types

The microscopy images in Figure 5.3 demonstrate the physical changes in the various starch types as a they are heated for 30 min at 5% w/w in water. As expected, the particles grew larger in size with increasing heating temperatures. It is interesting to note that, with some of the starch types, swelling does not occur uniformly within all of the granules in the sample. In addition, some granules appeared to remain relatively unswelled before rapidly swelling, rather than swelling gradually between the various temperatures. This "popcorn popping" effect has also been observed by Cai et al. (2013). In the samples we tested, this effect is most strongly observed with potato and wheat starch. This effect has implications for obtaining a uniform size distribution which could be a requirement for a starch-based drug delivery system.

Based on the optical microscopy results and the swelling power results in Section 5.4.1, we decided that potato was likely a poor option due to its rapid and extensive swelling. Further, with such similarities

between normal and waxy corn starch, and with amylose content likely not being important for our work, we could rule waxy corn starch out as a candidate.

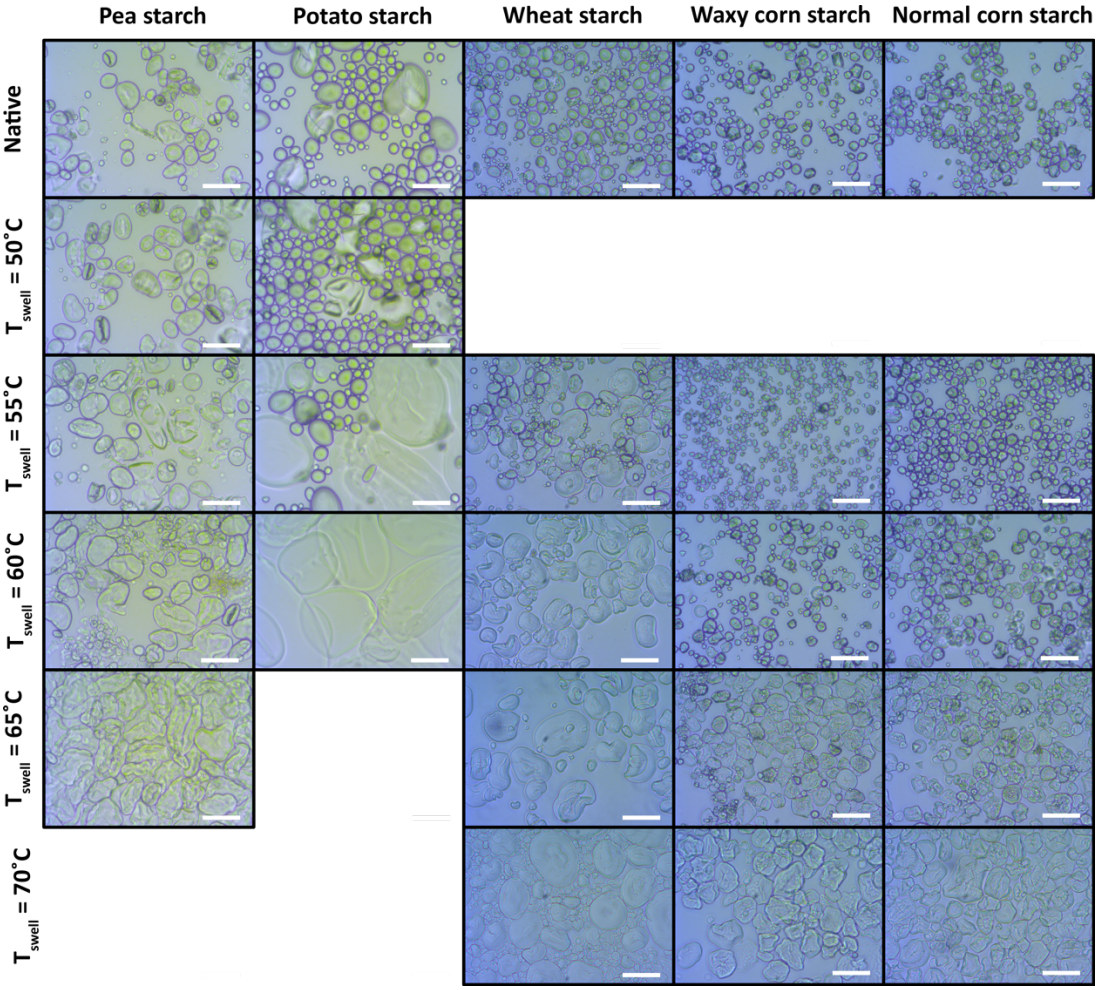

Figure 5.3: Brightfield microscopy images of pea, potato, wheat, waxy corn, and normal corn starch after swelling for 30 minutes at the indicated temperatures. Scale bars are 50 µm.

5.4.3 SEM images of swelled normal corn, pea, and wheat starch

At this point in evaluating the various starch types, the options we were still considering were normal corn, pea, and wheat starch. We swelled each of these starches and imaged them with SEM (Figure 5.4). Of

particular interest was the enlarged internal cavity that was observed in swelled normal corn and pea starch. Although such a structure has been previously described and imaged (Dhital et al., 2013; K C Huber & BeMiller, 2000; Sujka & Jamroz, 2013), our realization that the internal cavity increased size with partial swelling of the particles while the particles stayed mostly intact led to further investigating normal corn and pea starch for drug delivery. Normal corn starch appeared to swell more uniformly and to disintegrate less commonly, so it appeared to be a better choice for the application in mind compared to pea starch.

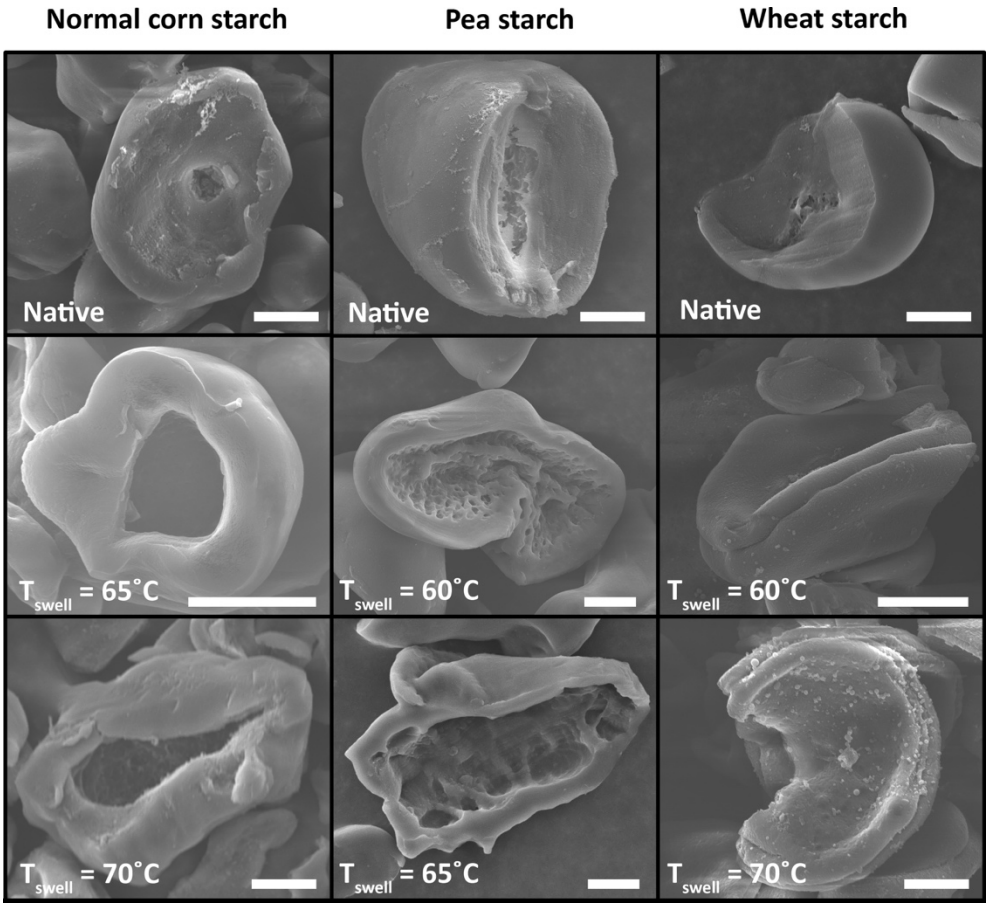

Figure 5.4: SEM images of normal corn, pea, and wheat starch after swelling for 30 minutes at the indicated temperatures. Scale bars are 5 µm.

5.4.4 Particle size distributions of normal corn starch

To evaluate the polydispersity of the starch samples, we measured particle size distributions of various starch normal corn (NC) starch samples (Figure 5.5). Data was obtained in 5˚C increments between 55˚C – 90˚C, however only selected data is shown in this figure for clarity (full data is provided in Appendix B). As expected, the particle size data confirms that larger particles were produced with increased swelling temperatures. The particle size distributions become wider with greater swelling.

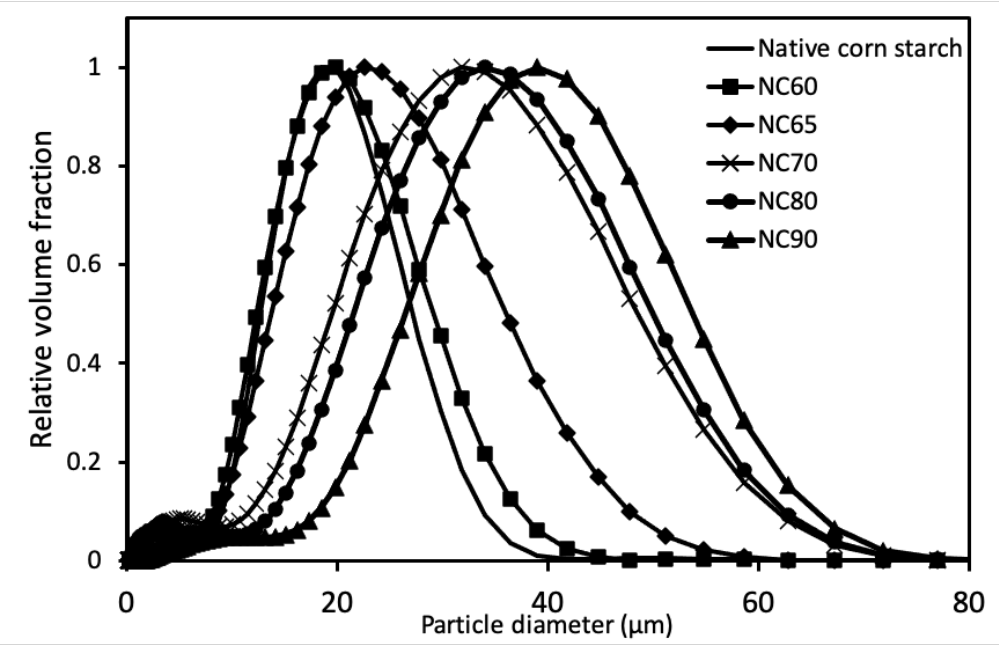

Figure 5.5: Particle size distributions of native normal corn (NC) starch and NC starch heated to 60˚C, 65˚C, 70˚C, 80˚C, and 90˚C for 30 minutes.

One method for quantifying polydispersity is to calculate the full width at half maximum (FWHM) for the particle size distributions. The FWHM is calculated by measuring the width of a distribution at a height

half of peak height. A lower FWHM indicates a more monodisperse distribution. The results of the FWHM calculations are given in Figure 5.6 and compared with the relative particle sizes. The relative particle is calculated by dividing each mean particle size by the mean particle size of native granules. If each particle within a sample swells the same amount proportionally, the FWHM should increase by that same amount proportionally. This trend is observed for particles with heating temperatures up to 70˚C. For temperatures above 70˚C, FWHM begins to decrease. This effect is likely due to one or both of two reasons: 1) the particles truly become more monodisperse as gradually all the particles achieve the "swelled" state and/or 2) the laser analyzer has difficultly with picking up some of most highly swelled particles due to their highly translucent nature. Both effects would narrow the size distribution. Our result is in agreement with results from Cai and colleagues who observed that most starch types they looked at had a range wherein individual granules start to swell and that the larger particles started swelling at lower temperature compared to smaller particles (Cai, Zhao, et al., 2014; Cai & Wei, 2013). Li and Yeh also observed a weak correlation between granule size and swelling power (2001).

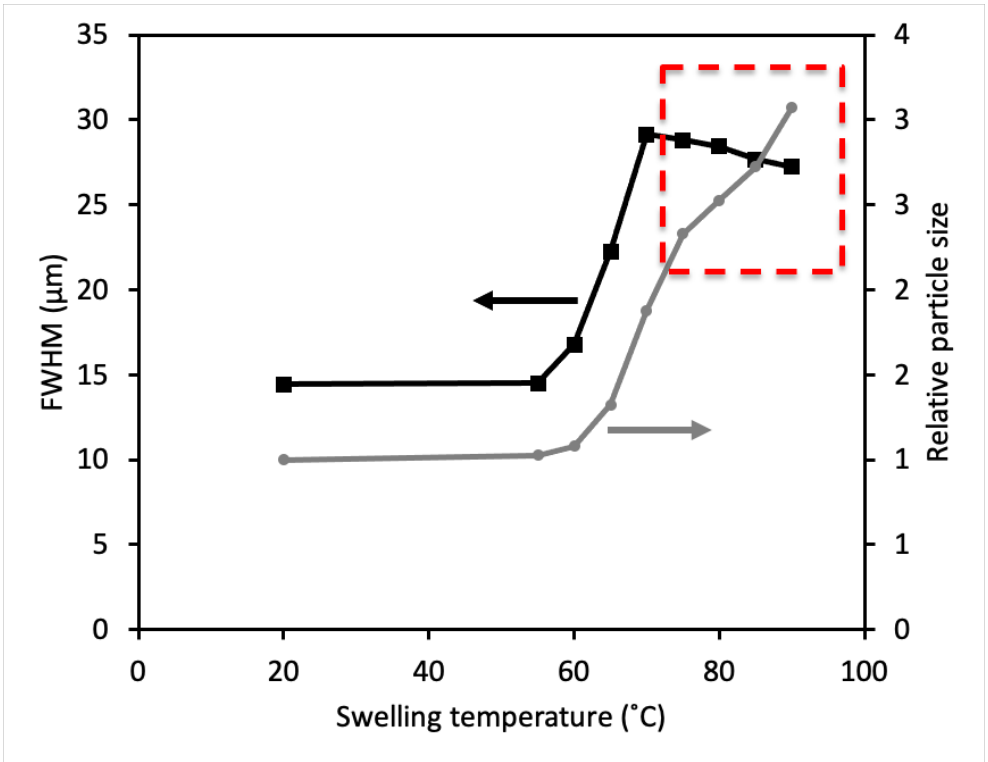

Figure 5.6: Calculated full width at half maximum (FWHM) for particle size distribution data of native normal corn (NC) starch and NC starch heated to 55˚C, 60˚C, 65˚C, 70˚C, 75˚C, 80˚C, 85˚C, and 90˚C for 30 minutes. The red dashed line demarcates samples for which the correlationbetween particle size and FHWM ends.

5.4.5 Effect of centrifugal force on swelling power

To roughly estimate the compressibility of partially swelled starch, we measured the swelling power at various centrifugal forces (Figure 5.7). We hypothesized that starch with little swelling would have very little compressibility and that highly swelled starch would be highly compressible. We also wanted to characterize the sensitivity of swelling power measurements to possible variations in centrifugal force, an important understanding for results that are heavily dependent on swelling power measurements. Our

results were as expected. Starch swelled at 70˚C had the greatest decrease in swelling power as the centrifugal force. This result suggests that more highly swelled starch is less rigid compared with less swelled starch or native starch.

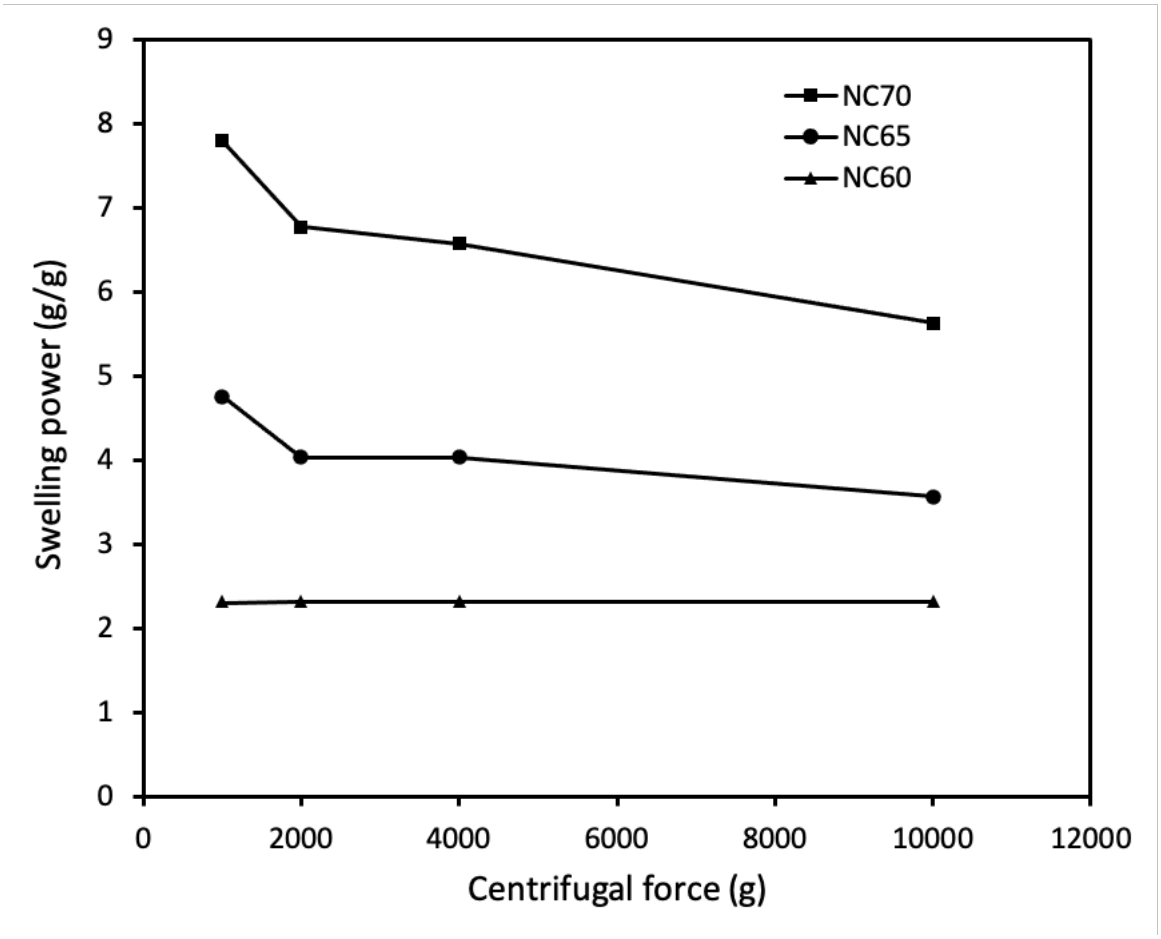

Figure 5.7: The effect of centrifugal force on the swelling power measurement of normal corn starch swelled for 30 minutes at 60˚C (NC60), 65˚C (NC65), and 70˚C (NC70).

5.4.6 Digestibility of native and swelled normal corn starch

An important factor when creating an oral drug delivery system is how it degrades as it traverses the digestive tract. For a starch-based system, its digestibility is particularly important since it is normally digested somewhat easily. Using the standard method for determining digestibility (Englyst et al., 1992), we analyzed native normal corn starch, and then freeze dried native starch, NC65, and NC70 (Figure 5.8). The digestibility is greatly increased as indicated by the large increase in the amount of rapidly digestible starch and the large decrease in slowly digestible starch and resistant starch. The increase in digestibility is primarily due to the swelled starch making more starch molecules accessible to amylase – the enzyme which hydrolyses starch polymer. Increased accessibility to amylase increases the rate at which starch is broken down into sugars. The increase in digestibility from the swelling process does not help with creating a digestion-resistant drug delivery system but being aware of this increase can allow us to create a solution.

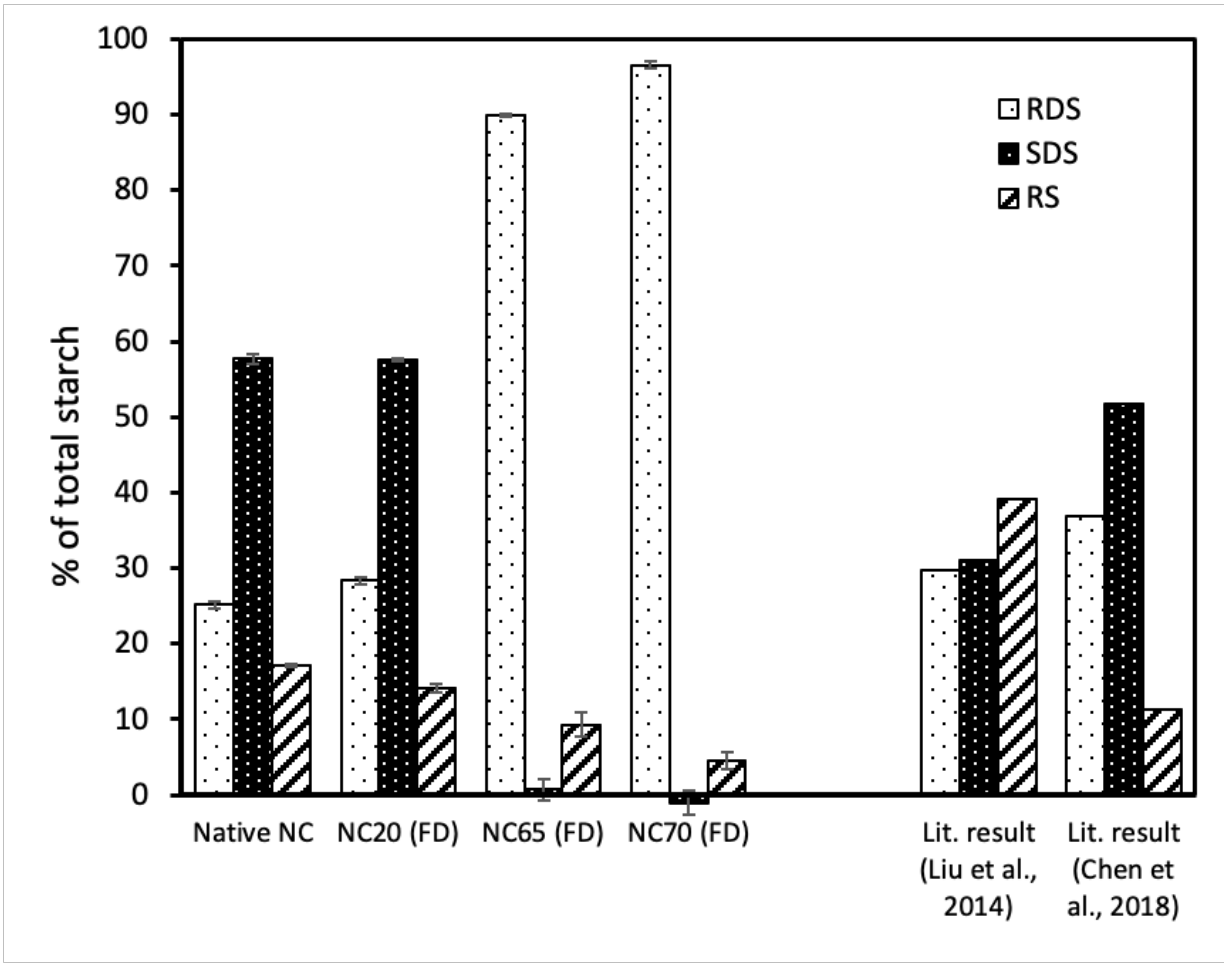

Figure 5.8: Fraction of rapidly digestible starch (RDS), slowly digestible starch (SDS), and resistant starch (RS) for native normal corn (NC) starch, freeze-dried (FD) normal corn starch with heating at 20˚C, 65˚C, and 70˚C. Error bars represent SD of three technical replicates. Literature digestibility results (X. Chen et al., 2018; H. Liu et al., 2014) for native normal corn starch are also included for comparison.

5.4.7 Amylose content of native normal corn starch and solubilized starch after swelling

To further characterize the partially swelled normal corn starch, we analyzed the amylose content of native normal corn starch and compared it with the supernatants of starch swelled at 65˚C and 70˚C (Figure 5.9).

The reason for analyzing the solubilized starch instead of the unsolubilized granules themselves is as follows: since the solubilized starch is a small amount (i.e. only 5% of the starch in NC70 granules become solubilized), any changes in the amylose content would be relatively small compared with directly measuring the solubilized fraction. The solubilized starch has over double the amylose content (>60% vs 28%) compared to that of native corn starch, which indicates that it is the amylose that preferentially leaches out, in agreement with work by Shujun Wang et al. (2012). This result could have implications for understanding internal structural changes that occur as result of swelling.

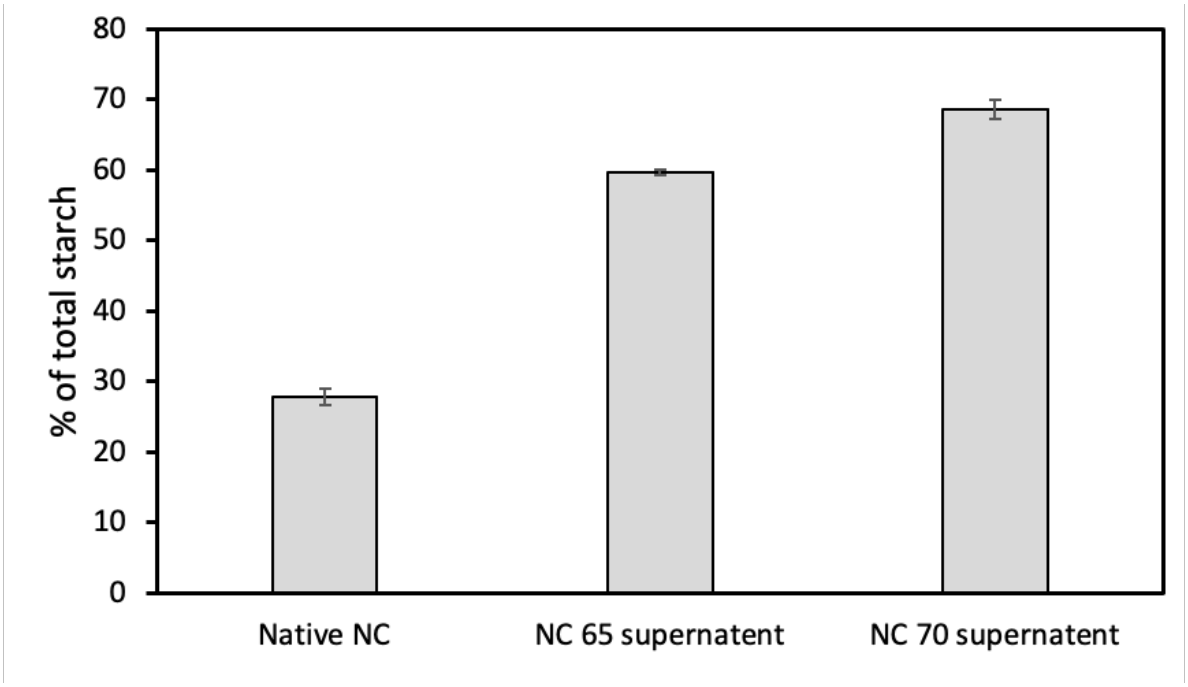

Figure 5.9: Amylose content of native normal corn starch, starch obtained from the supernatants when heating starch at 65˚C and 70˚C.

5.4.8 Inhibition of swelling as a result of cross-linking

When the goal of a controlled release drug delivery system is to prevent or slow the release of the encapsulated drug, there are many ways in which this can be done. One method for slowing release is to reduce the mesh size of hydrogel that is between the encapsulated drug and external environment. Based on our previous work, partially swelled starch appears to behave somewhat like a conventional hydrogel. Hydrogels are typically defined as being cross-linked polymers with a high water content (70-99%) that don't dissolve in water (Hoare & Kohane, 2008; J. Li & Mooney, 2016), and, while partially gelatinized starch isn't chemically cross-linked, it could be considered as physically cross-linked. We hypothesized that chemical cross-linking of partially swelled starch particles would increase their stiffness and could lock-in any encapsulated drugs. Measuring stiffness on a microparticle requires specialized equipment, and so we measured inhibition of swelling as an alternate method for quantifying the effect of cross-linking. To the best of our knowledge, cross-linking of partially swelled starch has not been studied before.

We first tested swelling inhibition with normal corn starch and pea starch that had been swelled at 65˚C; after cross-linking with STMP, we swelled the particles at a higher temperature of 90˚C (Figure 5.10). STMP was chosen as it commonly used for cross-linking starch (Fang et al., 2008; Gao et al., 2014; Wongsagonsup et al., 2014). We observed that cross-linked normal corn starch had a marked decrease in the swelling compared to the control. This was not the case for the cross-linked pea starch. We speculate that this difference could be the result either of poorer cross-linking extent for pea starch or, if equivalent cross-linking occurs, differences in starch polymer chain lengths which would impact the ability to prevent "slippage" between chains. Since gelatinization is a process where water imbibes the granules and results in the starch polymers gradually spreading further apart, cross-linking the polymer hinders this process.

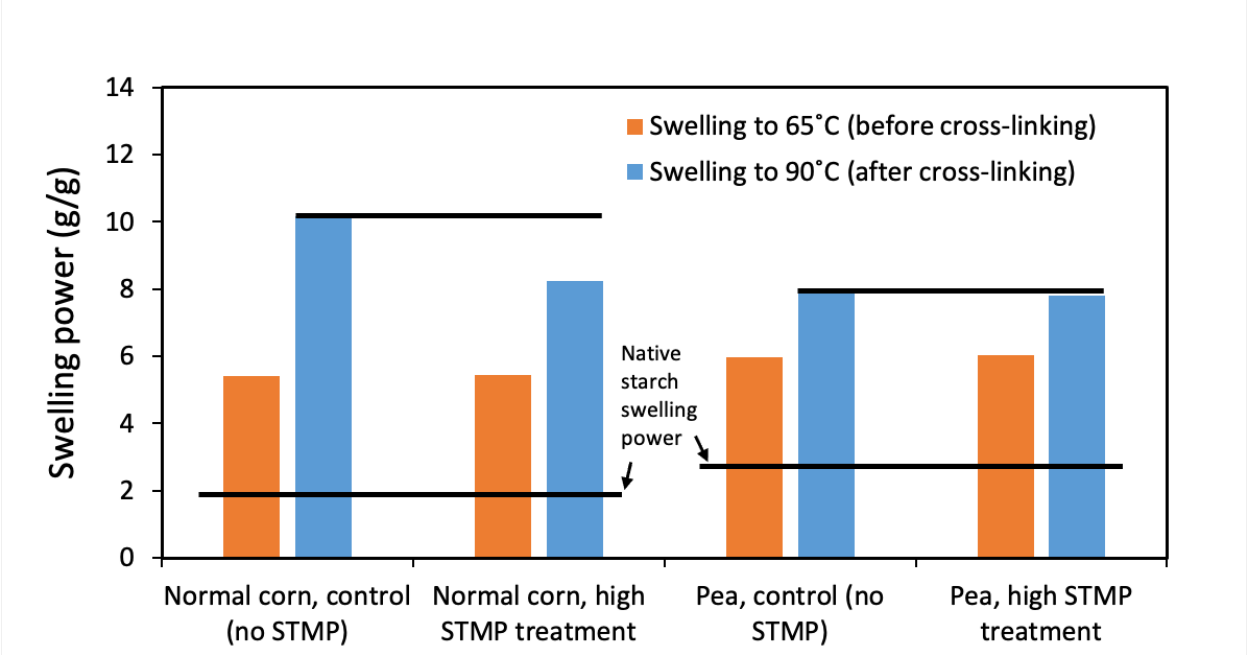

Figure 5.10: Swelling powers of normal corn (left) and pea (right) starch after initial swelling at 65˚C (orange) and then swelling at 90˚C after crosslinking with STMP (blue). The controls had the exact same heat treatment and all chemicals added for the cross-linking step other than the cross-linker (STMP) itself.

To evaluate the effect of different amounts of cross-linker, we performed the same experiment with normal corn with low and high amounts of cross-linker, with initial swelling at 65˚C (Figure 5.11). As expected, the particles cross-linked with a high amount of STMP demonstrated a greater extent of swelling inhibition. A pseudo-replicate was also performed with initial swelling at 70˚C with similar results (Figure 5.12). These results indicate that STMP cross-linking could likely be used to increase the stiffness of the starch microparticles and also to possibly prevent release of encapsulated drugs.

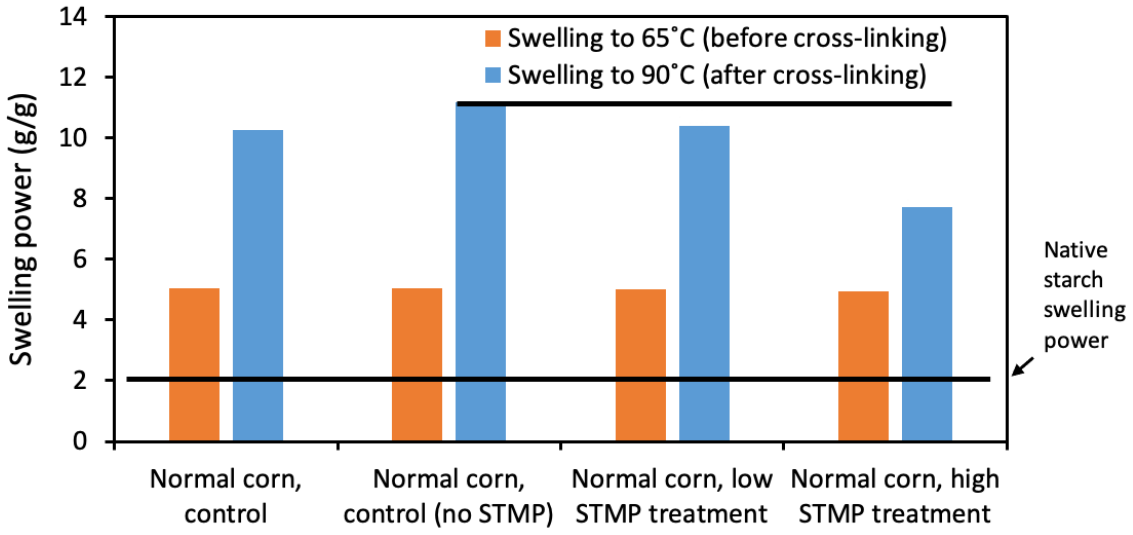

Figure 5.11: Swelling powers of normal corn starch after initial swelling at 65˚C (orange) and then swelling at 90˚C after crosslinking with STMP (blue). The first control had the exact same heat treatment, but no chemicals added. The second control, "no STMP," had the exact same heat treatment and all chemicals added for the cross-linking step other than the cross-linker (STMP) itself. The low and high treatments had 40 µg and 200 µg of STMP added during the cross-linking step, respectively.

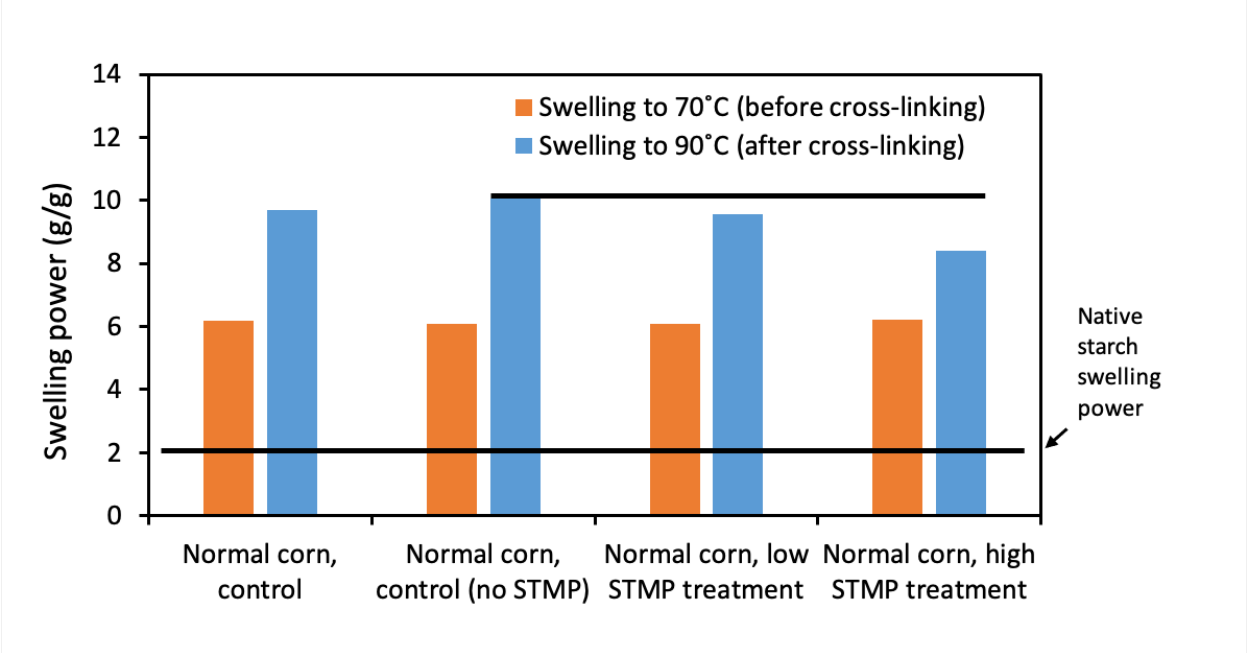

Figure 5.12: Swelling powers of normal corn starch after initial swelling at 70˚C (orange) and then swelling at 90˚C after crosslinking with STMP (blue). The first control had the exact same heat treatment, but no chemicals added. The second control, "no STMP," had the exact same heat treatment and all chemicals added for the cross-linking step other than the cross-linker (STMP) itself. The low and high treatments had 40 µg and 200 µg of STMP added during the cross-linking step, respectively.

5.4.9 Zeta potential of partially swelled normal corn starch

Zeta potential, a measure of the electrokinetic potential of a particle in solution, can provide insight on how drugs will interact with the particles. We measured this for native and swelled normal corn starch and found negative values for all, with native normal corn starch being the most negative (Figure 5.13). Our negative zeta potential result for native corn starch is in agreement with literature results where zeta potentials of roughly -39 mV for native rice starch (Wongsagonsup et al., 2005) and -40 mV for potato starch and -30 mV for wheat starch (Marsh & Waight, 1982) were reported. Since zeta potential depends on the density

of the surface charge of the particles, we speculate that the greater diameter of the more swelled starch is a key factor that results in weaker zeta potentials. The negative charge of native granules is thought to be due to lipids with zwitterionic species which are negatively charged at ~pH 7 (Marsh & Waight, 1982). It should also be noted that when converting the electrophoretic mobility to zeta potential, it is assumed that the particles are spherical, and while the starch particles are somewhat spherical, they are not perfect spheres. Our results indicate that positively charge species will interact more favorably with the microparticles than negatively charged species and could leader to higher loading capability.

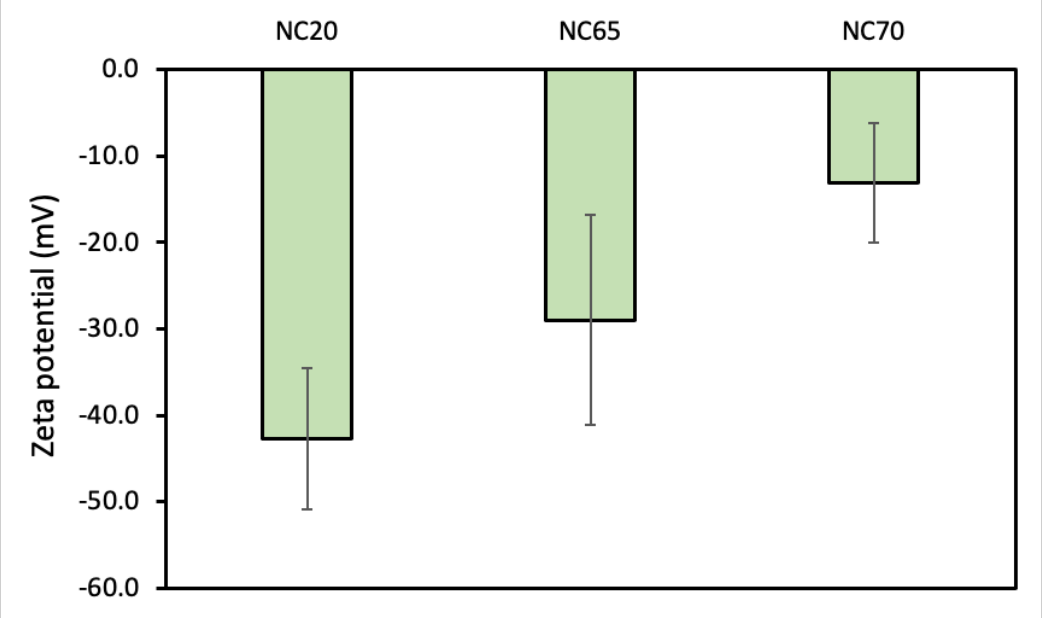

Figure 5.13: Zeta potential of native normal corn starch (NC20), NC65, and NC70. N=3, error bars represent SD.

5.4.10 Selective water uptake in native and swelled starch

A method for rough characterization of a hydrogel's pore sizes is to measure the amount of water that is selectively absorbed by the microparticles. The theory behind this method will be elaborated on further in

Chapter 6. We observed that all microparticle samples selectively uptake water. This is the result of hard sphere exclusion due to the relatively large size of BSA. We speculate that the decrease in water uptake for the NC100 could be the result of the polymer mesh size opening up, which allows for BSA to begin to enter the particles at this swelling extent.

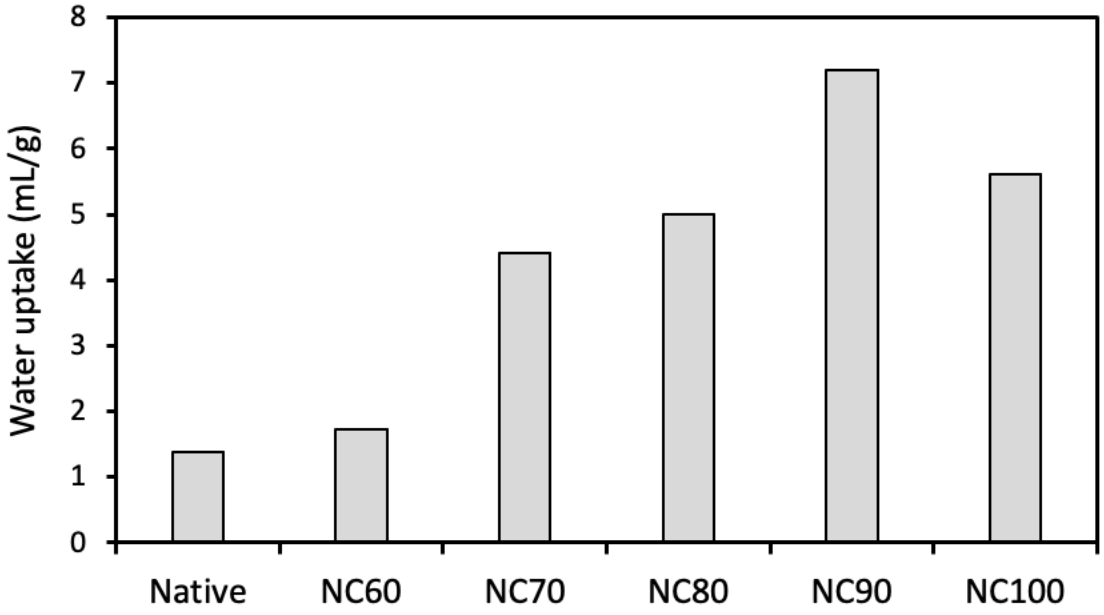

Figure 5.14: Selective water uptake by native and partially swelled normal corn starch when placed in a solution of 20 mg/mL BSA.

5.5 Conclusion

This work presented in this chapter investigated various properties of various types of starch with the goal of establishing what sort of microparticles would make the best candidate for use in a drug delivery system. Our characterization of swelling powers and images of swelled starch revealed that that normal corn, pea, and wheat starch seemed like good options based on the ability to control swelling and rudimentary

morphological observations. SEM imaging revealed distinct internal cavities in partially swelled normal corn starch, which moved it to be the top contender for use in a drug delivery system. The internal cavity seemed as though it could be used to encapsulate drugs.

Particle size distributions indicated that the particles have a somewhat polydisperse size distribution, in agreement with our microscopy images. Through measuring the FWHM for the distributions, it appeared as though the particles first became more polydisperse as the particles swell moderately, which is likely the result of differences in the susceptibility of particles to swelling at a given swelling temperature. However, as we increased the swelling temperature (and thus created more swelled particles) the particles became more monodisperse, which we conjecture is the result of unswelled particles catching up to the already-swelled particles. Swelling power, a useful measure of swelling extent, depends on the centrifugal pressure, with greater centrifugal force leading to smaller swelling pressures, the result of swelling reducing the mechanical rigidity of the microparticles.

Digestibility, an important characteristic of a microparticle system intended for oral drug delivery, was determined to be much higher for partially swelled starch compared to that of native granules. Through analysis of the supernatant after swelling we determined, in agreement with work by others, that amylose preferentially leaches out. Cross-linking of partially swelled normal corn and pea starch was tested as method for increasing stiffness. By measuring the swelling power of cross-linked starch when heated, we determined that cross-linking normal corn starch increased its rigidity. The effect on pea starch was comparably negligible.

An important characteristic of a microparticle that is intended to be loaded with drugs through adsorption is its surface charge. Negative zeta potentials, indicating negative surface charge, were measured for NC20, NC65, and NC70, with NC20 having the greatest negative charge. Lastly, selective absorption of water was

demonstrated with NC20 through to NC100; the mechanism for this selective absorption is hard sphere size exclusion of BSA due to BSA's relatively large size.

Chapter 6: Drug loading and release from starch microcapsules

6.1 Summary

Native and swelled starch were loaded with methylene blue (MB) at various concentrations to establish loading abilities. A unique problem with characterizing loading of microparticles in solution through adsorption is knowing the interstitial and intraparticle volumes. We describe the combination of both of these volumes as the drug-accessible-water volume. To deal with this unknown, it is necessary to perform the right set of experiments to allow for it to be solved for. We conducted these experiments with methylene blue and observed adsorption for native normal corn starch, SMC65, and SMC70 of 3.61, 2.14, and 2.06 mg/g and loading capacities of 3.81, 5.11, and 9.65 mg/g, respectively. We also conducted preliminary investigations into how the interstitial volume can be calculated, however more work beyond what is included here is required to calculate the value for each type of microparticle. Confocal laser scanning microscopy was also used to visualize the location of loaded RITC-dextran and FITC-BSA.

6.2 Introduction

Characterizing the ability of a microparticles to uptake and release drugs is a key step in creating a microparticle-based drug delivery system. In most cases, a high drug loading capacity is desired. Some microparticle systems are loaded during microparticle formation and others are loaded after. If the particles are loaded during formation, depending on the particle characteristics, the particle loading efficiency may be close to 100%. Particles loaded during particle formation also generally have a very high loading

capacity. When particles are loaded after formation, the primary mechanism for loading is generally adsorption; however, some drug will also be loaded through absorption. If loaded through soaking in the drug solution, the limitation is the maximum adsorption of the polymer in solution. If loaded through freeze drying or spray drying, typically more drug can be loaded as most of the drug in the initial solution ends up dried onto or into the microparticles.

In the work in this chapter, we attempt to characterize the loading characteristics of both native granules and swelled starch microcapsules (SMCs) from normal corn starch.

6.2.1 Measuring interactions between drugs and hydrogels

Since much of this chapter deals with characterizing the interactions between drugs and SMCs, a brief overview of drug-hydrogel interactions is provided. Although the term "drug" is used, this discussion applies to any solute. Characterizing adsorption of a drug with a hydrogel has been well studied. Adsorption is often used to measure the loading capacity of the hydrogel. The typical method for testing adsorption capacity is to place the hydrogel in a solution of the drug and measure how the drug concentration changes in the bulk solution. A simple mass balance can be done to calculate how much of the drug has been removed from the bulk. This amount of drug that is now in the hydrogel is used to calculate the loading capacity (LC) of the hydrogel, which is defined as

$$LC \stackrel{def}{\equiv} m_{drug}/m_{gel}$$

where m_{drug} and m_{gel} are the weights of the drug in the hydrogel and the weight of dry hydrogel polymer, respectively. Loading capacity is often interpreted to be the adsorption capacity of the hydrogel, but these two capacities are rarely equivalent. If there is a high water content of the hydrogel, it is likely that there is some drug in the hydrogel that is not actually adsorbed onto the hydrogel polymer. A better way to

characterize such a system is to calculate the equilibrium partition coefficient, k, which is defined by (Kotsmar et al., 2012)

$$k \stackrel{\text{def}}{\equiv} C_{gel}/C_{bulk}$$

where C_{gel} is the drug concentration in the hydrogel (per unit volume of the gel – both water and polymer) and C_{bulk} is the drug concentration of the external solution equilibrated with the gel.

To account for the water in the hydrogel that contains the drug at a concentration of C_{bulk}, it is useful to use what Kotsmar et al. (2012) have called an enhancement factor, E, which is defined by

$$E \stackrel{\text{def}}{\equiv} k/\phi_w$$

where ϕ_w is the water volume fraction of the hydrogel.

If E = 1, there is either no interaction between the drug and the polymer or there is equal competing specific adsorption and size exclusion, which balance each other out. If E>1, then adsorption dominates. If E<1, then size exclusion dominates. If the drug size is large enough to completely prevent permeation of drug into the hydrogel, then E = 0.

The factors that contribute to the enhancement factor, E, can be further defined, as described by Dursch et al (2014) when it is assumed that the free energies from different molecular combinations can be added together. This assumption is reasonable when the solution is dilute. With this assumption, the enhancement factor is defined as follows:

$$E \stackrel{\text{def}}{\equiv} E_{ex}E_{el}E_{spad}$$

where E_{ex} designates hard-sphere size exclusion, E_{el} designates nonspecific electrostatic interaction, and E_{spad} designates specific solute adsorption on the polymer strands. While these authors differentiate between E_{el} and E_{spad}, they can also be combined into E_{ad} to represent total adsorption where $E_{ad} = E_{el}E_{spad}$.

6.3 Materials and Methods

6.3.1 Materials

Normal corn (maize) starch was purchased from Sigma-Aldrich (S4126, Lot #: MKBT0621V) (Oakville, Canada). The apparent amylose content of the native starch was 27.8% as determined by the method of Williams et al. (1970). The moisture content was 14.3%, determined by the difference in weight as a fraction of the initial weight after drying for 16 hours at 100˚C. BSA, lysozyme, blue dextran, methylene blue, Fast Green FCF, FITC-BSA and RITC-dextran (MW: 70,000) were purchased from Sigma-Aldrich.

6.3.2 Preparation of starch microcapsules (SMCs) through heating in water

The starch microcapsules (SMCs) were prepared through a simple heat-treatment process. Native corn starch (0.7 g, dry basis), as received from the supplier, was added with Milli-Q water or PBS (14 mL) in a centrifuge tube at a concentration of 5% w/w (native, dried starch basis). To swell the starch, the centrifuge tube was placed in a water bath at the required heating temperature (65-75˚C) for 30 min with stirring of the water bath with a magnetic stirrer. The height of the water in water bath was carefully controlled to also cause gentle agitation of the centrifuge tube. After the starch was swelled, the starch mixture was cooled immediately to 20˚C by placing the centrifuge tube in a cold-water bath. For the MB adsorption experiment, the particles were freeze dried. For experiments where non-dried particles were required, the particles remained in solution and stored in the fridge until use.

6.3.3 Methylene blue adsorption

Freeze dried starch samples (~80 mg) were added to 1.7 mL microcentrifuge tubes with methylene blue solution at various concentrations. After 16 hours (with rotation to ensure mixing), the tubes were centrifuged at 1000g for 1 min and the supernatant was analyzed using UV-vis spectroscopy at 660 nm. The supernatants were diluted as needed to ensure they were the linear range for concentration measurement and concentrations were determined from a standard curve.

6.3.4 Model drug interactions with still-wet swelled starch

SMCs were prepared as previously described in 15 mL centrifuge tubes but with PBS as the solvent. After decanting the supernatant, 10 mL of drug solution was added and allowed to equilibrate for ~4 hours. Model drug solutions included the following: BSA at 2 mg/mL, lysozyme at 300 µg/mL, methylene blue (MB) at 100 µg/mL, blue dextran (BD) (2,000 kDa) at 1 mg/mL, Fast Green FCF at 200 µg/mL. Two measurements were taken to ensure the consistency of the results. The samples were then decanted, and 3 mL of PBS was added to act as the release media. Again, the mixture was allowed to equilibrate for ~4 hours and two measurements were taken.

Concentrations for proteins (BSA and lysozyme) were measured through use of the BCA (bicinchoninic acid) total protein assay method with BSA protein standard at 2 mg/mL used as the calibration standard. The standard curve was fit to a 2^{nd} order polynomial for the range from 0-2 mg/mL. Concentrations for MB, BD, and fast green FCF were determined through UV-vis spectroscopy at their highest peaks of 660 nm, 620 nm and 622 nm, respectively using linear standard curves in their linear concentration ranges.

6.3.5 Fluorescent microscopy of starch

Starch samples (native and SMC) were added to a solution of rhodamine B isothiocyanate conjugated with dextran (RITC-dextran) with a molecular weight of 70,000 g/mol at a concentration of 5 mg/mL and were left overnight at room temperature (~20˚C) for loading of the particles. After loading, and about 15 min before the images were captured, 100 µL of the wet loaded particles were placed on filter paper using a pipette to wick away excess liquid. The particles were then removed from the filter paper and place on a microscope slide. A drop (~50 µL) of fluorescein isothiocyanate conjugated with BSA (FITC-BSA) solution at a concentration of 5 mg/mL was placed on the particles already on the microscopy slide and a coverslip was placed on top. Nail polish was used to seal between the edges of the coverslip and the slide to prevent evaporation and movement. Once the nail polish was dry (~5 min), the slide was placed on the microscope and images were taken using a confocal microscope (LSM 700, Carl Zeiss, North York, Canada) with illumination by the 488 nm laser using a 100x oil emersion objective.

6.4 Results and Discussion

A goal of our work was to load the SMCs with drugs with the intent of being able to use them for drug delivery. Although beyond the scope of our current work, we imagined the particles could be used for controlled release for either oral or topical delivery of drugs. We did testing with several drug models: methylene blue, BSA, lysozyme, blue dextran, and fast green FCF. While we conducted various tests with the different molecules, we characterized the interaction of SMCs with methylene blue most thoroughly. We discuss this characterization first.

A key to characterizing interactions of various model drugs with SMCs is to understand both the internal structure of the SMCs and how the particles are packed together in solution.

6.4.1 Characterizing adsorption of methylene blue to SMCs

When microparticles are in solution, it is possible to measure the drug adsorption amount through calculating the change in concentration of the bulk volume. There is an added challenge in that the microparticles have drug solution between the individual microparticles, which we have called the interstitial volume However, one of two things is generally assumed depending on if the microparticles are already wet or not. If wet, it is assumed that the water already contained within the hydrogel does not dilute the drug loading solution. If dry, it is assumed that there is no interstitial volume between the microparticles (i.e. $E_{ex} = 1$). In some cases, these assumptions may not affect the results significantly. But, depending on the hydrogel mesh size, the drug size, the water content of the hydrogel/microparticles, and the adsorption capacity of hydrogel, these assumptions can mischaracterize the nature of the interactions.

Figure 6.1 demonstrates the various components of a system of microparticles and a drug solution in a test tube. In a conventional hydrogel system, the hydrogel takes up any volume that isn't V_{bulk}, however in microparticle system $V_{interstitial}$ must be considered as well. We refer to the combination of $V_{microparticles}$ and $V_{interstitial}$ as $V_{sediment}$:

$$V_{sediment} = V_{microparticles} + V_{interstitial}$$

We refer to the paste-like volume at the bottom of the test tube as "sediment". The sediment settles to the bottom over time due to the higher density of starch polymers compared to the density of water. We define V_{starch} as the volume of the microparticles that contains starch polymer only or starch polymer and water; it is the volume of the particle that does not contain methylene blue (MB) in solution. It is possible for MB solution to reach V_{intra} though the non-homogenous V_{starch} shell if there are pores or if there are areas with a mesh size large enough for MB to traverse through.

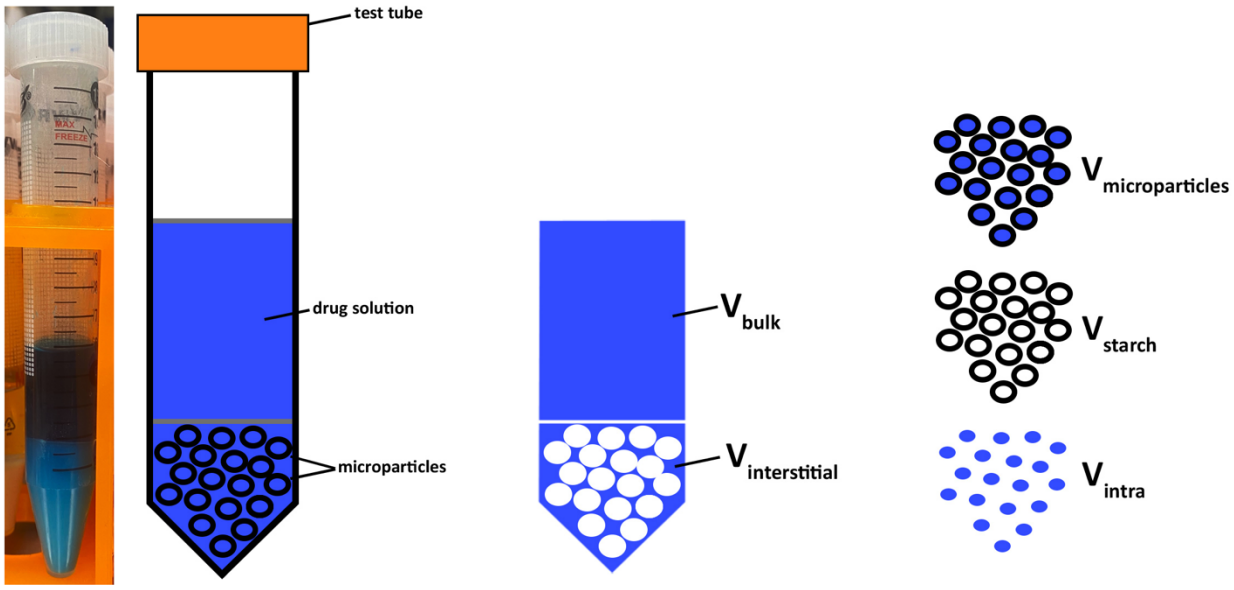

Figure 6.1: Schematic of microparticles in solution.

When a drug solution is added to a solution of dry microparticles and allowed to equilibrate, we can measure the change in concentration of the bulk to characterize nature of the interaction between the drug and the microparticles. This data is shown in Figure 6.2 for various concentrations of MB and with NC20, NC65, and NC70. We refer to SMCs starch type (normal corn – NC), and the heating temperature. The loading concentration is measured prior to adding the MB solution to the dry microparticles. When a high concentration of MB is added to the microparticles (e.g. Figure 6.2b), some MB is adsorbed onto the microparticle polymer; however, as the particles become saturated with MB, most of the MB remains in solution. Conversely, when a low concentration of MB is added to the microparticles (e.g. Figure 6.2g), most of the MB is adsorbed onto the microparticles polymer leaving little in solution. This observation is true for NC20, NC65, and NC70 microparticles. Another way to look at the data is to compare how NC20, NC65, and NC70 differ in how the MB solution concentration changes for a given loading concentration.

In Figure 6.2a, we observe that the concentration is reduced the most by the NC20 sample and the least by the NC70 sample, with the NC65 result falling in between. This indicates that the native starch is best at adsorbing MB.

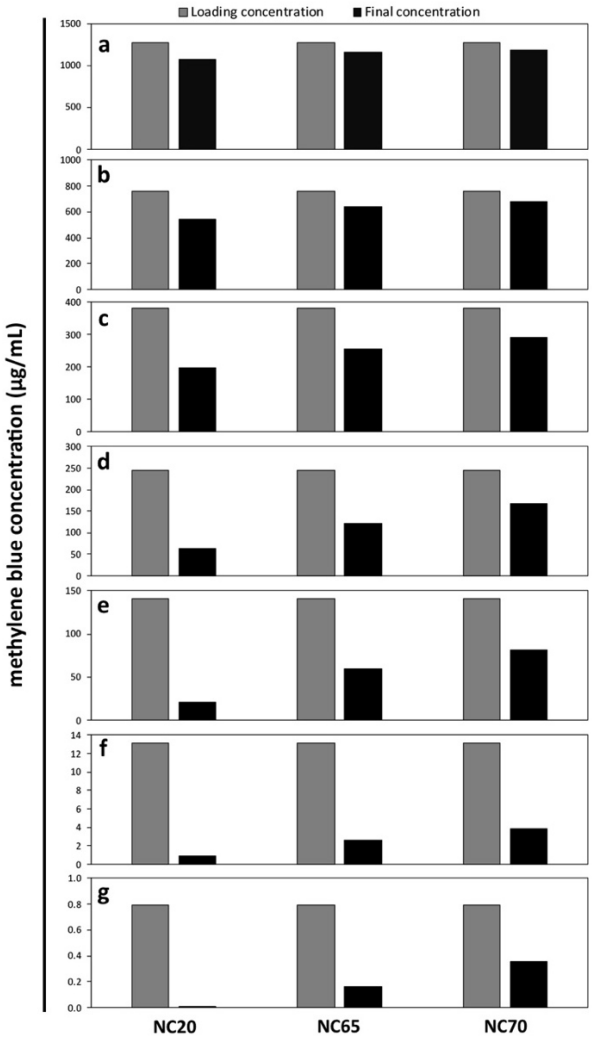

Figure 6.2: Methylene blue loading concentrations (grey) and final equilibrium concentrations after loading (black) for various initial loading concentrations with the highest loading concentrations (a) at the top to the lowest (g) at the bottom. Each test was conducted with NC20, NC65, and NC70 starch microparticles.

A more standard method for characterizing the hydrogel-drug interaction is to calculate the partition coefficient, as explained in Section 6.2.1. The coefficient will be a function of the bulk MB concentration. Since the bulk concentration is already known (i.e. the final concentration in Figure 6.2), only the microparticle concentrations must be calculated. Calculating the microparticle concentration is challenging because we have an unknown variable: the amount of MB within the microparticles. If it is assumed that $E_{ex} = 1$, then the reduction of MB in the bulk can only be attributed to adsorption. If $E_{ex} < 1$ and it is assumed that $E_{ex} = 1$, the measurement for the amount of MB adsorbed will be lower than what it really is. The assumption that $E_{ex}=1$, although probably not too incorrect for MB due to its small size, is not reasonable for larger molecules.

There is going to be MB in the sediment that is not adsorbed onto starch due to $V_{interstitial}$. Further, as long as V_{intra} is nonzero, there will also be MB that is in the microparticles, but not adsorbed. To account for the volume in the sediment that contains MB solution at a concentration of C_{bulk} (i.e. $V_{interstitial} + V_{intra}$), an experiment must be done in the range of C_{bulk} where the starch polymer is fully saturated with MB. We call the volume in the sediment that has MB at a concentration of C_{bulk} the drug-accessible water (DAW):

$$V_{DAW} = V_{interstitial} + V_{intra}$$

By making an assumption for what V_{DAW} is for each and using the data in Figure 6.2 we can plot C_{bulk} vs. q_e to determine how high C_{bulk} needs to be for the starch to be saturated with MB, where q_e (mg/g) is the amount of MB adsorbed at equilibrium per mass of starch. Once this concentration is known, we can do a mass balance for the amount of MB in the sediment between two experiments, one at a lower C_{bulk}, which we call $C_{bulk,a}$, and one at a higher $C_{bulk,}$ which we call $C_{bulk,b,}$, to calculate V_{DAW}. The resulting equations are:

$$m_{MB,sed,a} = C_{bulk,a} \cdot V_{DAW} \cdot m_{st,a} + q_{e,a} \cdot m_{st,a}$$

$$m_{MB,sed,b} = C_{bulk,b} \cdot V_{DAW} \cdot m_{st,b} + q_{e,b} \cdot m_{st,b}$$

In this case, V_{DAW} is the specific volume (mL/g) per mass of starch.

We then make the assumption that $q_{e,a} = q_{e,a} = q_e$ due to MB being fully saturated. After arranging we obtain

$$V_{DAW} = \frac{\frac{m_{MB,sed,a}}{m_{st,a}} - \frac{m_{MB,sed,b}}{m_{st,b}}}{C_{bulk,a} - C_{bulk,b}}$$

The result of calculating V_{DAW} with the results in Figure 6.2a-c and averaging the two results is given in Figure 6.3.

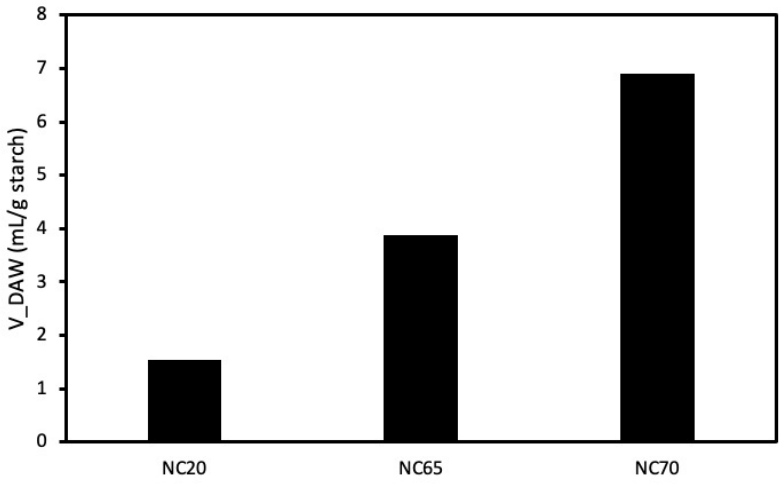

Figure 6.3: The volume of drug-accessible water (DAW) for NC20, NC65, and NC70 based on MB adsorption.

Although we now know V_{DAW}, we still do not know how much of it consists of $V_{interstitial}$ compared to V_{intra}. If the packing factor for the microparticles is known, then $V_{interstitial}$ can be calculated. The packing factor (PF) is defined as

$$PF = V_{microparticles}/V_{sediment}$$

The packing factor for native normal corn starch, or NC20, can be calculated geometrically based on the swelling power. However, assumptions for the porosity of the native granules and the density of starch polymer must be made. We measured the porosity of native normal corn starch using nitrogen gas adsorption to be about 0.01, however this method is not effective at measuring micropores (pores > 50 nm), which could be significant contributor to native granule porosity. We can however use the water content of native normal corn starch (~19 vol. %) as a rough estimate for porosity. Particle density was measured for corn starch as 1.5 g/mL for starch with a water content similar to ours by Marousis and Saravacous (1990), which is what we used. The resulting PF for native normal corn starch is calculated to be 0.505.

By assuming that the packing factor for swelled starch is the same as that of native granules, the swelling power for swelled starch can be estimated as a function of swelling extent, which we can compare to our experimental results. The swelling extent (α) is the ratio of swelled particle radius to the native granule radius (see discussion in Section 4.4.3). Due to some uncertainty from our assumptions, we performed a sensitivity analysis to evaluate the effect of changes in our assumptions (Figure 6.4). Most notably, at high swelling extents, the only way for our experimental results for swelling power to match geometrically calculated swelling powers, the packing factor must increase beyond the initial ~0.5 of the native starch granules to about PF = 1. Increasing the packing factor to 1 only helps for particles with $\alpha<2$. Beyond this swelling extent, packing factor must increase beyond 1 to match our experimental results. While PF>1 is

technically impossible for rigid particles, our particles are “squishy.” We speculate that, when centrifuged, the particles shrink through centrifugal pressure, effectively resulting in a PF>1. In other words, the original total particle volume prior to compression is greater than the total sediment volume when the particles are centrifuged. This speculation matched with results where we compared the effect of centrifugal force on swelling power (Section 5.4.5). We also observed decompression in NC70 of about 5% vol. in 20 minutes after centrifuging at 21,000g for 15 min, in agreement with our speculation. No decompression was observed for NC20 under the same conditions. This observation also indicates that the swelled particles have some compressive elasticity.

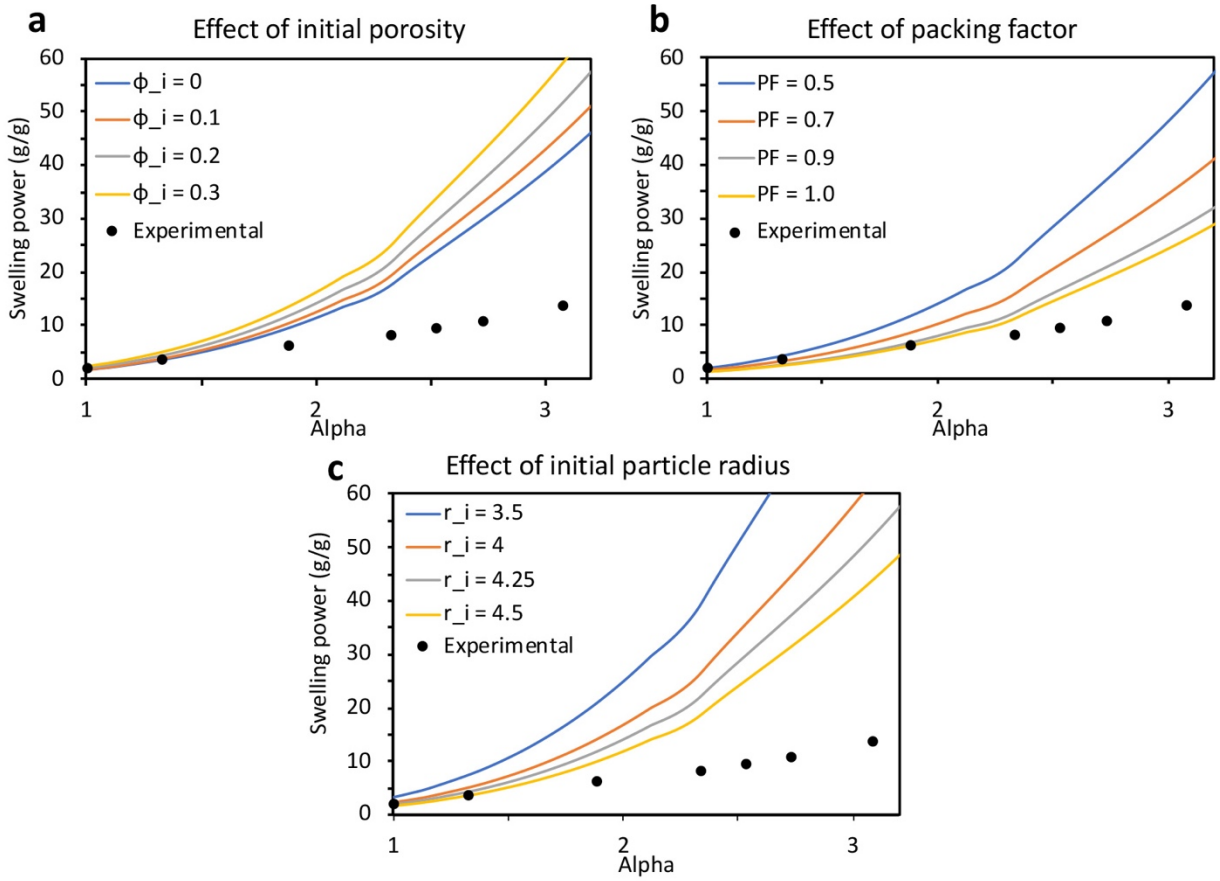

Figure 6.4: Sensitivity analysis on calculated swelling powers from swelling extent (alpha). The initial porosity was changed while the other variables were held constant with PF = 0.5 and r_i = 4.25 µm (a). Packing factor was changed while the other variables were held constant with r_i = 4.25 µm and ϕ_i = 0.2 (b). The initial particle radius was changed while the other variables were held constant with PF = 0.5 and ϕ_i = 0.2 (c).

Based on our comparison of theoretical calculations for swelling power from particle swelling extent and based on our PF calculation for native granule starch, for further calculations, we have assumed that PF_{NC20} = 0.5, PF_{NC65}= 0.75, and PF_{NC70} = 1. With these assumptions we are now able to calculate $V_{microparticles}$ for our MB adsorption experiments, and thus, enhancement factors can be calculated (Figure 6.5). We observed that our calculated enhancement factors decrease at C_{bulk} increases, as expected. Of greater significance is

that native normal corn starch has a much higher enhancement factor compared to NC65, and higher still compared with NC70. We speculate the surface charge of native starch plays a large role in the adsorption capacity, as suggested by the more negative zeta potential (Section 5.3.10) of native starch compared with the partially swelled starch.

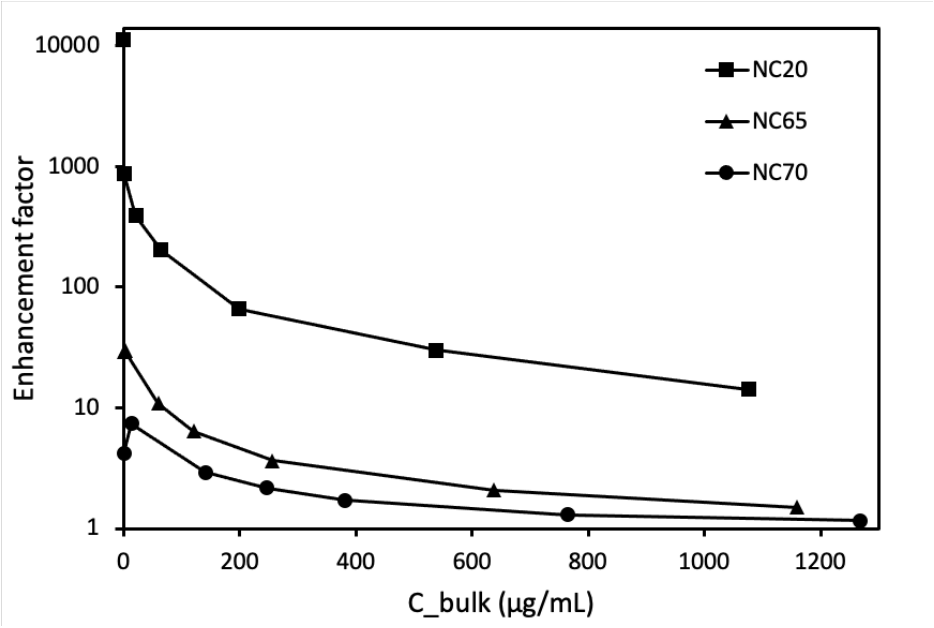

Figure 6.5: MB microparticle enhancement factors for NC20, NC65, and NC70 samples as a function of bulk MB concentration.

Unfortunately, we are not aware of any results in literature that has measured the enhancement factor for starch with MB. However, we can compare our results with others' by using the Langmuir adsorption model. The model, which assumes monolayer adsorption onto a flat plane, allows us to calculate q_m and b. While the assumptions are likely not particularly valid for a hydrogel, the model is often used in literature for modeling of drug adsorption onto hydrogel microparticles, and as such allows for comparison to others' results. We use the linear form of the equation,

$$\frac{C_{bulk}}{q_e} = \frac{1}{q_m b} + \frac{C_e}{q_m}$$

where q_e is the amount of MB adsorbed at equilibrium at a given C_{bulk}, q_m is the maximum adsorption capacity, and b is the Langmuir adsorption constant. Using the fitted equations (Figure 6.6), we obtain the results in Table 6.1.

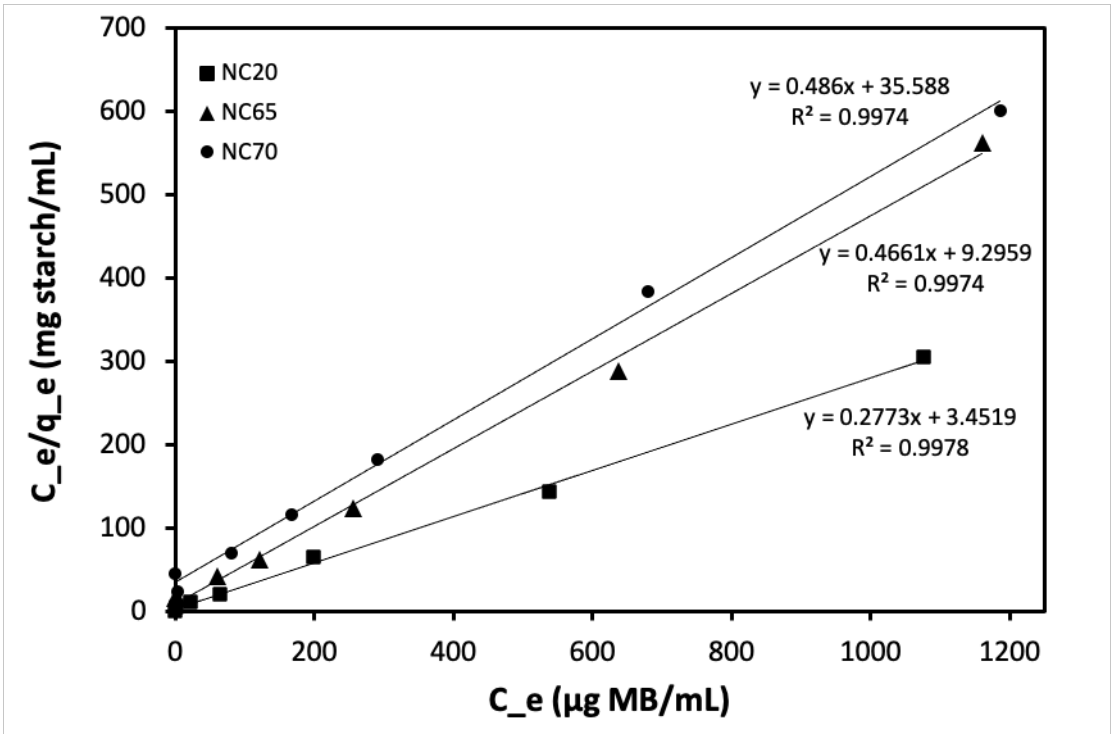

Figure 6.6: MB adsorption results with linear fits for calculating Langmuir isotherm parameters.

Although it is common to also model adsorption results with the Freundlich adsorption isotherm, based on work by others who looked at the adsorption of MB with cross-linked starch (Guo et al., 2013; X. F. Zhao et al., 2008), humic acid-functionalized starch (R. Chen et al., 2015), a porous graphene oxide/hydrogel nanocomposite (Pourjavadi et al., 2016), and Moroccan clay (El Mouzdahir et al., 2007) where they all

observed a much better fit with the Langmuir isotherm, we did not see the need for testing the Freundlich model with our results.

Table 6.1: Langmuir isotherm model parameters based on the adsorption of methylene blue (MB) into starch microcapsules.

Microparticle type	q_m (mg MB/g starch)	b (L/g starch)
NC20	3.61	0.080
NC65	2.14	0.050
NC70	2.06	0.014

R. Chen et al. (2015) studied the effect of starch grafted with humic acid on its ability to adsorb MB and measured adsorption capacity ($q_{e,max}$) of ~7 mg/g at neutral pH (compared to ~90 mg/mg for starch-humic acid). Unfortunately, they did not report the type of starch they used. Our result of q_m = 3.61 mg/g for native corn starch is comparable. Junlapong et al. (2020) reported an adsorption capacity of ~2000 mg/g with a hydrogel based on cassava starch and acrylamide, however this result seems unlikely as most reports of MB adsorption onto activated carbon are less than 500 mg/g.

A final comparison of MB adsorption to loading capacity illustrates the difference between the two characterization methods. The maximum loading capacities are given in Table 6.2. Loading capacity increases as swelling increases due to the higher volume of the microparticles, which led to a higher drug-accessible-water volume within the microparticles (i.e. V_{intra}).

Table 6.2: Loading capacities of methylene blue (MB) into normal corn microcapsules.

Microparticle type	LC_{max} (mg MB/g starch)
NC20	3.81
NC65	5.11
NC70	9.65

6.4.2 Analysis of drug-accessible water through drug loading and release

From our analysis in the previous section of loading of native and swelled starch, we had a good estimation of the drug-accessible water (DAW) for a starch-MB system which helped with charactering the absorbed MB amount. This DAW only applies to that system. Use of a different drug or adding another solvent could give different results. Our intent was to characterize the true interstitial volume ($V_{interstitial}$) rather than use our estimate based on geometrical calculation as we did in the previous section. We quantified how various model drug solutions would be diluted by adding the solution to the already "wet" microparticles (i.e. the sediment) whereby the drugs become loaded into the microparticles. After loading, we then decanted the supernatant – leaving the drug-loaded microparticles in sediment – and then added drug-free solution to the sediment to evaluate how much loading solution was left in the sediment based on dilution. If one of our model drugs was both a) large enough that through size exclusion no drug would enter the microparticles (i.e. $E_{ex} = 0$) and b) non-adsorbent towards the outside of the microparticles (or at least this adsorption was negligible), $V_{interstitial}$ could be calculated. The amount of $V_{interstitial}$ for each of our model drugs, with making both those assumptions, is shown in Figure 6.7. Our results are somewhat inconclusive, but some

observations can be made. Unlike with the previous loading experiments, these particles were swelled in PBS instead of in water.

Since BSA and blue dextran are the largest two molecules, we would expect one of these to give the lowest values of the specific volume. The lower the specific volume, the more size exclusion dominates over adsorption. However, while the results for BSA are all positive values and reasonable, some of our results from blue dextran were negative, which cannot be the case as there is no mechanism to cause the blue dextran concentration to increase.

Also of interest is that for the BSA results, the specific volume increased as the particles became more swelled. This increase could be the result of greater interstitial volume simply due to granule swelling; however, for the interstitial volume to be the main reason for the increased specific volume, the packing factor needs to stay close to the packing factor of the unswelled granules. However, an unchanging packing factor seems unlikely due to the high compressibility of the particles. What is more likely is that the increase could be the result of the mesh size of the swelled starch increasing enough to let BSA enter the swelled particles, which effectively allows for greater reduction in $C_{bulk,BSA}$, which results in a higher specific volume. In other words, the native starch might not be permeable to BSA, but upon swelling the increased mesh size allows for diffusion of BSA into the particles.

One final observation is that with methylene blue, we observed an opposite trend compared to our similar experiments in pure water: greater swelling of PBS-swelled particles led to higher adsorption of MB. We speculate that this result could be from competition and/or shielding by ions in PBS with regard to the starch polymer.

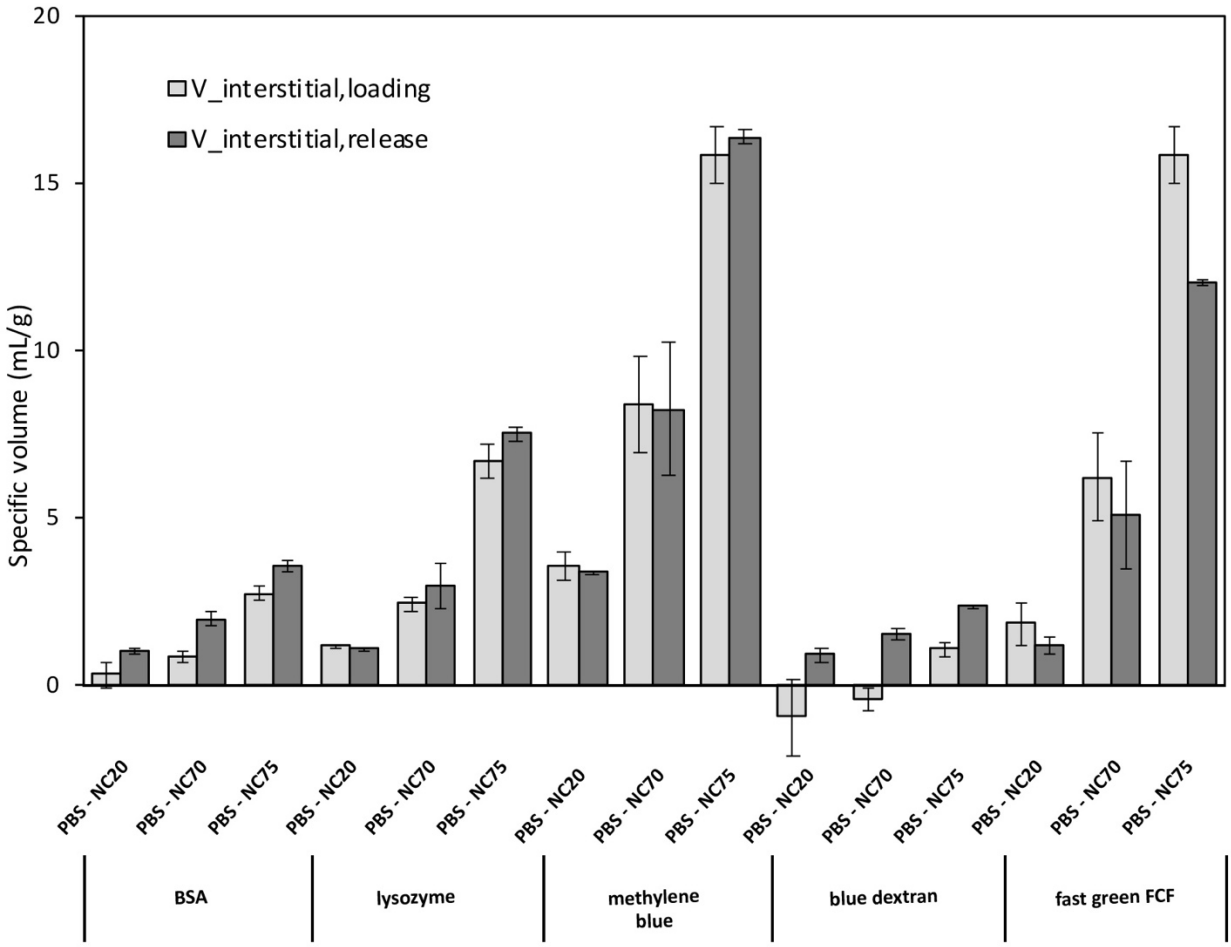

Figure 6.7: $V_{interstitial}$ results for loading and release of BSA, lysozyme, methylene blue, blue dextran, and fast green FCF. N=2. Error bars represent SD.

6.4.3 Confocal laser scanning microscopy of microparticles loaded with model drugs

Confocal laser scanning microscopy can be a useful tool for observing the interior of microparticles. The ability to only observe a cross-section of a sample that contains a fluorescent dye can allow the observer to see exactly where that dye is spatially. The images are particularly useful with a rather nonhomogeneous system like we have with the SMCs. The result of loading our particles with RITC-dextran (70kDA)

followed by brief washing with a solution of FITC-BSA and then immediate observation is shown in Figure 6.8 The initial loading step with RITC-dextran allowed for equilibrium loading of RITC-dextran (stokes radius: 5.8 nm). The washing with FITC-BSA washed out any free RITC-dextran. We observe that with NC20, both RITC-dextran and FITC-BSA appear to adsorb onto the outer edge of the granules. For NC70, we notice that while most particles that likely previously contained RITC-dextran solution are washed out by the FITC-BSA, there are three particles (white arrows in Figure 6.8) that easily retain the RITC-dextran solution, indicating that the particles have walls that are fully intact and, at a minimum, prevent quick leakage of the encapsulated solution.

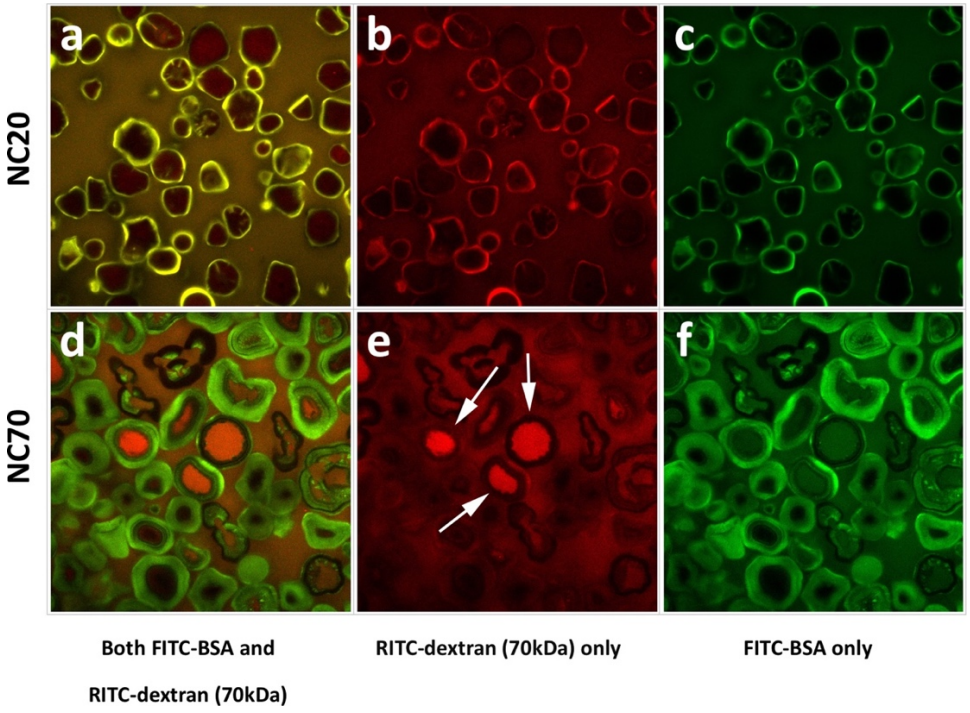

Figure 6.8: Confocal laser scanning microscopy of NC20 and NC70 microparticles. Each set (NC20 and NC70) of images were all taken moments apart with images (a) and (d) depicting excitation/emission of both FITC-BSA and 70kDa RITC-dextran, with images (b) and (e) depicting excitation/emission of only RITC-dextran, and with images (c) and (f) depicting excitation/emission of only FITC-BSA.

6.5 Conclusion

Our work in this chapter demonstrated a novel method for characterizing adsorption of a solute onto and into microparticles in a way that accounts for the interstitial volume and the volume inside the microparticles themselves. This method is helpful for isolating the amount of drug that is truly adsorbed on the microparticles and not just encapsulated simply due absorbed solution at the bulk concentration. Using this method, we calculated the volume that methylene blue (MB) can access within the starch sediment, and we observed that greater swelling led to a higher volume of this drug-accessible water.

The relationship between swelling extent and swelling power can be calculated geometrically after using some assumption and estimates for some variables. Our comparison with our experimental results revealed that it seems likely that the packing factor increases from about 0.5 for native normal corn starch granules to roughly 1 for NC70. For particles with greater swelling than NC70, for our results to match the theoretical swelling powers, the packing factor must be greater than one. We interpret this result to mean that our particles are greatly compressed during centrifugation, resulting in the total sediment volume being smaller than the initial total microparticle volume prior to centrifugation. Estimations of the packing factor for each type of microparticle made it possible to calculate the concentration of MB for the microparticles themselves. These concentrations made it possible to calculate the enhancement factor for the MB-microparticle system for NC20, NC65, and NC70 as a function of bulk MB concentration. As expected, NC20 has the highest enhancement factor. Through Langmuir isotherm modeling, we established that native normal corn starch has a higher adsorption capacity compared with swelled SMCs. However, due to the higher water content and higher swelled volume, the loading capacity is technically higher for NC70 compared with NC20.

In order to evaluate the capacity of microparticles for drug delivery, it is useful to characterize the interaction between several model drugs with the microparticles. We conducted a set of experiments where we added solutions of five different model drugs to already-wet starch. Our hope was also that one of our drugs would be large enough that hard-sphere size exclusion would dominate, which would allow for calculation of the interstitial volume for each microparticles type. The starch-BSA interaction appears to be dominated by size exclusion. The volume in the sediment that can be diluted by a BSA solution increases as swelling extent increases. We speculate that this increased volume is the result of the increased mesh size from swelling, which allows entry of the relatively large-sized BSA.

Confocal laser scanning microscopy is a useful tool for observing the interaction between fluorescent dyes and microparticles. Through loading with 70 kDa RITC-dextran followed by washing with FITC-BSA, we observed differences in how particular microparticles interact with the dyes. Some particles clearly demonstrated their capacity for encapsulating dye that, at a minimum, does not leak out rapidly.

Chapter 7: Conclusions and Recommendations

7.1 Contributions

In our work, we thoroughly studied the swelling process of various starch types, with a focus on normal corn starch, in pursuit of using partially swelled starch for use in controlled release drug delivery. We refer to the partially swelled starch as starch microcapsules (SMCs).

First, we reported on application of helium ion microscopy (HIM) for imaging of native corn starch granules. We used a novel sectioning technique to allow access to the internal structure for observation with minor disturbance. We determined that HIM is a useful technique for probing starch structure and that it

can resolve features smaller than 10 nm in size. New mesh-like features not previously reported on with AFM or SEM were observed. A comparison to SEM images revealed the significant improvement in imaging resolution. HIM offers a new way to better understand the internal structure of starch granules.

Next, we studied the starch gelatinization process for normal corn starch, with an emphasis on the intermediate steps before full gelatinization. We demonstrated that swelling extent can be easily controlled through modulation of swelling temperatures and swelling times. As a result of swelling extent being closely correlated with particle size and solubility, these properties may also be controlled. The ability to tune the particles could be useful for applications in drug delivery. We characterized SMCs to understand their change in morphology as a result of swelling. The internal cavity present in native normal was shown to increase in size as the particles increase in size. We observed the structural changes in the swelling process through use of SEM, HIM, and CSLM imaging. Due to the geometry of the SMCs and their internal cavities, only a small change in particle size is required to cause a large change in the internal cavity size. We modeled this change mathematically and fit this model to our experimental data, which matched very closely.

Before proceeding further with investigation on the ability of partially swelled starch for use in drug delivery, we evaluated a few starch types to determine the best candidate for the task. Due to controllability uniformity of the internal cavity, we choose normal corn starch as the best option. We conducted extensive characterization of SMCs made from normal corn starch to help understand various aspects of its polydispersity and chemical and physical properties. We compared the changes in these properties with native starch granules. With characterizing swelling extent being vital to our work, we concluded that centrifugal force influences swelling power measurement and that the SMC are somewhat compressible. When microparticles are to be used orally, their degradation in the gastrointestinal tract is important for

how drugs are released. To understand how SMCs could react to this environment, we measured the digestibility for SMCs and established that the swelling process greatly increased the digestibility of the particles. Cross-linking could provide a method for either reducing digestibility or slowing the diffusion of drugs out of the microparticles. We cross-linked starch and used measurement of swelling inhibition to determine that the rigidity of normal corn SMCs starch increased. When drugs are to be loaded through adsorption, surface charge is important, and, using measurement of zeta potential, we determined the surface charge of normal corn starch to be negative, with greater swelling leading to less negative surface charge. Selective absorption of water in a solution of BSA demonstrated that size exclusion plays a factor, which could have implications for the loading capacities of SMCs.

In the last section of our work, we quantified the adsorption capacity of normal corn SMCs with methylene blue (MB). Work in literature has quantified adsorption of MB into starch microparticles but has failed to account for possible size exclusion. In other cases, loading capacity is determined but fails to account for the interstitial water between the particles. We quantified the interaction between MB and SMCs with taking these factors into consideration. We determined that while adsorption onto native granules was the highest, swelled SMCs allowed for the highest loading capacities. To determine the interstitial volume, a solute that exhibits complete size exclusion and no adsorption must be used. We used five different model drugs to see if any would display such behaviour. While our results were somewhat inconclusive for determining the interstitial volume, we were able to make other observations. The trend of highest adsorption of MB in native granules compared with SMCs in water was flipped when conducting the same experiment with SMCs in PBS. Finally, with use of confocal laser scanning microscopy, we observed the interaction between particles loaded with RITC-dextran followed by quick rinsing with FITC-BSA and

were able to conclude that some particles demonstrate the capacity for at least brief encapsulation of RITC-dextran.

7.2 Recommendations

To better evaluate the loading and release capability of SMCs, further testing should be done with a wider variety of large solute to determine the interstitial volume with confidence. Some of our later experiments revealed that solubilized starch affected accuracy of determining solute concentrations. While this effect can be mitigated through use of controls that can be used to subtract the effect of solubilized starch, a better solution could be to wash the microcapsules prior to conducting loading and release experiments to remove all solubilized starch.

A potential limitation for applicability of SMCs is their wide size distribution which could lead to higher variability in characteristics. Further experiments should be conducted to determine what the effect of particle size is on drug loading and release. If the effect is significant, it could be useful for develop a method for sorting the SMCs by size. It is likely that a microfluidic process could be used to take advantage of differences in particles sizes or densities.

Based on our results, drug loading and release occurs relatively quickly. Quick equilibrium is typically not ideal for a system where the idea is to have the drugs be released over a long period of time. It could be very useful to develop a method for locking in the drug after having loaded them into the particles. We suggest that cross-linking of the outer shell of normal corn SMCs could provide this ability. Another option could involve coating the microparticles with a different polymer. When the goal of a drug delivery system is to target the intestine or the colon, a pH-controlled release is generally useful. Adding a pH-responsive

polymer could allow such controlled release, with the SMCs contributing by allowing for high encapsulation with its large internal cavity.

One way to tune the properties of SMCs is to control where gelatinization occurs within the particle as a result of heating. We speculate that it might be possible to only swell the outermost part of the starch granule by rapidly passing single granules through a short heated section of tube. The rate would need be fast enough that only the outer portion of the starch granule is exposed to the high-enough heat to cause gelatinization (e.g. 70-100˚C), but that the interior remains cool due to a thermal gradient. On this scale, an individual particle likely reaches thermal equilibrium in less than a second, so the process would need to be very quick. A microfluid system with a very short heated section followed by immediate cooling would likely work.

It could be useful to allow control of each particle to allow for reaction with a specific amount of reagent or to allow for loading of a precise amount of drug. We speculate that this control could be achieved using a water-in-oil emulsion where a single particle in an aqueous solution would be isolated into an oleic carrier phase. It is conceivable that a system could be set up that adds a variable amount of the reagent based on the previously measured size of the particular microparticle. A small microneedle would be needed to inject reagents or drugs; however, these chemicals could probably be added either right before encapsulation in the oleic phase or after.

Partially swelled starch could also be investigated for use in a low porosity scaffold or foam whereby the starch microparticles would act as the template for the void spaces. Due to the apparent “squishy” nature of the particles, the contact area between particles is relatively high compared to non-compressible spheres. A polymer would be added to fill the intraparticle space that would then be cross-linked. After cross-linking, a solution of amylase would be used to selectively hydrolyze the amylose and amylopectin, leaving the

cross-linked polymer as the scaffold. Since swelled starch microparticles are roughly the same size as cells, this could work well for system where a single cell is required in each void space.

References

Achayuthakan, P., Suphantharika, M., & Bemiller, J. N. (2012). Confocal laser scanning microscopy of dextran-rice starch mixtures. *Carbohydrate Polymers*, *87*(1), 557–563. https://doi.org/10.1016/j.carbpol.2011.08.020

Adejoro, F. A., Hassen, A., & Thantsha, M. S. (2019). Characterization of starch and gum Arabic-maltodextrin microparticles encapsulating acacia tannin extract and evaluation of their potential use in ruminant nutrition. *Asian-Australasian Journal of Animal Sciences*, *32*(7), 977–987. https://doi.org/10.5713/ajas.18.0632

Ahmad, M. Z., Akhter, S., Ahmad, I., Singh, A., Anwar, M., Shamim, M., & Ahmad, F. J. (2012). In vitro and in vivo evaluation of Assam Bora rice starch-based bioadhesive microsphere as a drug carrier for colon targeting. *Expert Opinion on Drug Delivery*, *9*(2), 141–149. https://doi.org/10.1517/17425247.2012.633507

Ahmad, M. Z., Akhter, S., Anwar, M., & Ahmad, F. J. (2012). Assam bora rice starch based biocompatible mucoadhesive microsphere for targeted delivery of 5-fluorouracil in colorectal cancer. *Molecular Pharmaceutics*, *9*(11), 2986–2994. https://doi.org/10.1021/mp300289y

Ahmad, M. Z., Akhter, S., Anwar, M., Kumar, A., Rahman, M., Talasaz, A. H., & Ahmad, F. J. (2013). Colorectal cancer targeted Irinotecan-Assam Bora rice starch based microspheres: A mechanistic, pharmacokinetic and biochemical investigation. *Drug Development and Industrial Pharmacy*, *39*(12), 1936–1943. https://doi.org/10.3109/03639045.2012.719906

Ai, Y., & Jane, J. L. (2015). Gelatinization and rheological properties of starch. *Starch - Stärke*, *67*(3–4), 213–224. https://doi.org/10.1002/star.201400201

Avila-Reyes, S. V, Garcia-Suarez, F. J., Jiménez, M. T., San Martín-Gonzalez, M. F., & Bello-Perez, L. A. (2014). Protection of L. rhamnosus by spray-drying using two prebiotics colloids to enhance the viability. *Carbohydrate Polymers*, *102*(1), 423–430. https://doi.org/10.1016/j.carbpol.2013.11.033

Badenhuizen, N. P. (1956). The structure of the starch granule. *Protoplasma*, *45*(3), 315–326. https://doi.org/10.1007/BF01247977

Baimark, Y., & Srisuwan, Y. (2013). Preparation of polysaccharide-based microspheres by a water-in-oil emulsion solvent diffusion method for drug carriers. *International Journal of Polymer Science*, *2013*, 1–6. https://doi.org/10.1155/2013/761870

Baker, A. A., Miles, M. J., & Helbert, W. (2001). Internal structure of the starch granule revealed by AFM. *Carbohydrate Research*, *330*(2), 249–256. https://doi.org/10.1016/S0008-6215(00)00275-5

Baldwin, P. M., Adler, J., Davies, M. C., & Melia, C. D. (1994). Holes in Starch Granules: Confocal, SEM and Light Microscopy Studies of Starch Granule Structure. *Starch - Stärke*, *46*(9), 341–346. https://doi.org/10.1002/star.19940460906

Balmayor, E. R., Feichtinger, G. A., Azevedo, H. S., Van Griensven, M., & Reis, R. L. (2009). Starch-poly-ε-caprolactone microparticles reduce the needed amount of BMP-2. *Clinical Orthopaedics and Related Research*, *467*(12), 3138–3148. https://doi.org/10.1007/s11999-009-0954-z

Balmayor, E. R., Tuzlakoglu, K., Azevedo, H. S., & Reis, R. L. (2009). Preparation and characterization of starch-poly-ε-caprolactone microparticles incorporating bioactive agents for drug delivery and tissue engineering applications. *Acta Biomaterialia*, *5*(4), 1035–1045. https://doi.org/10.1016/j.actbio.2008.11.006

Bertoft, E. (2017). Understanding Starch Structure: Recent Progress. *Agronomy*, *7*(3), 56. https://doi.org/10.3390/agronomy7030056

Bie, P., Chen, L., Li, X., & Li, L. (2016). Characterization of concanavalin A-conjugated resistant starch acetate bioadhesive film for oral colon-targeting microcapsule delivery system. *Industrial Crops and Products*, *84*, 320–329. https://doi.org/10.1016/j.indcrop.2016.02.023

Błaszczak, W., Fornal, J., Valverde, S., & Garrido, L. (2005). Pressure-induced changes in the structure of corn starches with different amylose content. *Carbohydrate Polymers*, *61*(2), 132–140. https://doi.org/10.1016/j.carbpol.2005.04.005

Blemur, L., Le, T. C., Marcocci, L., Pietrangeli, P., & Mateescu, M. A. (2016). Carboxymethyl starch/alginate microspheres containing diamine oxidase for intestinal targeting. *Biotechnology and Applied Biochemistry*, *63*(3), 344–353. https://doi.org/10.1002/bab.1369

Bogracheva, T. Y., Morris, V. J., Ring, S. G., & Hedley, C. L. (1998). The granular structure of C-type pea starch and its role in gelatinization. *Biopolymers*, *45*(4), 323–332. https://doi.org/10.1002/(SICI)1097-0282(19980405)45:4<323::AID-BIP6>3.0.CO;2-N

Bordenave, N., Janaswamy, S., & Yao, Y. (2014). Influence of glucan structure on the swelling and leaching properties of starch microparticles. *Carbohydrate Polymers*, *103*(1), 234–243. https://doi.org/10.1016/j.carbpol.2013.11.031

Builders, P. F., & Arhewoh, M. I. (2016). Pharmaceutical applications of native starch in conventional drug delivery. In *Starch/Staerke* (Vol. 68, Issues 9–10). https://doi.org/10.1002/star.201500337

Buléon, A., Colonna, P., Planchot, V., & Ball, S. (1998). Starch granules: structure and biosynthesis. *International Journal of Biological Macromolecules*, *23*(2), 85–112. https://doi.org/10.1016/S0141-8130(98)00040-3

Burch, M. J., Ievlev, A. V, Mahady, K., Hysmith, H., Rack, P. D., Belianinov, A., & Ovchinnikova, O. S. (2018). Helium Ion Microscopy for Imaging and Quantifying Porosity at the Nanoscale. *Analytical Chemistry*, *90*(2), 1370–1375. https://doi.org/10.1021/acs.analchem.7b04418

Cai, C., Cai, J., Zhao, L., & Wei, C. (2014). In situ gelatinization of starch using hot stage microscopy. *Food Science and Biotechnology*, *23*(1), 15–22. https://doi.org/10.1007/s10068-014-0003-x

Cai, C., & Wei, C. (2013). In situ observation of crystallinity disruption patterns during starch gelatinization. *Carbohydrate Polymers*, *92*(1), 469–478. https://doi.org/10.1016/j.carbpol.2012.09.073

Cai, C., Zhao, L., Huang, J., Chen, Y., & Wei, C. (2014). Morphology, structure and gelatinization properties of heterogeneous starch granules from high-amylose maize. *Carbohydrate Polymers*, *102*(1), 606–614. https://doi.org/10.1016/j.carbpol.2013.12.010

Chen, H., Yang, M., Shan, Z., Mansouri, S., May, B. K., Chen, X., Chen, H., & Woo, M. W. (2017). On

spray drying of oxidized corn starch cross-linked gelatin microcapsules for drug release. *Materials Science and Engineering C*, *74*, 493–500. https://doi.org/10.1016/j.msec.2016.12.047

Chen, J., Li, X., Chen, L., & Xie, F. (2018). Starch film-coated microparticles for oral colon-specific drug delivery. *Carbohydrate Polymers*, *191*, 242–254. https://doi.org/10.1016/j.carbpol.2018.03.025

Chen, L., Ma, R., Zhang, Z., Huang, M., Cai, C., Zhang, R., McClements, D. J., Tian, Y., & Jin, Z. (2019). Comprehensive investigation and comparison of surface microstructure of fractionated potato starches. *Food Hydrocolloids*, *89*, 11–19. https://doi.org/10.1016/j.foodhyd.2018.10.017

Chen, P., Yu, L., Simon, G. P., Liu, X., Dean, K., & Chen, L. (2011). Internal structures and phase-transitions of starch granules during gelatinization. *Carbohydrate Polymers*, *83*(4), 1975–1983. https://doi.org/10.1016/j.carbpol.2010.11.001

Chen, P., Yu, L., Simon, G., Petinakis, E., Dean, K., & Chen, L. (2009). Morphologies and microstructures of cornstarches with different amylose-amylopectin ratios studied by confocal laser scanning microscope. *Journal of Cereal Science*, *50*(2), 241–247. https://doi.org/10.1016/j.jcs.2009.06.001

Chen, R., Zhang, Y., Shen, L., Wang, X., Chen, J., Ma, A., & Jiang, W. (2015). Lead(II) and methylene blue removal using a fully biodegradable hydrogel based on starch immobilized humic acid. *Chemical Engineering Journal*, *268*, 348–355. https://doi.org/10.1016/j.cej.2015.01.081

Chen, W., Palazzo, A., Hennink, W. E., & Kok, R. J. (2017). Effect of particle size on drug loading and release kinetics of gefitinib-loaded PLGA microspheres. *Molecular Pharmaceutics*, *14*(2), 459–467. https://doi.org/10.1021/acs.molpharmaceut.6b00896

Chen, X., He, X., Zhang, B., Fu, X., Li, L., & Huang, Q. (2018). Structure, physicochemical and in vitro digestion properties of ternary blends containing swollen maize starch, maize oil and zein protein. *Food Hydrocolloids*. https://doi.org/10.1016/j.foodhyd.2017.04.025

Daly, A. C., Riley, L., Segura, T., & Burdick, J. A. (2020). Hydrogel microparticles for biomedical applications. In *Nature Reviews Materials* (Vol. 5, Issue 1, pp. 20–43). Nature Research. https://doi.org/10.1038/s41578-019-0148-6

Dash, S., Murthy, P. N., Nath, L., & Chowdhury, P. (2010). Kinetic modeling on drug release from controlled drug delivery systems. In *Acta Poloniae Pharmaceutica - Drug Research* (Vol. 67, Issue 3, pp. 217–223). https://pubmed.ncbi.nlm.nih.gov/20524422/

de Oliveira Cardoso, V. M., Evangelista, R. C., Daflon Gremião, M. P., & Stringhetti Ferreira Cury, B. (2020). Insights into the impact of cross-linking processes on physicochemical characteristics and mucoadhesive potential of gellan gum/retrograded starch microparticles as a platform for colonic drug release. *Journal of Drug Delivery Science and Technology*, *55*, 101445. https://doi.org/10.1016/j.jddst.2019.101445

Debet, M. R., & Gidley, M. J. (2007). Why do gelatinized starch granules not dissolve completely? Roles for amylose, protein, and lipid in granule "ghost" integrity. *Journal of Agricultural and Food Chemistry*, *55*(12), 4752–4760. https://doi.org/10.1021/jf070004o

Deng, X. X., Chen, Z., Huang, Q., Fu, X., & Tang, C. H. (2014). Spray-drying microencapsulation of β-carotene by soy protein isolate and/or OSA-modified starch. *Journal of Applied Polymer Science*, *131*(12), n/a-n/a. https://doi.org/10.1002/app.40399

Desai, K. G. (2007). Properties of tableted high-amylose corn starch-pectin blend microparticles intended for controlled delivery of diclofenac sodium. *Journal of Biomaterials Applications*, *21*(3), 217–233. https://doi.org/10.1177/0885328206056771

Desam, G. P., Li, J., Chen, G., Campanella, O., & Narsimhan, G. (2018). A mechanistic model for swelling kinetics of waxy maize starch suspension. *Journal of Food Engineering*, *222*, 237–249. https://doi.org/10.1016/j.jfoodeng.2017.11.017

Dhital, S., Shelat, K. J., Shrestha, A. K., & Gidley, M. J. (2013). Heterogeneity in maize starch granule internal architecture deduced from diffusion of fluorescent dextran probes. *Carbohydrate Polymers*, *93*(2), 365–373. https://doi.org/10.1016/j.carbpol.2012.12.017

Dhital, S., Shrestha, A. K., & Gidley, M. J. (2010). Relationship between granule size and in vitro digestibility of maize and potato starches. *Carbohydrate Polymers*, *82*(2), 480–488. https://doi.org/10.1016/j.carbpol.2010.05.018

Doblado-Maldonado, A. F., Janssen, F., Gomand, S. V, De Ketelaere, B., Goderis, B., & Delcour, J. A. (2017). A response surface analysis of the aqueous leaching of amylose from maize starch. *Food Hydrocolloids*, *63*, 265–272. https://doi.org/10.1016/j.foodhyd.2016.09.006

Dursch, T. J., Taylor, N. O., Liu, D. E., Wu, R. Y., Prausnitz, J. M., & Radke, C. J. (2014). Water-soluble drug partitioning and adsorption in HEMA/MAA hydrogels. *Biomaterials*, *35*(2), 620–629. https://doi.org/10.1016/j.biomaterials.2013.09.109

El Mouzdahir, Y., Elmchaouri, A., Mahboub, R., Gil, A., & Korili, S. A. (2007). Adsorption of methylene blue from aqueous solutions on a moroccan clay. *Journal of Chemical and Engineering Data*, *52*(5), 1621–1625. https://doi.org/10.1021/je700008g

Elfstrand, L., Eliasson, A. C., & Wahlgren, M. (2009). The effect of starch material, encapsulated protein and production conditions on the protein release from starch microspheres. *Journal of Pharmaceutical Sciences*, *98*(10), 3802–3815. https://doi.org/10.1002/jps.21693

Englyst, H. N., Kingman, S. M., & Cummings, J. H. (1992). Classification and measurement of nutritionally important starch fractions. *European Journal of Clinical Nutrition*, *46*(SUPPL. 2), S33-50. https://doi.org/10.1016/S0271-5317(97)00010-9

Fang, Y., Wang, L. jun, Li, D., Li, B. zheng, Bhandari, B., Chen, X. D., & Mao, Z. huai. (2008). Preparation of crosslinked starch microspheres and their drug loading and releasing properties. *Carbohydrate Polymers*, *74*(3), 379–384. https://doi.org/10.1016/j.carbpol.2008.03.005

Farrag, Y., Ide, W., Montero, B., Rico, M., Rodríguez-Llamazares, S., Barral, L., & Bouza, R. (2018). Starch films loaded with donut-shaped starch-quercetin microparticles: Characterization and release kinetics. *International Journal of Biological Macromolecules*, *118*, 2201–2207. https://doi.org/10.1016/j.ijbiomac.2018.07.087

Farrag, Y., Sabando, C., Rodríguez-Llamazares, S., Bouza, R., Rojas, C., & Barral, L. (2018). Preparation of donut-shaped starch microparticles by aqueous-alcoholic treatment. *Food Chemistry*, *246*, 1–5. https://doi.org/10.1016/j.foodchem.2017.10.147

Fundueanu, G., Constantin, M., Ascenzi, P., & Simionescu, B. C. (2010). An intelligent multicompartmental system based on thermo-sensitive starch microspheres for temperature-

controlled release of drugs. *Biomedical Microdevices*, *12*(4), 693–704. https://doi.org/10.1007/s10544-010-9422-5

Gallant, D. J., Bouchet, B., & Baldwin, P. M. (1997). Microscopy of starch: evidence of a new level of granule organization. *Carbohydrate Polymers*, *32*, 177–191. https://doi.org/10.1016/S0144-8617(97)00008-8

Gao, F., Li, D., Bi, C. H., Mao, Z. H., & Adhikari, B. (2014). Preparation and characterization of starch crosslinked with sodium trimetaphosphate and hydrolyzed by enzymes. *Carbohydrate Polymers*, *103*(1), 310–318. https://doi.org/10.1016/j.carbpol.2013.12.028

García-González, C. A., Uy, J. J., Alnaief, M., & Smirnova, I. (2012). Preparation of tailor-made starch-based aerogel microspheres by the emulsion-gelation method. *Carbohydrate Polymers*, *88*(4), 1378–1386. https://doi.org/10.1016/j.carbpol.2012.02.023

Goerg, F., Zimmermann, M., Bruners, P., Neumann, U., Luedde, T., & Kuhl, C. (2019). Chemoembolization with Degradable Starch Microspheres for Treatment of Patients with Primary or Recurrent Unresectable, Locally Advanced Intrahepatic Cholangiocarcinoma: A Pilot Study. *CardioVascular and Interventional Radiology*, *42*(12), 1709–1717. https://doi.org/10.1007/s00270-019-02344-0

Gómez-Luría, D., Vernon-Carter, E. J., & Alvarez-Ramirez, J. (2017). Films from corn, wheat, and rice starch ghost phase fractions display overall superior performance than whole starch films. *Starch/Staerke*, *69*(11–12). https://doi.org/10.1002/star.201700059

Guo, L., Li, G., Liu, J., Meng, Y., & Tang, Y. (2013). Adsorptive decolorization of methylene blue by crosslinked porous starch. *Carbohydrate Polymers*, *93*(2), 374–379. https://doi.org/10.1016/j.carbpol.2012.12.019

Hall, D. M., & Sayre, J. G. (1970). Internal Architecture of Potato and Canna Starch - Part I: Crushing Studies. *Textile Research Journal*, *40*(3), 147–157. https://doi.org/10.1177/004051757004000208

Hall, D. M., & Sayre, J. G. (1971). Internal Architecture of Potato and Canna Starch - Part II: Swelling Studies. *Textile Research Journal*, *41*(5), 404–414. https://doi.org/10.1177/004051757104100506

He, H., Hong, Y., Gu, Z., Liu, G., Cheng, L., & Li, Z. (2016). Improved stability and controlled release of CLA with spray-dried microcapsules of OSA-modified starch and xanthan gum. *Carbohydrate Polymers*, *147*, 243–250. https://doi.org/10.1016/j.carbpol.2016.03.078

Hoare, T. R., & Kohane, D. S. (2008). Hydrogels in drug delivery: Progress and challenges. *Polymer*, *49*(8), 1993–2007. https://doi.org/10.1016/j.polymer.2008.01.027

Hoyos-Leyva, J. D., Chavez-Salazar, A., Castellanos-Galeano, F., Bello-Perez, L. A., & Alvarez-Ramirez, J. (2018). Physical and chemical stability of L-ascorbic acid microencapsulated into taro starch spherical aggregates by spray drying. *Food Hydrocolloids*, *83*, 143–152. https://doi.org/10.1016/j.foodhyd.2018.05.002

Huber, K C, & BeMiller, J. N. (2000). Channels of maize and sorghum starch granules. *Carbohydrate Polymers*, *41*(3), 269–276. https://doi.org/10.1016/S0144-8617(99)00145-9

Huber, Kerry C., & BeMiller, J. N. (1997). Visualization of channels and cavities of corn and sorghum

starch granules. *Cereal Chemistry*, *74*(5), 537–541. https://doi.org/10.1094/CCHEM.1997.74.5.537

Huo, W., Xie, G., Zhang, W., Wang, W., Shan, J., Liu, H., & Zhou, X. (2016). Preparation of a novel chitosan-microcapsules/starch blend film and the study of its drug-release mechanism. *International Journal of Biological Macromolecules*, *87*, 114–122. https://doi.org/10.1016/j.ijbiomac.2016.02.049

Ismail, S., Mansor, N., Majeed, Z., & Man, Z. (2016). Effect of Water and [Emim][OAc] as Plasticizer on Gelatinization of Starch. *Procedia Engineering*, *148*, 524–529. https://doi.org/10.1016/j.proeng.2016.06.542

Jane, Jay-Lin. (1993). Mechanism of Starch Gelatinization in Neutral Salt Solutions. *Starch - Stärke*, *45*(5), 161–166. https://doi.org/10.1002/star.19930450502

Jane, Jay-lin, & Shen, J. J. (1993). Internal structure of the potato starch granule revealed by chemical gelatinization. *Carbohydrate Research*, *247*, 279–290. https://ac.els-cdn.com/000862159384260D/1-s2.0-000862159384260D-main.pdf?_tid=38bfd60d-1458-443a-a92b-d3f1c2eea86d&acdnat=1549479136_70f972bf9a44570993adb5ba65c6bcc3

Jenkins, P. J., & Donald, A. M. (1998). Gelatinisation of starch: A combined SAXS/WAXS/DSC and SANS study. *Carbohydrate Research*, *308*(1–2), 133–147. https://doi.org/10.1016/S0008-6215(98)00079-2

Jiang, T., Wu, C., Gao, Y., Zhu, W., Wan, L., Wang, Z., & Wang, S. (2014). Preparation of novel porous starch microsphere foam for loading and release of poorly water soluble drug. *Drug Development and Industrial Pharmacy*, *40*(2), 252–259. https://doi.org/10.3109/03639045.2012.756511

Joens, M. S., Huynh, C., Kasuboski, J. M., Ferranti, D., Sigal, Y. J., Zeitvogel, F., Obst, M., Burkhardt, C. J., Curran, K. P., Chalasani, S. H., Stern, L. A., Goetze, B., & Fitzpatrick, J. A. J. (2013). Helium Ion Microscopy (HIM) for the imaging of biological samples at sub-nanometer resolution. *Scientific Reports*, *3*. https://doi.org/10.1038/srep03514

Junlapong, K., Maijan, P., Chaibundit, C., & Chantarak, S. (2020). Effective adsorption of methylene blue by biodegradable superabsorbent cassava starch-based hydrogel. *International Journal of Biological Macromolecules*, *158*, 258–264. https://doi.org/10.1016/j.ijbiomac.2020.04.247

Karim, A. A. A., Norziah, M. . H., & Seow, C. . C. (2000). Methods for the study of starch retrogradation. *Food Chemistry*, *71*(1), 9–36. https://doi.org/10.1016/S0308-8146(00)00130-8

Ketola, A. E., Leppänen, M., Turpeinen, T., Papponen, P., Strand, A., Sundberg, A., Arstila, K., & Retulainen, E. (2019). Cellulose nanofibrils prepared by gentle drying methods reveal the limits of helium ion microscopy imaging. *RSC Advances*, *9*(27), 15668–15677. https://doi.org/10.1039/c9ra01447k

Kim, J.-Y., & Huber, K. C. (2013). Corn starch granules with enhanced load-carrying capacity via citric acid treatment. *Carbohydrate Polymers*, *91*(1), 39–47. https://doi.org/10.1016/j.carbpol.2012.07.049

Kittipongpatana, O. S. (2013). *Physicochemical, in vitro digestibility and functional properties of carboxymethyl rice starch cross-linked with epichlorohydrin*. *141*(2), 1438–1444. http://resolver.scholarsportal.info/resolve/03088146/v141i0002/1438_pivdafcrscwe.xml

Kotsmar, C., Sells, T., Taylor, N., Liu, D. E., Prausnitz, J. M., & Radke, C. J. (2012). Aqueous solute partitioning and mesh size in HEMA/MAA hydrogels. *Macromolecules*, *45*(22), 9177–9187.

https://doi.org/10.1021/ma3018487

Kowalski, G., & Ptaszek, P. (2016). The effect of swelling time on rheological properties of hydrogels, consisting of high -amylose carboxymethyl corn starch and acrylic polymers. *Starch - Stärke*, *68*(5–6), 381–388. https://doi.org/10.1002/star.201400253

Kumar, L., Brennan, M., Zheng, H., & Brennan, C. (2018). The effects of dairy ingredients on the pasting, textural, rheological, freeze-thaw properties and swelling behaviour of oat starch. *Food Chemistry*, *245*, 518–524. https://doi.org/10.1016/j.foodchem.2017.10.125

Lara, S. C., & Salcedo, F. (2016). Gelatinization and retrogradation phenomena in starch/montmorillonite nanocomposites plasticized with different glycerol/water ratios. *Carbohydrate Polymers*, *151*, 206–212. https://doi.org/10.1016/j.carbpol.2016.05.065

Lecorre, D., Bras, J., & Dufresne, A. (2012). Influence of native starch's properties on starch nanocrystals thermal properties. *Carbohydrate Polymers*, *87*(1), 658–666. https://doi.org/10.1016/j.carbpol.2011.08.042

Lemieux, M., Gosselin, P., & Mateescu, M. A. (2009). Carboxymethyl high amylose starch as excipient for controlled drug release: Mechanistic study and the influence of degree of substitution. *International Journal of Pharmaceutics*, *382*(1–2), 172–182. https://doi.org/10.1016/j.ijpharm.2009.08.030

Lemieux, M., Gosselin, P., & Mateescu, M. A. (2015). Carboxymethyl starch mucoadhesive microspheres as gastroretentive dosage form. *International Journal of Pharmaceutics*, *496*(2), 497–508. https://doi.org/10.1016/j.ijpharm.2015.10.027

Lenaerts, V., Dumoulin, Y., & Mateescu, M. A. (1991). Controlled release of theophylline from cross-linked amylose tablets. *Journal of Controlled Release*, *15*(1), 39–46. https://doi.org/10.1016/0168-3659(91)90101-I

Li, B., Wang, L., Li, D., Chiu, Y. L., Zhang, Z., Shi, J., Chen, X. D., & Mao, Z. huai. (2009). Physical properties and loading capacity of starch-based microparticles crosslinked with trisodium trimetaphosphate. *Journal of Food Engineering*, *92*(3), 255–260. https://doi.org/10.1016/j.jfoodeng.2008.10.008

Li, C., Fu, X., Luo, F., & Huang, Q. (2013). Effects of maltose on stability and rheological properties of orange oil-in-water emulsion formed by OSA modified starch. *Food Hydrocolloids*, *32*(1), 79–86. https://doi.org/10.1016/j.foodhyd.2012.12.004

Li, D., Liu, A., Liu, M., Li, X., Guo, H., Zuo, C., & Li, Y. (2020). The intestine-responsive lysozyme nanoparticles-in-oxidized starch microgels with mucoadhesive and penetrating properties for improved epithelium absorption of quercetin. *Food Hydrocolloids*, *99*. https://doi.org/10.1016/j.foodhyd.2019.105309

Li, J., & Mooney, D. J. (2016). Designing hydrogels for controlled drug delivery. In *Nature Reviews Materials* (Vol. 1, Issue 12). Nature Publishing Group. https://doi.org/10.1038/natrevmats.2016.71

Li, J. Y., & Yeh, A. I. (2001). Relationships between thermal, rheological characteristics and swelling power for various starches. *Journal of Food Engineering*, *50*(3), 141–148. https://doi.org/10.1016/S0260-8774(00)00236-3

Li, Q., Xie, Q., Yu, S., & Gao, Q. (2013). New approach to study starch gelatinization applying a combination of hot-stage light microscopy and differential scanning calorimetry. *Journal of Agricultural and Food Chemistry*, *61*(6), 1212–1218. https://doi.org/10.1021/jf304201r

Li, Yuan, De Vries, R., Slaghek, T., Timmermans, J., Cohen Stuart, M. A., & Norde, W. (2009). Preparation and characterization of oxidized starch polymer microgels for encapsulation and controlled release of functional ingredients. *Biomacromolecules*, *10*(7), 1931–1938. https://doi.org/10.1021/bm900337n

Li, Yuan, Kadam, S., Abee, T., Slaghek, T. M., Timmermans, J. W., Cohen Stuart, M. A., Norde, W., & Kleijn, M. J. (2012). Antimicrobial lysozyme-containing starch microgel to target and inhibit amylase-producing microorganisms. *Food Hydrocolloids*, *28*(1), 28–35. https://doi.org/10.1016/j.foodhyd.2011.11.011

Li, Yuan, Kleijn, J. M., Cohen Stuart, M. A., Slaghek, T., Timmermans, J., & Norde, W. (2011). Mobility of lysozyme inside oxidized starch polymer microgels. *Soft Matter*, *7*(5), 1926–1935. https://doi.org/10.1039/c0sm00962h

Li, Yuan, Norde, W., & Kleijn, J. M. (2012). Stabilization of protein-loaded starch microgel by polyelectrolytes. *Langmuir*, *28*(2), 1545–1551. https://doi.org/10.1021/la204014q

Li, Yuan, Zhang, Z., Van Leeuwen, H. P., Cohen Stuart, M. A., Norde, W., & Kleijn, J. M. (2011). Uptake and release kinetics of lysozyme in and from an oxidized starch polymer microgel. *Soft Matter*, *7*(21), 10377–10385. https://doi.org/10.1039/c1sm06072d

Li, Yuhua, Zhang, Y., Zhao, J., Han, N., & Bian, L. (2019). Studies on the Adsorption and Thermodynamics of Theophylline, Vitamin C and Bovine Serum Albumin on Microporous Corn Starch. *Starch/Staerke*, *71*(3–4), 1800042. https://doi.org/10.1002/star.201800042

Liu, C.-S., Desai, K. G. H., Meng, X.-H., & Chen, X.-G. (2007). Sweet Potato Starch Microparticles as Controlled Drug Release Carriers: Preparation and In Vitro Drug Release. *Drying Technology*, *25*(4), 689–693. https://doi.org/10.1080/07373930701290977

Liu, H., Liang, R., Antoniou, J., Liu, F., Shoemaker, C. F., Li, Y., & Zhong, F. (2014). The effect of high moisture heat-acid treatment on the structure and digestion property of normal maize starch. *Food Chemistry*, *159*, 222–229. https://doi.org/10.1016/j.foodchem.2014.02.162

Liu, Q. (2005). Food Carbohydrates: Chemistry, Physical Properties, and Applications. In *Food Carbohydrates*.

Luo, K., Jeong, K. B., You, S. M., Lee, D. H., & Kim, Y. R. (2018). Molecular Rearrangement of Glucans from Natural Starch to Form Size-Controlled Functional Magnetic Polymer Beads. *Journal of Agricultural and Food Chemistry*, *66*(26), 6806–6813. https://doi.org/10.1021/acs.jafc.8b01590

Luo, K., Lee, D. H., Adra, H. J., & Kim, Y. R. (2019). Synthesis of monodisperse starch microparticles through molecular rearrangement of short-chain glucans from natural waxy maize starch. *Carbohydrate Polymers*, *218*, 261–268. https://doi.org/10.1016/j.carbpol.2019.05.001

Maaran, S., Hoover, R., Donner, E., & Liu, Q. (2014). Composition, structure, morphology and physicochemical properties of lablab bean, navy bean, rice bean, tepary bean and velvet bean starches. *Food Chemistry*, *152*, 491–499. https://doi.org/10.1016/j.foodchem.2013.12.014

Maia, P. D. D. S., dos Santos Baião, D., da Silva, V. P. F., de Araújo Calado, V. M., Queiroz, C., Pedrosa, C., Valente-Mesquita, V. L., & Pierucci, A. P. T. R. (2019). Highly Stable Microparticles of Cashew Apple (Anacardium occidentale L.) Juice with Maltodextrin and Chemically Modified Starch. *Food and Bioprocess Technology*, *12*(12), 2107–2119. https://doi.org/10.1007/s11947-019-02376-x

Mao, S., Chen, J., Wei, Z., Liu, H., & Bi, D. (2004). Intranasal administration of melatonin starch microspheres. *International Journal of Pharmaceutics*, *272*(1–2), 37–43. https://doi.org/10.1016/j.ijpharm.2003.11.028

Marousis, S. N., & Saravacos, G. D. (1990). Density and Porosity in Drying Starch Materials. *Journal of Food Science*, *55*(5), 1367–1372. https://doi.org/10.1111/j.1365-2621.1990.tb03939.x

Marsh, R. A., & Waight, S. G. (1982). The Effect of pH on the Zeta Potential of Wheat and Potato Starch. *Starch - Stärke*, *34*(5), 149–152. https://doi.org/10.1002/star.19820340502

Momeni, A., & Mohammadi, M. H. (2009). Respiratory delivery of theophylline by size-targeted starch microspheres for treatment of asthma. *Journal of Microencapsulation*, *26*(8), 701–710. https://doi.org/10.3109/02652040802685043

Moreno-Mendieta, S., Barrera-Rosales, A., Mata-Espinosa, D., Barrios-Payán, J., Sánchez, S., Hernández-Pando, R., & Rodríguez-Sanoja, R. (2019). Raw starch microparticles as BCG adjuvant: Their efficacy depends on the virulence of the infection strains. *Vaccine*, *37*(38), 5731–5737. https://doi.org/10.1016/j.vaccine.2019.04.027

Moreno-Mendieta, S., Barrios-Payán, J., Mata-Espinosa, D., Sánchez, S., Hernández-Pando, R., & Rodríguez-Sanoja, R. (2017). Raw starch microparticles have immunostimulant activity in mice vaccinated with BCG and challenged with Mycobacterium tuberculosis. *Vaccine*, *35*(38), 5123–5130. https://doi.org/10.1016/j.vaccine.2017.08.012

Muhammad, Z., Ramzan, R., Zhang, S., Hu, H., Hameed, A., Bakry, A. M., Dong, Y., Wang, L., & Pan, S. (2018). Comparative assessment of the bioremedial potentials of potato resistant starch-based microencapsulated and non-encapsulated Lactobacillus plantarum to alleviate the effects of chronic lead toxicity. *Frontiers in Microbiology*, *9*(JUN). https://doi.org/10.3389/fmicb.2018.01306

Nashed, G., Rutgers, R. P. G., & Sopade, P. A. (2003). The plasticisation effect of glycerol and water on the gelatinisation of wheat starch. *Starch/Staerke*, *55*(3–4), 131–137. https://doi.org/10.1002/star.200390027

Nayak, A. K., Malakar, J., Pal, D., Hasnain, M. S., & Beg, S. (2018). Soluble starch-blended Ca2+-Zn2+-alginate composites-based microparticles of aceclofenac: Formulation development and in vitro characterization. *Future Journal of Pharmaceutical Sciences*, *4*(1), 63–70. https://doi.org/10.1016/J.FJPS.2017.10.001

Nogueira, G. F., Soares, C. T., Martin, L. G. P., Fakhouri, F. M., & de Oliveira, R. A. (2020). Influence of spray drying on bioactive compounds of blackberry pulp microencapsulated with arrowroot starch and gum arabic mixture. *Journal of Microencapsulation*, *37*(1), 65–76. https://doi.org/10.1080/02652048.2019.1693646

Ohtani, T., Yoshino, T., Hagiwara, S., & Maekawa, T. (2000). High-resolution Imaging of Starch Granule Structure using Atomic Force Microscopy. *Starch/Staerke*, *52*(5), 150–153. https://doi.org/10.1002/1521-379X(200006)52:5<150::AID-STAR150>3.0.CO;2-F

Okunlola, A., Adebayo, A. S., & Adeyeye, M. C. (2017). Development of repaglinide microspheres using novel acetylated starches of bitter and Chinese yams as polymers. *International Journal of Biological Macromolecules*, *94*, 544–553. https://doi.org/10.1016/j.ijbiomac.2016.10.032

Östh, K., Strindelius, L., Larhed, A., Ahlander, A., Roomans, G. M., Sjöholm, I., & Björk, E. (2003). Uptake of ovalbumin-conjugated starch microparticles by pig respiratory nasal mucosa in vitro. *Journal of Drug Targeting*, *11*(1), 75–82. https://doi.org/10.1080/1061186031000093254

Palma-Rodriguez, H. M., Agama-Acevedo, E., Gonzalez-Soto, R. A., Vernon-Carter, E. J., Alvarez-Ramirez, J., & Bello-Perez, L. A. (2013). Ascorbic acid microencapsulation by spray-drying in native and acid-modified starches from different botanical sources. *Starch/Staerke*, *65*(7–8), 584–592. https://doi.org/10.1002/star.201200200

Panyoyai, N., Shanks, R. A., & Kasapis, S. (2017). Tocopheryl acetate release from microcapsules of waxy maize starch. *Carbohydrate Polymers*, *167*, 27–35. https://doi.org/10.1016/j.carbpol.2017.03.005

Park, H., Xu, S., & Seetharaman, K. (2011). A novel in situ atomic force microscopy imaging technique to probe surface morphological features of starch granules. *Carbohydrate Research*, *346*(6), 847–853. https://doi.org/10.1016/j.carres.2011.01.036

Parker, R., & Ring, S. G. (2001). Aspects of the physical chemistry of starch. In *Journal of Cereal Science* (Vol. 34, Issue 1, pp. 1–17). https://doi.org/10.1006/jcrs.2000.0402

Peng, H., Xiong, H., Wang, S., Li, J., Chen, L., & Zhao, Q. (2011). Soluble starch-based biodegradable and microporous microspheres as potential adsorbent for stabilization and controlled release of coix seed oil. *European Food Research and Technology*, *232*(4), 693–702. https://doi.org/10.1007/s00217-011-1438-4

Pereira, A. G. B., Fajardo, A. R., Nocchi, S., Nakamura, C. V, Rubira, A. F., & Muniz, E. C. (2013). Starch-based microspheres for sustained-release of curcumin: Preparation and cytotoxic effect on tumor cells. *Carbohydrate Polymers*, *98*(1), 711–720. https://doi.org/10.1016/j.carbpol.2013.06.013

Pérez, S., & Bertoft, E. (2010). The molecular structures of starch components and their contribution to the architecture of starch granules: A comprehensive review. In *Starch/Staerke* (Vol. 62, Issue 8, pp. 389–420). https://doi.org/10.1002/star.201000013

Phromsopha, T., & Baimark, Y. (2014). Preparation of starch/gelatin blend microparticles by a water-in-oil emulsion method for controlled release drug delivery. *International Journal of Biomaterials*, *2014*, 829490. https://doi.org/10.1155/2014/829490

Pourjavadi, A., Nazari, M., Kabiri, B., Hosseini, S. H., & Bennett, C. (2016). Preparation of porous graphene oxide/hydrogel nanocomposites and their ability for efficient adsorption of methylene blue. *RSC Adv.*, *6*(13), 10430–10437. https://doi.org/10.1039/C5RA21629J

Quadrado, R. F. N., & Fajardo, A. R. (2020). Microparticles based on carboxymethyl starch/chitosan polyelectrolyte complex as vehicles for drug delivery systems. *Arabian Journal of Chemistry*, *13*(1), 2183–2194. https://doi.org/10.1016/j.arabjc.2018.04.004

Ragheb, A. A., Abdel-Thalouth, I., & Tawfik, S. (1995). Gelatinization of Starch in Aqueous Alkaline Solutions. *Starch - Stärke*, *47*(9), 338–345. https://doi.org/10.1002/star.19950470904

Ratnayake, W. S., & Jackson, D. S. (2007). A new insight into the gelatinization process of native starches. *Carbohydrate Polymers*, *67*(4), 511–529. https://doi.org/10.1016/j.carbpol.2006.06.025

Rehan, M., Ahmed-Farid, O. A., Ibrahim, S. R., Hassan, A. A., Abdelrazek, A. M., Khafaga, N. I. M., & Khattab, T. A. (2019). Green and Sustainable Encapsulation of Guava Leaf Extracts (Psidium guajava L.) into Alginate/Starch Microcapsules for Multifunctional Finish over Cotton Gauze. *ACS Sustainable Chemistry and Engineering*. https://doi.org/10.1021/acssuschemeng.9b04952

Ridout, M. J., Gunning, A. P., Parker, M. L., Wilson, R. H., & Morris, V. J. (2002). Using AFM to image the internal structure of starch granules. *Carbohydrate Polymers*, *50*(2), 123–132. https://doi.org/10.1016/S0144-8617(02)00021-8

Rochelle, C., & Lee, G. (2007). Dextran or hydroxyethyl starch in spray-freeze-dried trehalose/mannitol microparticles intended as ballistic particulate carriers for proteins. *Journal of Pharmaceutical Sciences*, *96*(9), 2296–2309. https://doi.org/10.1002/jps.20861

Roger, P., & Colonna, P. (1996). Molecular weight distribution of amylose fractions obtained by aqueous leaching of corn starch. *International Journal of Biological Macromolecules*, *19*(1), 51–61. https://doi.org/10.1016/0141-8130(96)01101-4

Rosicka - Kaczmarek, J., Makowski, B., Nebesny, E., Tkaczyk, M., Komisarczyk, A., & Nita, Z. (2016). Composition and thermodynamic properties of starches from facultative wheat varieties. *Food Hydrocolloids*, *54*, 66–76. https://doi.org/10.1016/j.foodhyd.2015.09.014

Sajeesh, P., & Sen, A. K. (2014). Particle separation and sorting in microfluidic devices: A review. In *Microfluidics and Nanofluidics* (Vol. 17, Issue 1, pp. 1–52). https://doi.org/10.1007/s10404-013-1291-9

Sasaki, T., & Matsuki, J. (1998). Effect of wheat starch structure on swelling power. *Cereal Chemistry*, *75*(4), 525–529. https://doi.org/10.1094/CCHEM.1998.75.4.525

Sato, C., Sato, M., & Ogawa, S. (2018). Imaging of immunogold labeling in cells and tissues by helium ion microscopy. *International Journal of Molecular Medicine*, *42*(1), 309–321. https://doi.org/10.3892/ijmm.2018.3604

Schicho, A., Pereira, P. L., Michalik, K., Beyer, L. P., Stroszczynski, C., & Wiggermann, P. (2018). Safety and efficacy of transarterial chemoembolization with degradable starch microspheres (DSM-TACE) in the treatment of secondary liver malignancies. *OncoTargets and Therapy*, *11*, 345–350. https://doi.org/10.2147/OTT.S147852

Schirmer, M, Höchstötter, A., Jekle, M., Arendt, E., & Becker, T. (2013). Physicochemical and morphological characterization of different starches with variable amylose/amylopectin ratio. *Food Hydrocolloids*, *32*(1), 52–63. https://doi.org/10.1016/j.foodhyd.2012.11.032

Schirmer, Markus, Jekle, M., & Becker, T. (2015). Starch gelatinization and its complexity for analysis. In *Starch/Staerke* (Vol. 67, Issues 1–2, pp. 30–41). https://doi.org/10.1002/star.201400071

Schneider Teixeira, A., Deladino, L., García, M. A., Zaritzky, N. E., Sanz, P. D., & Molina-García, A. D. (2018). Microstructure analysis of high pressure induced gelatinization of maize starch in the presence of hydrocolloids. *Food and Bioproducts Processing*, *112*, 119–130. https://doi.org/10.1016/j.fbp.2018.09.009

Shi, M., Gu, F., Wu, J., Yu, S., & Gao, Q. (2013). Preparation, physicochemical properties, and in vitro digestibility of cross-linked resistant starch from pea starch. *Starch/Staerke*, *65*(11–12), 947–953. https://doi.org/10.1002/star.201300008

Simonin, H., Guyon, C., Orlowska, M., de Lamballerie, M., & Le-Bail, A. (2011). Gelatinization of waxy starches under high pressure as influenced by pH and osmolarity: Gelatinization kinetics, final structure and pasting properties. *LWT - Food Science and Technology*, *44*(3), 779–786. https://doi.org/10.1016/j.lwt.2010.07.002

Singh, N., Singh, J., Kaur, L., Sodhi, N. S., & Gill, B. S. (2003a). Morphological, thermal and rheological properties of starches from different botanical sources. In *Food Chemistry* (Vol. 81, Issue 2, pp. 219–231). https://doi.org/10.1016/S0308-8146(02)00416-8

Singh, N., Singh, J., Kaur, L., Sodhi, N. S., & Gill, B. S. (2003b). Morphological, thermal and rheological properties of starches from different botanical sources. *Food Chemistry*, *81*(2), 219–231. https://doi.org/10.1016/S0308-8146(02)00416-8

Situ, W., Chen, L., Wang, X., & Li, X. (2014). Resistant starch film-coated microparticles for an oral colon-specific polypeptide delivery system and its release behaviors. *Journal of Agricultural and Food Chemistry*, *62*(16), 3599–3609. https://doi.org/10.1021/jf500472b

Situ, W., Li, X., Liu, J., & Chen, L. (2015). Preparation and characterization of glycoprotein-resistant starch complex as a coating material for oral bioadhesive microparticles for colon-targeted polypeptide delivery. *Journal of Agricultural and Food Chemistry*, *63*(16), 4138–4147. https://doi.org/10.1021/acs.jafc.5b00393

Su, H., Wei, S., Chen, F., Cui, R., & Liu, C. (2019). Tranexamic acid-loaded starch hemostatic microspheres. *RSC Advances*, *9*(11), 6245–6253. https://doi.org/10.1039/c8ra06662k

Sujka, M., & Jamroz, J. (2013). Ultrasound-treated starch: SEM and TEM imaging, and functional behaviour. *Food Hydrocolloids*, *31*(2), 413–419. https://doi.org/10.1016/j.foodhyd.2012.11.027

Sun, Y., Shi, C., Yang, J., Zhong, S., Li, Z., Xu, L., Zhao, S., Gao, Y., & Cui, X. (2018). Fabrication of folic acid decorated reductive-responsive starch-based microcapsules for targeted drug delivery via sonochemical method. *Carbohydrate Polymers*, *200*, 508–515. https://doi.org/10.1016/j.carbpol.2018.08.036

Tester, R. F., Karkalas, J., & Qi, X. (2004). Starch - Composition, fine structure and architecture. *Journal of Cereal Science*, *39*(2), 151–165. https://doi.org/10.1016/j.jcs.2003.12.001

Tester, R. F., & Morrison, W. R. (1990). Swelling and gelatinization of cereal starches. I. Effects of amylopectin, amylose, and lipids. *Cereal Chemistry*, *67*(6), 551–557.

Trindade, M. A., & Grosso, C. R. F. (2000). The stability of ascorbic acid microencapsulated in granules of rice starch and in gum arabic. *Journal of Microencapsulation*, *17*(2), 169–176. https://doi.org/10.1080/026520400288409

Tsukamoto, K., Ohtani, T., & Sugiyama, S. (2012). Effect of sectioning and water on resin-embedded sections of corn starch granules to analyze inner structure. *Carbohydrate Polymers*, *89*(4), 1138–1149. https://doi.org/10.1016/j.carbpol.2012.03.087

Tuovinen, L., Peltonen, S., Liikola, M., Hotakainen, M., Lahtela-Kakkonen, M., Poso, A., & Järvinen, K. (2004). Drug release from starch-acetate microparticles and films with and without incorporated α-amylase. *Biomaterials*, *25*(18), 4355–4362. https://doi.org/10.1016/j.biomaterials.2003.11.026

Vamadevan, V., & Bertoft, E. (2015). Structure-function relationships of starch components. In *Starch/Staerke* (Vol. 67, Issues 1–2, pp. 55–68). https://doi.org/10.1002/star.201400188

Vamadevan, V., & Bertoft, E. (2020). Observations on the impact of amylopectin and amylose structure on the swelling of starch granules. *Food Hydrocolloids*, *103*. https://doi.org/10.1016/j.foodhyd.2020.105663

Vandeputte, G. E., & Delcour, J. A. (2004). From sucrose to starch granule to starch physical behaviour: A focus on rice starch. *Carbohydrate Polymers*, *58*(3), 245–266. https://doi.org/10.1016/j.carbpol.2004.06.003

Waigh, T. A., Gidley, M. J., Komanshek, B. U., & Donald, A. M. (2000). The phase transformations in starch during gelatinisation: A liquid crystalline approach. *Carbohydrate Research*, *328*(2), 165–176. https://doi.org/10.1016/S0008-6215(00)00098-7

Wang, Shanshan, Chen, X., Shi, M., Zhao, L., Li, W., Chen, Y., Lu, M., Wu, J., Yuan, Q., & Li, Y. (2015). Absorption of whey protein isolated (WPI)-stabilized β-Carotene emulsions by oppositely charged oxidized starch microgels. *Food Research International*, *67*, 315–322. https://doi.org/10.1016/j.foodres.2014.11.041

Wang, Shanshan, Chen, Y., Liang, H., Chen, Y., Shi, M., Wu, J., Liu, X., Li, Z., Liu, B., Yuan, Q., & Li, Y. (2015). Intestine-Specific Delivery of Hydrophobic Bioactives from Oxidized Starch Microspheres with an Enhanced Stability. *Journal of Agricultural and Food Chemistry*, *63*(39), 8669–8675. https://doi.org/10.1021/acs.jafc.5b03575

Wang, Shujun, Blazek, J., Gilbert, E., & Copeland, L. (2012). New insights on the mechanism of acid degradation of pea starch. *Carbohydrate Polymers*, *87*(3), 1941–1949. https://doi.org/10.1016/j.carbpol.2011.09.093

Wang, Shujun, & Copeland, L. (2012). New insights into loss of swelling power and pasting profiles of acid hydrolyzed starch granules. *Starch/Staerke*, *64*(7), 538–544. https://doi.org/10.1002/star.201100186

Wang, Shujun, & Copeland, L. (2015). Effect of Acid Hydrolysis on Starch Structure and Functionality: A Review. *Critical Reviews in Food Science and Nutrition*, *55*(8), 1081–1097. https://doi.org/10.1080/10408398.2012.684551

Wang, Shujun, Li, C., Yu, J., Copeland, L., & Wang, S. (2014). Phase transition and swelling behaviour of different starch granules over a wide range of water content. *LWT - Food Science and Technology*, *59*(2), 597–604. https://doi.org/10.1016/j.lwt.2014.06.028

Wang, Shujun, Zhang, X., Wang, S., & Copeland, L. (2016). Changes of multi-scale structure during mimicked DSC heating reveal the nature of starch gelatinization. *Scientific Reports*, *6*(1), 28271. https://doi.org/10.1038/srep28271

Wang, W., Zhou, H., Yang, H., Zhao, S., Liu, Y., & Liu, R. (2017). Effects of salts on the gelatinization and retrogradation properties of maize starch and waxy maize starch. *Food Chemistry*, *214*, 319–327.

https://doi.org/10.1016/j.foodchem.2016.07.040

Wang, Z., Li, Y., Chen, L., Xin, X., & Yuan, Q. (2013). A study of controlled uptake and release of anthocyanins by oxidized starch microgels. *Journal of Agricultural and Food Chemistry*, *61*(24), 5880–5887. https://doi.org/10.1021/jf400275m

Ward, B. W., Notte, J. A., & Economou, N. P. (2006). Helium ion microscope: A new tool for nanoscale microscopy and metrology. *Journal of Vacuum Science and Technology B: Microelectronics and Nanometer Structures*, *24*(6), 2871–2874. https://doi.org/10.1116/1.2357967

Wikingsson, L. D., & Sjöholm, I. (2002). Polyacryl starch microparticles as adjuvant in oral immunisation, inducing mucosal and systemic immune responses in mice. *Vaccine*, *20*(27–28), 3355–3363. https://doi.org/10.1016/S0264-410X(02)00288-8

Williams, P. C., Kuzina, F. D., & Hylnka, I. (1970). A Rapid Colorimetric Procedure for Estimating the Amylose Content of Starches and Flours. In *Cereal Chemistry* (Vol. 47, Issue 4, pp. 411–420).

Wöhl-Bruhn, S., Bertz, A., Harling, S., Menzel, H., & Bunjes, H. (2012). Hydroxyethyl starch-based polymers for the controlled release of biomacromolecules from hydrogel microspheres. *European Journal of Pharmaceutics and Biopharmaceutics*, *81*(3), 573–581. https://doi.org/10.1016/j.ejpb.2012.04.017

Wojtasz, J., Carlstedt, J., Fyhr, P., & Kocherbitov, V. (2016). Hydration and swelling of amorphous cross-linked starch microspheres. *Carbohydrate Polymers*, *135*, 225–233. https://doi.org/10.1016/j.carbpol.2015.08.085

Wongsagonsup, R., Pujchakarn, T., Jitrakbumrung, S., Chaiwat, W., Fuongfuchat, A., Varavinit, S., Dangtip, S., & Suphantharika, M. (2014). Effect of cross-linking on physicochemical properties of tapioca starch and its application in soup product. *Carbohydrate Polymers*, *101*(1), 656–665. https://doi.org/10.1016/j.carbpol.2013.09.100

Wongsagonsup, R., Shobsngob, S., Oonkhanond, B., & Varavinit, S. (2005). Zeta potential (ζ) and pasting properties of phosphorylated or crosslinked rice starches. *Starch/Staerke*, *57*(1), 32–37. https://doi.org/10.1002/star.200400311

Wulff, D., Aucoin, M. G., & Gu, F. X. (2020). Helium Ion Microscopy of Corn Starch. *Starch/Staerke*, 1900267. https://doi.org/10.1002/star.201900267

Wulff, D., Chan, A., Liu, Q., Gu, F. X., & Aucoin, M. G. (2020). Characterizing internal cavity modulation of corn starch microcapsules. *Heliyon*, *6*(10). https://doi.org/10.1016/j.heliyon.2020.e05294

Xi, H. D., Zheng, H., Guo, W., Gañán-Calvo, A. M., Ai, Y., Tsao, C. W., Zhou, J., Li, W., Huang, Y., Nguyen, N. T., & Tan, S. H. (2017). Active droplet sorting in microfluidics: a review. *Lab on a Chip*, *17*(5), 751–771. https://doi.org/10.1039/c6lc01435f

Xiao, Z., Kang, Y., Hou, W., Niu, Y., & Kou, X. (2019). Microcapsules based on octenyl succinic anhydride (OSA)-modified starch and maltodextrins changing the composition and release property of rose essential oil. *International Journal of Biological Macromolecules*, *137*, 132–138. https://doi.org/10.1016/j.ijbiomac.2019.06.178

Xu, L., Zhong, S., Shi, C., Sun, Y., Zhao, S., Gao, Y., & Cui, X. (2018). Sonochemical fabrication of

reduction-responsive magnetic starch-based microcapsules. *Ultrasonics Sonochemistry*, *49*, 169–174. https://doi.org/10.1016/j.ultsonch.2018.07.047

Yang, J., Xie, F., Wen, W., Chen, L., Shang, X., & Liu, P. (2016). Understanding the structural features of high-amylose maize starch through hydrothermal treatment. *International Journal of Biological Macromolecules*, *84*, 268–274. https://doi.org/10.1016/j.ijbiomac.2015.12.033

Yusoff, A., & Murray, B. S. (2011). Modified starch granules as particle-stabilizers of oil-in-water emulsions. *Food Hydrocolloids*, *25*(1), 42–55. https://doi.org/10.1016/j.foodhyd.2010.05.004

Zhang, Bao, Li, H., Li, X., Cheng, C., Jin, Z., Xu, X., & Tian, Y. (2015). Preparation, characterization, and in vitro release of carboxymethyl starch/β-cyclodextrin microgel-ascorbic acid inclusion complexes. *RSC Advances*, *5*(76), 61815–61820. https://doi.org/10.1039/c5ra09944g

Zhang, Bao, Pan, Y., Chen, H., Liu, T., Tao, H., & Tian, Y. (2017). Stabilization of starch-based microgel-lysozyme complexes using a layer-by-layer assembly technique. *Food Chemistry*, *214*, 213–217. https://doi.org/10.1016/j.foodchem.2016.07.076

Zhang, Bao, Tao, H., Wei, B., Jin, Z., Xu, X., & Tian, Y. (2014). Characterization of Different Substituted Carboxymethyl Starch Microgels and Their Interactions with Lysozyme. *PLoS ONE*, *9*(12). https://doi.org/10.1371/journal.pone

Zhang, Bao, Wei, B., Hu, X., Jin, Z., Xu, X., & Tian, Y. (2015). Preparation and characterization of carboxymethyl starch microgel with different crosslinking densities. *Carbohydrate Polymers*, *124*, 245–253. https://doi.org/10.1016/j.carbpol.2015.01.075

Zhang, Bin, Dhital, S., Flanagan, B. M., & Gidley, M. J. (2014). Mechanism for starch granule ghost formation deduced from structural and enzyme digestion properties. *Journal of Agricultural and Food Chemistry*, *62*(3), 760–771. https://doi.org/10.1021/jf404697v

Zhao, L., Chen, Y., Li, W., Lu, M., Wang, S., Chen, X., Shi, M., Wu, J., Yuan, Q., & Li, Y. (2015). Controlled uptake and release of lysozyme from glycerol diglycidyl ether cross-linked oxidized starch microgel. *Carbohydrate Polymers*, *121*, 276–283. https://doi.org/10.1016/j.carbpol.2015.01.002

Zhao, X. F., Li, Z. J., Wang, L., & Lai, X. J. (2008). Synthesis, characterization, and adsorption capacity of crosslinked starch microspheres with N,N′-methylene bisacrylamide. *Journal of Applied Polymer Science*, *109*(4), 2571–2575. https://doi.org/10.1002/app.28220

Zhao, Y., Wu, C., Zhao, Z., Hao, Y., Xu, J., Yu, T., Qiu, Y., & Jiang, J. (2015). Preparation of starch macrocellular foam for increasing the dissolution rate of poorly water-soluble drugs. *Pharmaceutical Development and Technology*, *21*(6), 749–754. https://doi.org/10.3109/10837450.2015.1055763

Zhong, F., Yokoyama, W., Wang, Q., & Shoemaker, C. F. (2006). Rice starch, amylopectin, and amylose: Molecular weight and solubility in dimethyl sulfoxide-based solvents. *Journal of Agricultural and Food Chemistry*, *54*(6), 2320–2326. https://doi.org/10.1021/jf051918i

Zhou, J., Mukherjee, P., Gao, H., Luan, Q., & Papautsky, I. (2019). Label-free microfluidic sorting of microparticles. *APL Bioengineering*, *3*(4), 041504. https://doi.org/10.1063/1.5120501

Zhu, F. (2015). Composition, structure, physicochemical properties, and modifications of cassava starch. In *Carbohydrate Polymers* (Vol. 122, pp. 456–480). https://doi.org/10.1016/j.carbpol.2014.10.063

Zhu, F. (2018). Relationships between amylopectin internal molecular structure and physicochemical properties of starch. In *Trends in Food Science and Technology* (Vol. 78, pp. 234–242). https://doi.org/10.1016/j.tifs.2018.05.024

Appendix A – Supplementary Information for Chapter 3

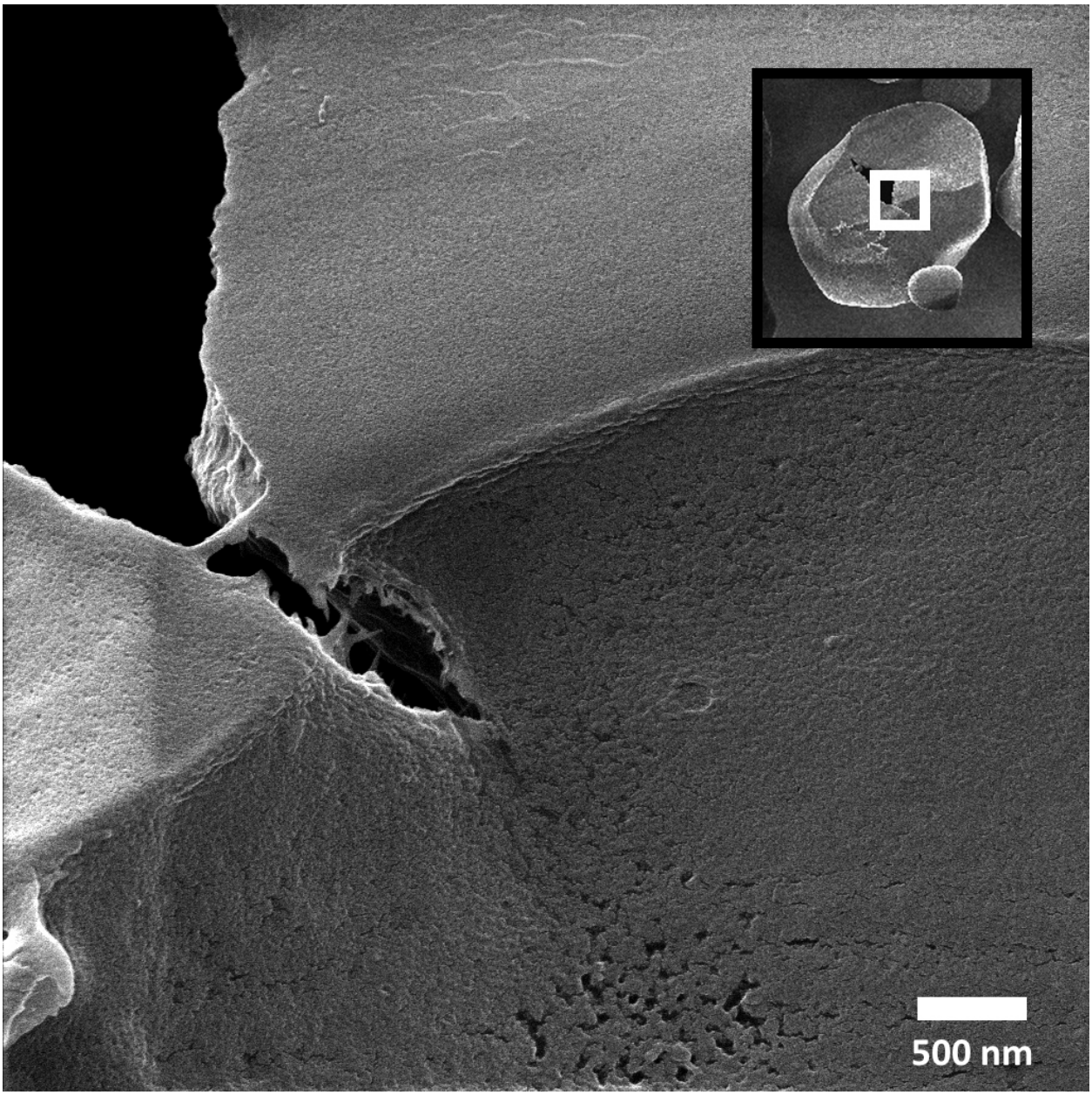

Figure A.1: HIM image of a sectioned native Hylon VII starch granule. The inset in the black box is an image of the granule at lower magnification where the white box demarcates the section of the granule that is imaged at high magnification.

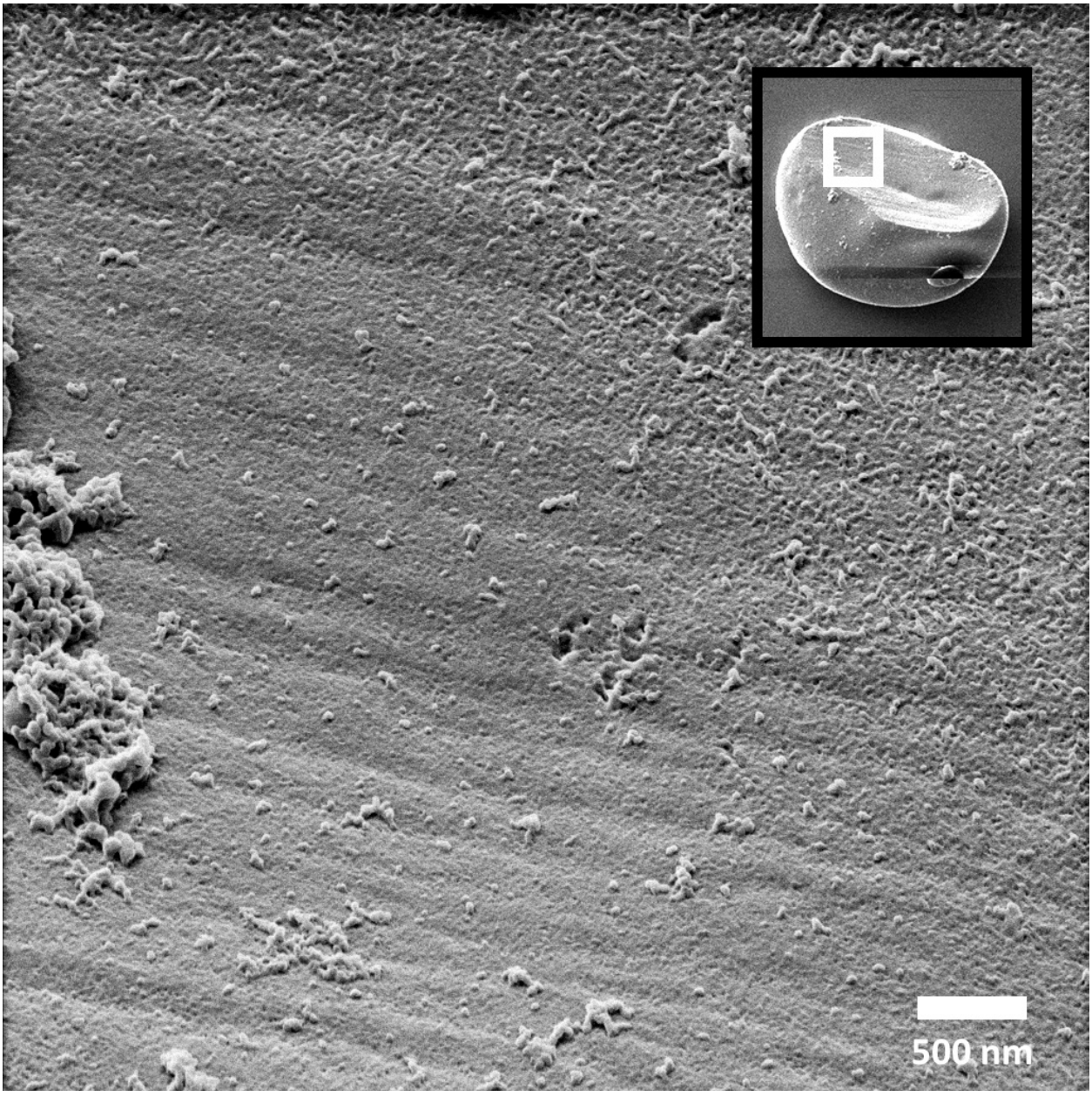

Figure A.2: HIM image of a sectioned native potato starch granule. The inset in the black box is an image of the granule at lower magnification where the white box demarcates the section of the granule that is imaged at high magnification.

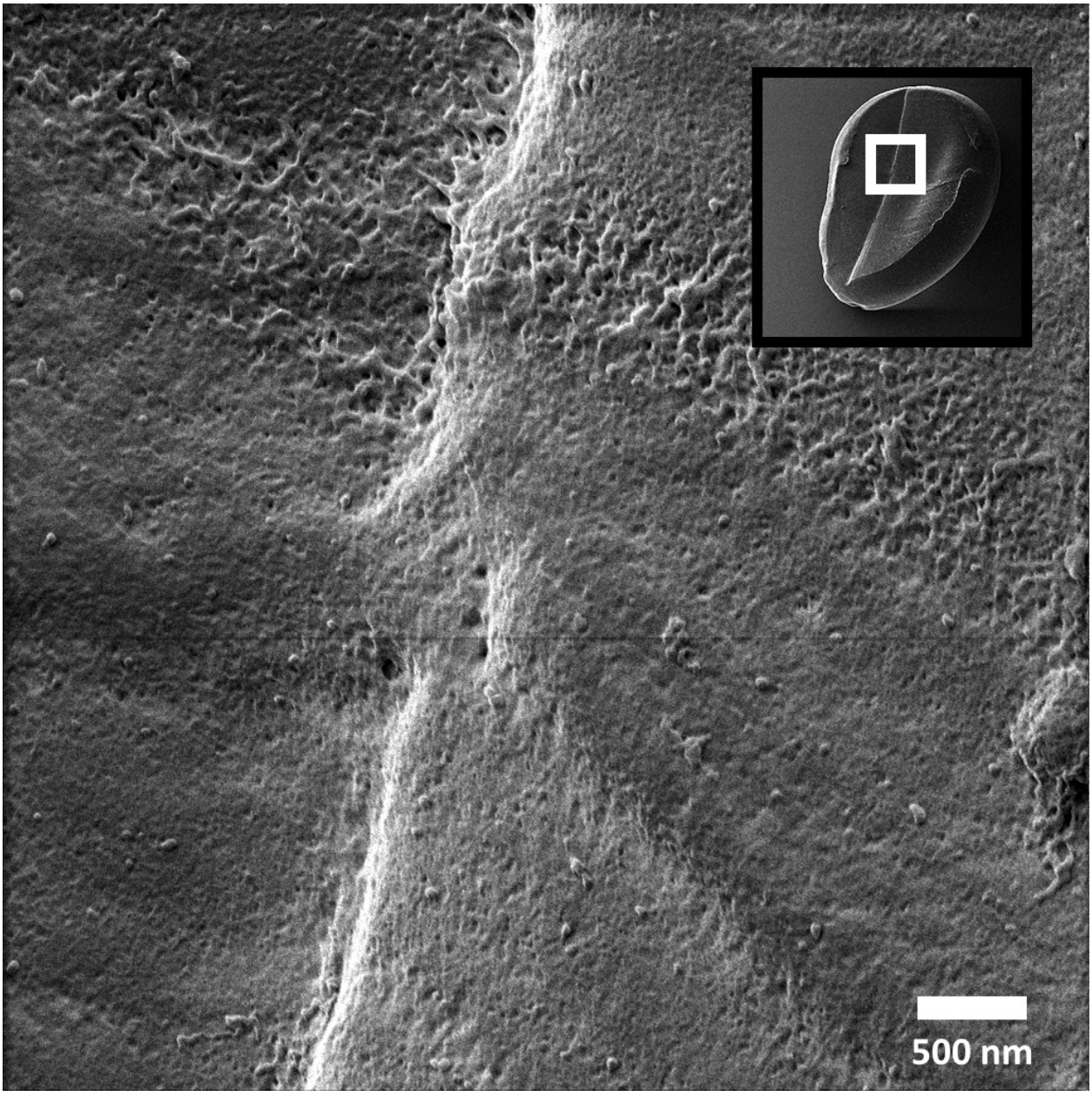

Figure A.3: HIM image of a sectioned native wheat starch granule. The inset in the black box is an image of the granule at lower magnification where the white box demarcates the section of the granule that is imaged at high magnification.

Appendix B – Supplementary Information for Chapter 5

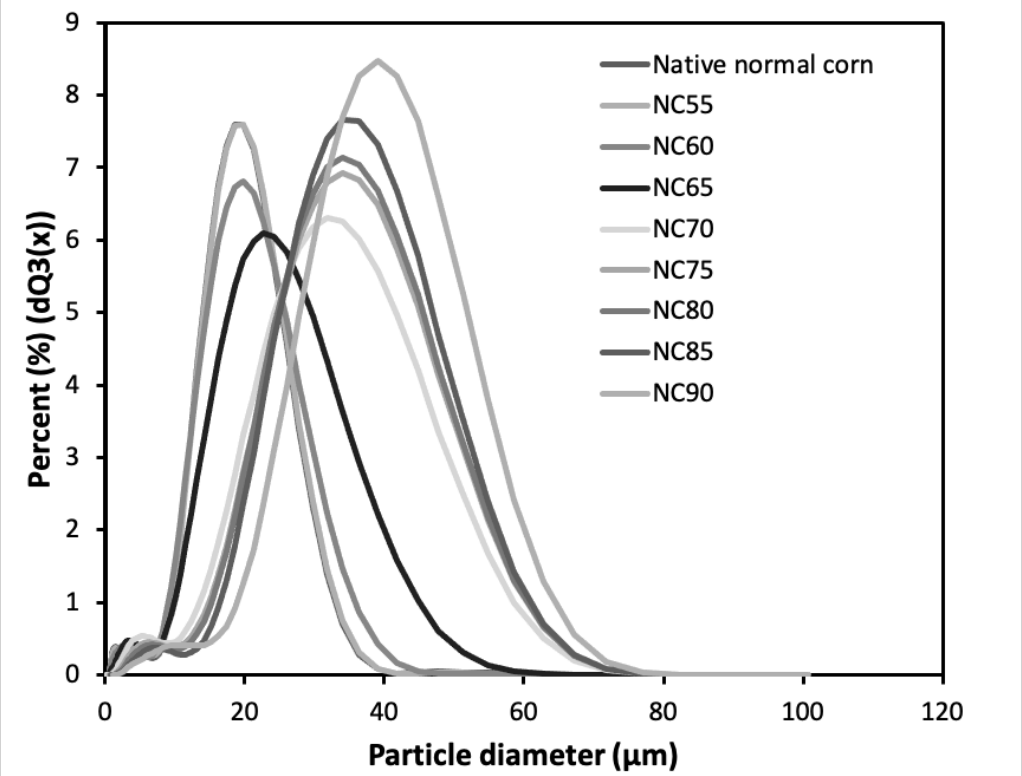

Figure A.4: Particle size distributions for native normal corn starch and swelled starch with heating for 30 minutes at 55, 60, 65, 70, 75, 80, 85, and 90˚C. Data has not been normalized with respect to peak distribution height. For this data, peak height is meaningless and is simply the result of the bins used for the assigning the individual particles size data.